UNIVERSITY OF CALIFORNIA, SAN DIEGO

Shock Environment Characterization: Experimental and Numerical Methods

A thesis submitted in partial satisfaction of the
requirements for the degree
Master of Science

in

Structural Engineering

by

Bradley Durant

Committee in charge:

Professor Gilbert Hegemier, Chair
Professor David Benson
Professor Hyonny Kim

2013

The thesis of Bradley Durant is approved, and it is acceptable in quality and form for publication on microfilm and electronically:

_____

_____

_____

Chair

University of California, San Diego

2013

DEDICATION

To my wife, Rebecca.

TABLE OF CONTENTS

LIST OF FIGURES

LIST OF TABLES

ACKNOWLEDGEMENTS

I would first like to thank my advisor, Professor Hegemier, for his continuous support and encouragement in all of my research at UCSD, particularly my work for this thesis project. He has provided me with numerous opportunities to study the effects of blast and shock loading on structural elements as well as connected me with people who have been instrumental in the development of this work at UCSD. His faith in me to conduct this research has motivated me to further pursue work in this field.

I am also very thankful for the support and guidance of my committee members, Professor Hyonny Kim and Professor David Benson. Being able to glean from their expertise in their respective fields has been very helpul for me, and I appreciate their willingness to provide me with assistance.

I would also like to thank Lauren Stewart for her guidance, assistance, and motivation over the last three years. She is the primary reason why I have had the opportunity to conduct graduate research at UCSD and has taken me under her wing in helping me to pursue my ambitions in the field. Her value of hard work and complete dedication to each project at hand has been my example to model since the beginning of my work with the research group. In addition to being a vital component in bringing the project which is examined in this thesis to the university, she developed the original experimental setup and helped me better understand the use of the laboratory devices to conduct my own research.

Furthermore, I must thank Peter Huson for his encouragement and insight during my time at UCSD. Through trusting me to work extensively with his research project during my time as an undergraduate, he helped me to gain an understanding of the experimental process and setup at the laboratory used to run my own tests. His willingness to explain the intricacies of the system and discuss methods for improving my simulations was very beneficial to my progress. I have been very thankful to be able to glean from his expertise.

I also am very grateful for the extensive help from my right-hand man, Aaron Freidenberg. In addition to teaching me most of what I know about finite element modeling, he always made himself available to help with my experimental setup and

data analysis. The numerous tests examined in this thesis were made possible by his assistance at the lab and willingness to offer hours of assistance to me each week during the experimental series. He has also gone above and beyond the call of duty to help me understand the software tools used to pursue this research.

I cannot neglect to thank all of the Englekirk staff for their commitment to the progress of this research - Alex, Lonnie, Steve, Hector, Dan, Andy, and Robert all went above and beyond the call of duty out at the laboratory to make these experiments successful. Their commitment to patiently train me as a white hat during my undergraduate years at UCSD also provided me with a solid foundation for pursuing experimental research.

The project examined in this thesis was made possible by the support of the staff at the Air Force Research Laboratory at Eglin Air Force Base, Florida. I would especially like to thank Dr. Janet Wolfson and Dr. Jason Foley for their provision of this project and all of the support and assistance along the way.

I would like to thank my parents for their constant support and prayers throughout the duration of my research. I cannot fully express my gratitude for all that they have done for me and the motivation that they have provided for me to press on in my work.

Also, I would like to thank my wonderful wife, Rebecca, for being the best helper that I could ever find. Her encouragement and reminders of how blessed I am to be able to conduct this research are some of my greatest motivation.

Above all, I thank God for all His wonderful blessings in my life. In addition to providing me with an undeserved salvation through the work of Jesus Christ, He has blessed me with all of the people listed above and the opportunities to pursue my ambitions as I seek to honor Him with my work.

It shall be noted that portions of Chapter 2 and Chapter 4 are a reprint of the material as it appears in Blast Simulator Testing for High-g Shock Environment Characterization (2013). Durant, Brad, Stewart, Lauren, Wolfson, Janet, Hegemier, Gilbert. *Proceedings of the 83rd Shock and Vibration Symposium.* The thesis author was the primary investigator and author of this paper.

ABSTRACT OF THE THESIS

Shock Environment Characterization: Experimental and Numerical Methods

by

Bradley Durant

Master of Science in Structural Engineering

University of California, San Diego, 2013

Professor Gilbert Hegemier, Chair

Reliable experimental characterization of high-g shock environments is a long-standing problem which faces much difficulty. The shock levels experienced by various defense-related structural and mechanical components are not always easily obtained in the true environments but are known to span a significant range of peak accelerations and pulse durations. The reproduction of these high-g shock levels in a controlled setting is highly important but also quite complicated. A system which is characterized by substantial energy output, a high level of precision, and adjustability is ideal for producing the varying and intense conditions experienced by components subjected to shock loads.

The UCSD Blast Simulator, a complex experimental device which simulates

explosive blasts without a fireball or the use of explosive materials, has proven to be an appropriate tool for this application. The system uses high-precision, computer-controlled hydraulic actuators to fire a piston mounted with various impact materials at high velocities into the specified test article. In the developed experimental series, a cylindrical steel specimen is launched by the Blast Simulator from a set of custom pedestals into a catcher pit. The response of the test article to the impact is acquired and analyzed with various methods.

The experimental shock environment characterization and analysis is supplemented by a set of numerical models developed with an advanced finite element tool. The simulations examine the loading arrangements of several tests and the resulting specimen response. With the calibrated models, extrapolation to other possible experimental configurations and the prediction of corresponding shock levels is produced.

Chapter 1

Introduction

The proper function of structures and mechanical components can be suddenly brought to a halt by the presence of a high-energy, short-duration load. This type of threat, known as a shock load, can cause critical damage to a wide range of components which are vital to the operation of various structures and mechanical devices such as buildings, bridges, military craft and vehicles, and aerospace components. Because of the need to properly design such structures to resist shock loading, effective experimental techniques must be developed to characterize the loading environments experienced by the various components found in these systems.

The UCSD Blast Simulator has proven to be an effective tool for the application of shock loads. Typically used for the simulation of blast-like pressure pulses upon various structural components such as columns and walls, the simulator is capable of producing high-intensity loading scenarios. Using a set of programmable pressures, hydraulic oil, and an adjustable impacting ram, the device is ideal for developing a series of varying shock loads for a provided specimen.

The Air Force Research Laboratory at Eglin Air Force Base, Florida, provided a special steel cylinder for shock testing at the Blast Simulator testing facility. The ultimate objectives of the thesis were related to the examination of the various shock environments which would be experienced by the test article and are provided as follows:

- Provide information on the shock response spectrum and its effective use as an analytical tool for the characterization of shock environments

- Provide experimental methods for applying various shock loads to a steel test article using the UCSD Blast Simulator
- Display the effectiveness of the Blast Simulator as a shock loading tool
- Compare the specimen response resulting from different experimental loading arrangements and examine the effects of modifying various testing parameters
- Using the experimental results, calibrate numerical models which can be extrapolated to a wide range of shock loading configurations

The thesis is composed of six chapters. Chapter 2 provides information on the fundamentals of shock loading and examples of structures which often are threatened by such loading. The use of the shock response spectrum as a tool for both analysis and design of structures and mechanical components is also explained.

Chapter 3 provides information on the UCSD Blast Simulator and its use for producing extreme loading conditions. The design of the device and its use for the application of both blast-like loads and mechanical shock is explained.

Chapter 4 presents a thorough description of the experimental test series. The specimen and data acquisition setup, various loading configurations, and results and discussion of each test are provided.

Chapter 5 presents the numerical simulations of specified tests from the experimental series. Modeling approaches and comparisons of results between the tests and models are provided. The usefulness of the models for designing new experimental tests is also explained.

Chapter 6 concludes and summarizes the shock environment characterization study. The practical implications of the results are discussed to display the usefulness of the research, and recommendations for future work are provided. Additional data and images which were not included in the main body of the thesis are given in the appendices.

Chapter 2

Shock Response Fundamentals

2.1 Shock Loading

Mechanical shock is a complex loading event which involves the application of a large force over a duration which is significantly shorter than the natural period of the structure being loaded. A basic definition of mechanical shock was provided at the first Shock and Vibration Symposium in 1947: "a sudden and violent change in the state of motion of the component parts or particles of a body or medium resulting from the sudden application of a relatively large external force, such as a blow or impact. [2]" The study of the effects of shock loading on structures and development of design approaches for resisting such loads is highly important to the defense industry.

Structures and mechanical components can experience various types of shock. Earthquake ground motions are a form of shock load which can induce damaging oscillatory accelerations in buildings and bridges. Ballistic shock occurs when a projectile impacts another object and induces a rapid velocity change in the loaded surface. An example of this would be the collision of an artillery shell with a military vehicle as shown in Figure 2.1. This thesis provides specific analysis for ballistic shock in subsequent chapters. Another military application for this type of extreme loading is naval shock (Figure 2.1), which occurs when a sudden force (such as an underwater explosion) is applied to the hull of a ship and transmits loads to various components throughout the craft [2]. Pyroshock is a specific type of shock which is often expe-

rienced by aerospace vehicles during staging events. Small charges are detonated to initiate these processes and often produce shocks which can be damaging to various mechanical and electrical components of the spacecraft.[19]

Figure 2.1: Ballistic and Naval Shock Loading (taken directly from [2])

It is important to note that two different types of shock loads are commonly experienced by structures. The first, an oscillatory shock, is often encountered by aerospace components during various staging events of a spacecraft or missile. An example of this type of shock is provided by Tom Irvine and displayed in Figure 2.2. The second, a single-cycle pulse shock, is often induced during impact events. This type of shock is displayed in the schematic of Figure 2.6 and in the results shown in Chapter 4.

Because of the need for specially-designed structures and mechanical devices which can withstand shock loads, experimental techniques are necessary for testing these components. Drop towers, gas guns, resonant fixtures, and hydraulic actuators are all typical experimental methods for inducing shock. A drop tower, which uses gravity and often times tension cables to rapidly accelerate a mass towards a test article, is discussed by Richard Chalmers [8]. Gas guns utilize the sudden release of a large amount of pressure to accelerate a small projectile towards a specimen as discussed by Luo [13]. With knowledge of the fundamental frequency of a test article, a resonant fixture uses an impactor to strike a rod or platform which is designed to vibrate at the primary natural frequency of the specimen, thus inducing large accelerations. This approach to shock loading is explained in a pyroshock test

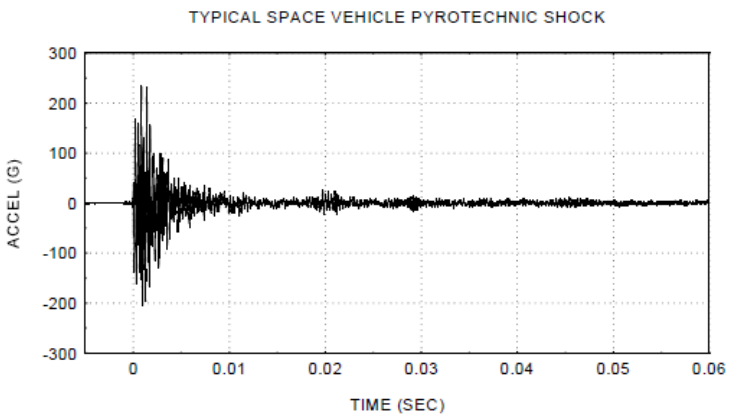

Figure 2.2: Example of oscillatory shock (taken directly from [11])

procedures report produced by staff at the US Army White Sands Missile Range [1]. The UCSD Blast Simulator, which is discussed in Chapter 3, uses special hydraulic actuators to impart shock loads.

Engineers and analysts working with experimental shock testing will often want to know the capabilities of a test configuration in terms of its ability to induce specific levels of peak accelerations and pulse durations in a test article. While determination of the peak acceleration is generally straightforward, there is some discrepancy over the best method for computing the width of the pulse duration. One method simply calculates the integral of the curve and sets the duration equal to the time value at which the slope of the integral levels off (no further contribution of area under the pulse curve) minus the starting time of the pulse. This approach is considered to be non-conservative because it will include the contributions of noisy oscillations which exist beyond the main pulse of interest and produce a higher duration value than is reasonable. An example of a pulse which exhibits this behavior is shown in Figure 2.3. Another method is to simply locate the points at which the front and back of the signal cross the time axis on each end of the signal (corresponding to zero acceleration). This method can also be considered non-conservative because it will include slow rise or fall times at each end of the pulse which should not be considered as part of the true pulse (see Figure 2.4).

A typical and more conservative approach to determining the pulse duration

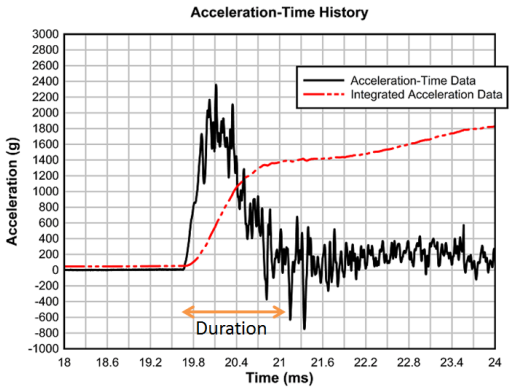

Figure 2.3: Example of Non-conservative Approach to Duration Calculation: Signal Integration

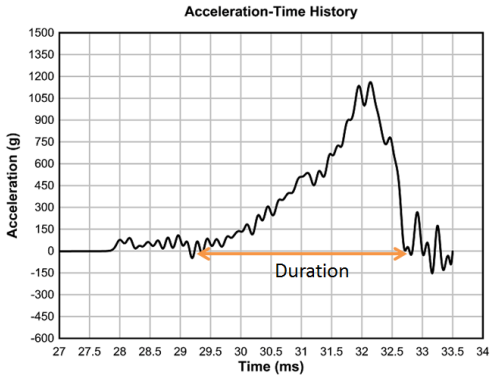

Figure 2.4: Example of Non-conservative Approach to Duration Calculation: Zeros Method

involves calculating 10% of the peak acceleration and locating the time values at each end of the pulse which correspond to this acceleration value. Thus, the potential problems discussed in the previous examples will be avoided, and a conservative value will be determined. This approach is used for all duration calculations in this thesis, and an example of the method is displayed using a simple haversine curve in Figure 2.5 for visual clarification.

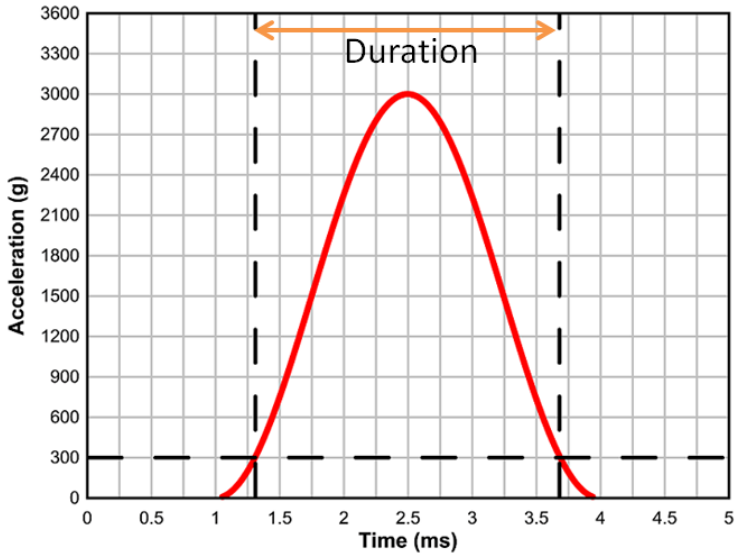

Figure 2.5: Conservative Approach to Duration Calculation: 10% Method

2.2 Shock Response Spectrum

The shock response spectrum (SRS) is an analytical tool often used in shock applications to understand the risks faced by various components in a given structural or mechanical system. When a system is loaded with a short duration pulse and undergoes transient dynamic stresses, the response will be a candidate for evaluation with the shock response spectrum. George Henderson and Allan Piersol broadly define the shock response spectrum as "the peak response of a simple oscillator (single-degree-of-freedom) to an excitation as a function of the natural frequency of the oscillator [9]." Thus, for a system characterized by a wide range of frequencies, the expected peak response at each of the frequencies can be determined using the method.

To calculate the response, a given excitation is applied to a set of single-degree-of-freedom oscillators, each with equal mass, spring constants, and damping values but varying natural frequencies. The equations of motion and relevant variables describing the event are given as follows [11]:

m - mass
k - spring constant
c - damping coefficient
x - absolute displacement of mass
y - displacement of base
z - relative displacement of mass
ω_n - natural angular frequency
ξ - damping ratio
ω_d - damped natural angular frequency

The differential equation of motion for the oscillating system:

$$m\ddot{x} + c\dot{x} + kx = c\dot{y} + ky \tag{2.1}$$

Considering the relative displacement of the mass $z = x - y$, the equation can be simplified:

$$m\ddot{z} + c\dot{z} + kz = -m\ddot{y} \tag{2.2}$$

Forming relations for the natural frequency and damping values:

$$\omega_n = \sqrt{\frac{k}{m}} \tag{2.3}$$

$$\xi = \frac{c}{2\sqrt{km}} \tag{2.4}$$

$$\omega_d = \omega_n \sqrt{1 - \xi^2} \tag{2.5}$$

Relating the relative motion of the mass to the base (input) acceleration:

$$\ddot{z} + 2\xi\omega_n \dot{z} + {\omega_n}^2 z = -\ddot{y}(t) \tag{2.6}$$

Using a convolution integral, the absolute acceleration of each single-degree-of-freedom oscillator is determined as a function of its natural frequency:

$$\begin{aligned} \ddot{x}_i = {} & 2e^{-\xi\omega_n \Delta t} cos\left[\omega_d \Delta t\right] \ddot{x}_{i-1} - e^{-2\xi\omega_n \Delta t} \ddot{x}_{i-2} + 2\xi\omega_n \Delta t \ddot{y}_i \\ & + \omega_n \Delta t e^{-\xi\omega_n \Delta t} \Bigg\{ \left[\frac{\omega_n}{\omega_d}(1 - \xi^2)\right] sin\left[\omega_d \Delta t\right] \\ & - 2\xi cos\left[\omega_d \Delta t\right] - 2\xi cos\left[\omega_d \Delta t\right] \Bigg\} \ddot{y}_{i-1} \end{aligned} \tag{2.7}$$

Using the result in Equation (2.7), the threat (in terms of peak acceleration) faced by a component of any given natural frequency in the system can be analyzed. The analyst can determine the range of natural frequencies which are relevant for the given system and specify this set to be used in the calculation. For an accurate response, the sampling frequency of the data acquisition system must be considered when determining the maximum frequency value to use in the results. The IES Handbook for Dynamic Data Acquisition and Analysis [10] provides guidelines for determining cutoff frequencies when performing analysis in either the time or frequency domain. Since the shock response spectrum calculations are performed in the time domain, a sampling rate which is 10 times greater than the maximum frequency response is recommended to produce a magnitude error which is less than 5%. Be-

cause the system being used for the test series was characterized by a 1 MHz sampling rate, a maximum frequency value of 100 kHz was used in the results produced in this thesis. The analytical approach for forming the response spectrums seen in Chapter 4 was formulated by David Smallwood [17]. Figure 2.6 shows a schematic of the shock response computation process.

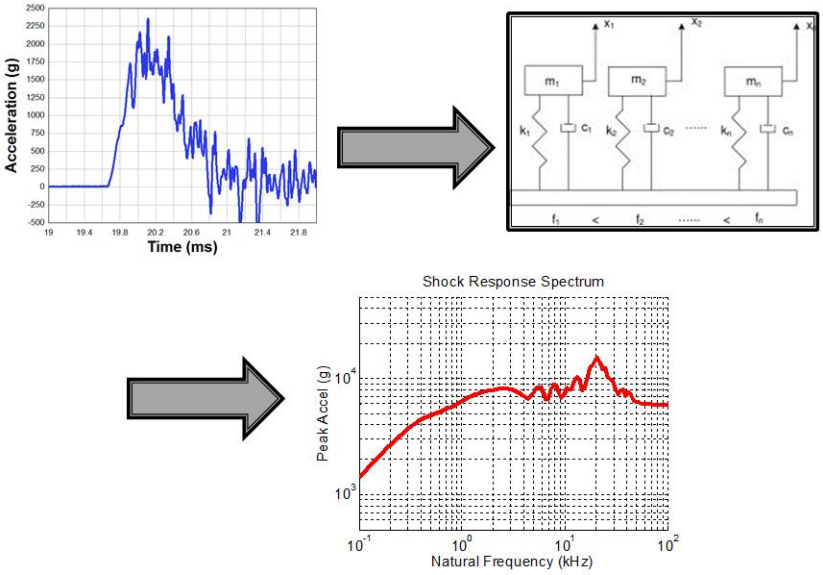

Figure 2.6: Schematic of Shock Response Spectrum Calculation

When studying a specific response spectrum, it is necessary to know the characteristics of the structure being examined for the data to be useful. Because different structural and mechanical components will have various stress threshold values, the maximum shock response at a given frequency value may or may not be threatening to the structure. While an aerospace component may be perfectly safe when subjected to a specific shock, a computer circuit board may reach critical damage when facing the same shock. Thus, the shock response spectrum is applicable specifically to the component(s) being evaluated.

As discussed in [12], specific properties of the input acceleration-time history have noteworthy effects on the resulting shock response spectrum. For example, in the high-frequency region of the plot (>1,000 Hz for the purposes of this thesis), the shock response curve will tend towards the peak acceleration found in the input signal when the damping is small. An examination of Equation 2.7 shows how the response

is scaled linearly with the input acceleration when the natural frequency is very high. Further details on the convolution integral approach and detailed equations which are used for the computation are provided in [11]. For a given peak acceleration, an increase in pulse duration will increase the response values in the low-frequency region (<100 Hz) of the shock response spectrum. Thus, an increase in area under the pulse curve will naturally raise the values in this region. Concepts which are commonly used in earthquake engineering can be used to explain this phenomenon. Tall structures which have longer periods (smaller natural frequencies) are more prone to be excited to high acceleration levels by ground motions which have a significant amount of low-frequency content than those with mostly high-frequency content. Similarly, a mechanical component with a low natural frequency will generally face greater risk from an input pulse with a long duration than from one characterized by a short duration. Multiple examples which display this effect are provided in Chapter 4.

Depending on the application, there are five different shock response values which may be of particular interest. These can be characterized as the maximum acceleration response values experienced by the theoretical SDOF oscillators within specific frames. The names of these SRS values and their corresponding conditions are as follows [15]:

- Primary SRS - Response only during the application of the shock
- Residual SRS - Response experienced after completion of the shock
- Positive SRS - Response in the positive direction
- Negative SRS - Response in the negative direction (oscillatory shocks)
- Maximax SRS - Maximum of the positive and negative direction responses

The shock responses produced in this thesis use the maximax computation approach. In addition to this specification, it is important to note that every shock response spectrum is characterized by a "Q-factor," or quality factor, which is directly related to the specified damping value: $Q = \frac{1}{2\xi}$. The spectrum is incomplete without the specification of this term. For all shock responses computed in this thesis, the damping is set to 5%, which is equivalent to a Q-factor of 10.

A portion of Chapter 2 is a reprint of the material as it appears in Blast Simulator Testing for High-g Shock Environment Characterization (2013). Durant, Brad, Stewart, Lauren, Wolfson, Janet, Hegemier, Gilbert. *Proceedings of the 83rd Shock and Vibration Symposium.* The thesis author was the primary investigator and author of this paper.

Chapter 3

UCSD Blast Simulator

The UCSD Blast Simulator is a complex experimental device which is capable of delivering shock loads in a controlled environment. This chapter explains the more typical use of the simulator for applying blast-like pressure pulses and provides examples of past experimental series which analyzed the response of structural columns and walls to blast loads. The components which comprise the simulator and a discussion on the mechanical process involved in the reproduction of impulsive loading is also provided. The chapter concludes with information regarding the use of the device for applying shock loads as seen in the experimental series being specifically examined in this thesis.

3.1 Blast Simulation Methodologies and Operational Components

The typical approach for analyzing the effects of blast loads on structures is to conduct a field test involving the detonation of a column or pile of explosives which is placed at a specified distance from the test article. However, this approach has several limitations. First, reproducing the same explosive charge configuration (density of explosive material, shape, etc.) for subsequent tests is very difficult and, thus, it is unreasonable to expect repeatable conditions during an experimental series. Second, the fireball and/or dust cloud produced by the explosion will typically disturb any camera view of the specimen during loading. As a result, visual examination of the progression of deformation in the structure being studied is not possible. Finally, field tests are typically very costly and conducted in difficult work environments which are offset from civilization. While ultimately being necessary for a full characterization of a structure's ability to withstand blast loads, field tests are clearly limited in these specific areas.

In contrast to a standard field test, the Blast Simulator applies a blast-like load in a laboratory environment without the use of explosive materials or a fireball. Consequently, a full qualitative analysis of the loading and test article response can be conducted using video captured with high-speed cameras. Because the Simulator function is controlled electronically, a high level of repeatability in results between identical test setups is readily obtainable as seen in Figure 3.9. The device has proven to be an effective tool for a comprehensive examination of the response of various structural components to impulsive loading.

In order to reproduce the types of pressures created by explosions, the simulator system uses a combination of pressurized nitrogen and hydraulic oil in conjunction with unique actuator systems known as Blast Generators. Two types of these devices are typically used at the Blast Simulator facility. The smaller device, known as a BG 25, is capable of producing peak velocities at specimen impact of approximately 25-30 m/s and is often used for tests involving wall systems. The larger option, the BG 50, can reach peak impact velocities of 50-60 m/s and is used for articles such as columns, defense-related components, and other structures which require a very high

level of loading. The BG 50 is used in the experimental series for this thesis and is shown in Figure 3.1.

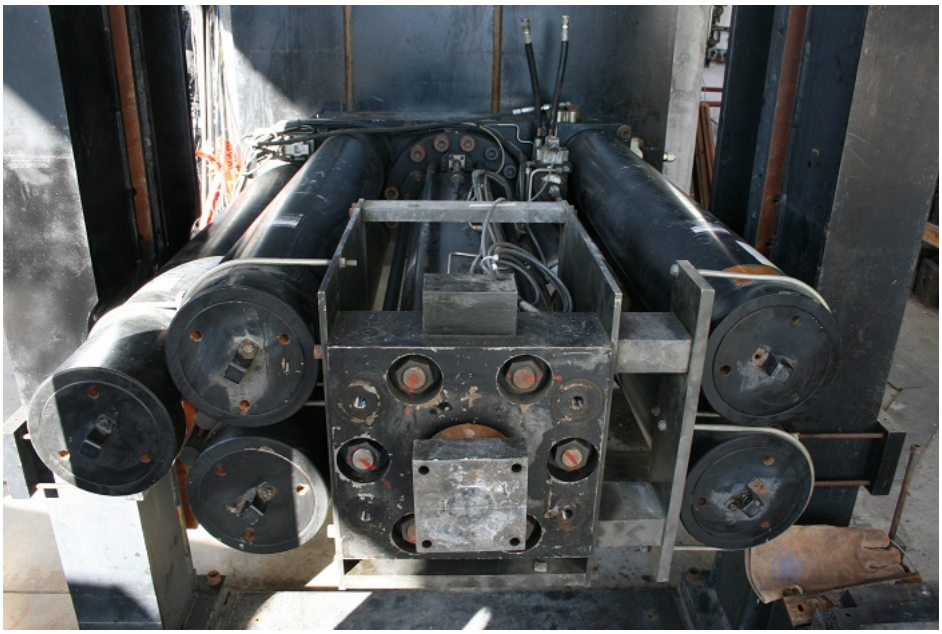

Figure 3.1: BG 50

The generators operate through interactions between accumulated pressure, hydraulic oil, and a piston assembly which is rapidly forced out of the generator. Pressure transducers and high-precision poppet valves are used to monitor and control the flow of oil and and transfer of pressure to produce a very specific motion of the piston. This motion is programmed by specifying various input parameters including pressure levels and the starting position of the piston before the test. A schematic of a BG 50 showing its operational components is provided Figure 3.2.

Typically mounted to the piston is an aluminum or steel plate known as the "impacting mass." Because the size of this mass can be adjusted, the total weight being applied to the specimen and, thus, the incoming energy can be easily modified to impart different loads. Attached to the mass is a specially designed urethane pad with a specific geometry shown in Figure 3.3. The pyramids extending from the front face were designed specifically to reproduce the types of loading durations experienced during blast events. An examination of the adiprene material which comprises the pad is provided in [6]. The combination of the metal plate, programmer, and any

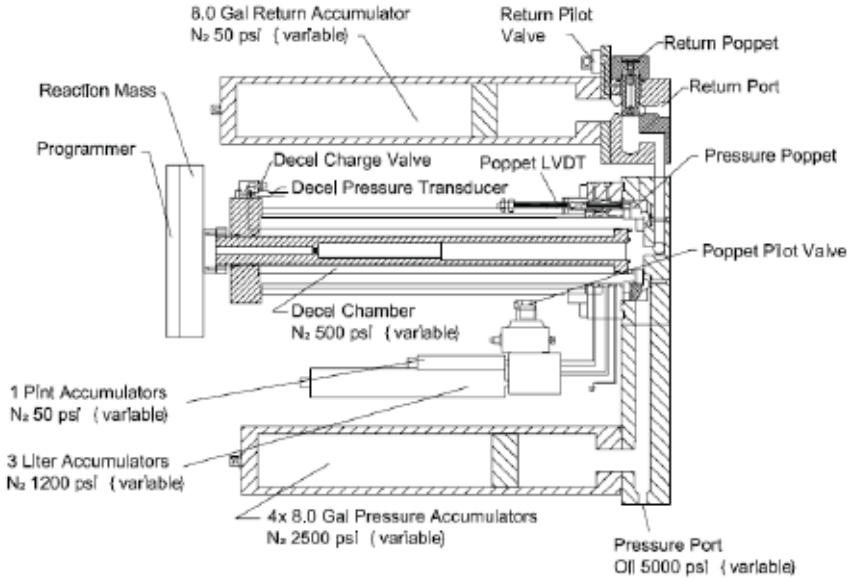

Figure 3.2: Schematic of BG 50

other attachments will collectively be referred to as the "impacting mass" for the purposes of this thesis. Also, the velocity at which the impacting mass collides with the test article will be known as the "impact velocity." The desired impact velocity programmed for the test, which is typically not identical to the true impact velocity but very close, will be known as the "target impact velocity" in subsequent sections.

A set of rails and sliders are used to guide the impacting mass along a level path towards the test specimen. The rails are bolted securely to both the blast generator and a set of steel support towers and checked with a leveling device between tests. The sliders are composed of a phenolic material and designed to have greater strength in a specific direction such that they resist the unique loads experienced during the blast simulations. Because of the importance of keeping the impacting mass at a specific height for collision, the rails and sliders are very important for maintaining the predictable and repeatable nature of the tests. A display of the impacting mass, rails, and slider is shown in Figure 3.4.

The Blast Simulator has the unique option of applying a particular loading pattern to test articles. The "punch" is described as the forward motion of the

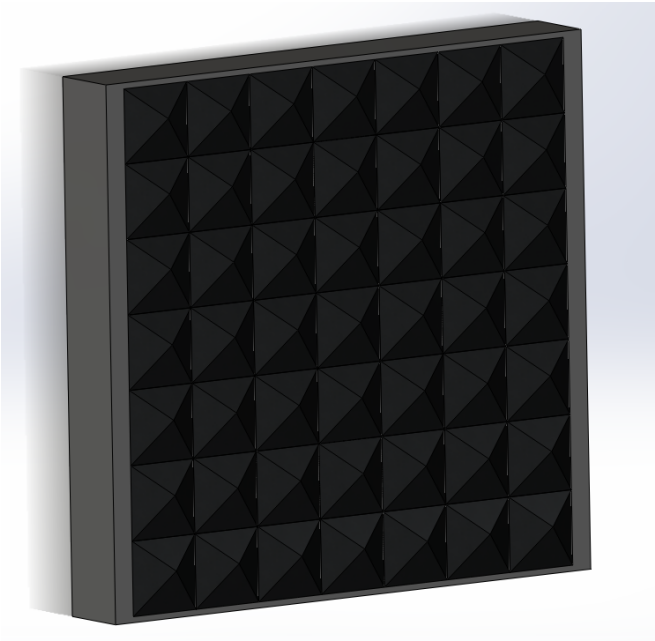

Figure 3.3: Rendering of Programmer

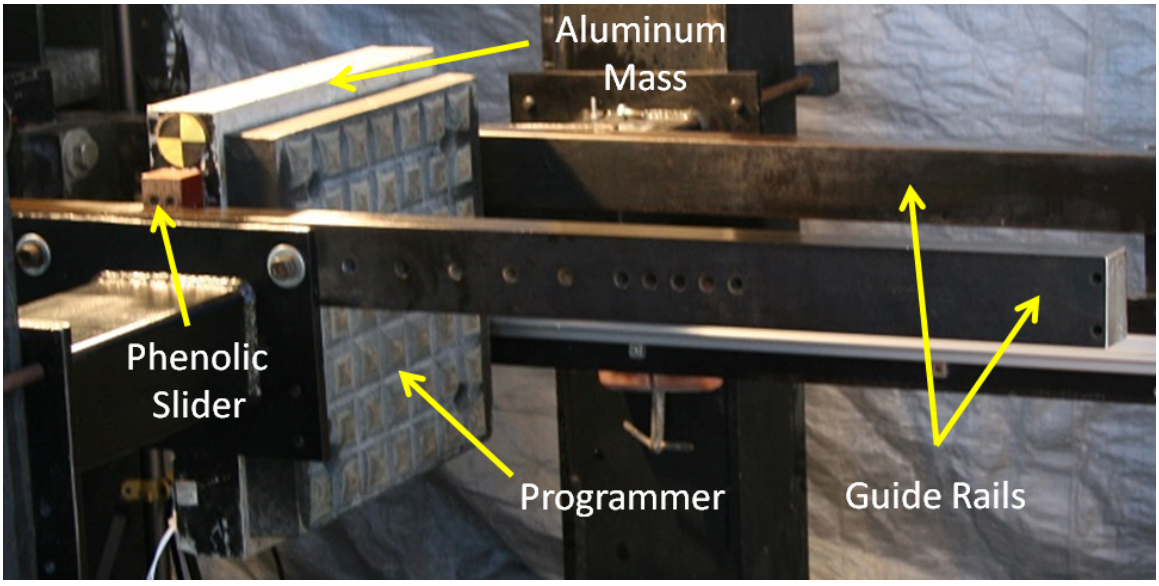

Figure 3.4: Impacting Mass and Guide Assembly

impacting mass into the test article up to a very specific point followed by a regression back towards the Blast Generator. While other impulsive loading devices such as drop towers and gas guns can impart high-energy loads, any return of the impactor towards its origin will be a result of natural rebound rather than a programmable event as with the Blast Simulator. This unique capability allows for effective modification of the types of loading required for blast simulations.

The Blast Generator used in the test series being examined is mounted to a reinforced concrete reaction structure which is located on a base-isolated platform. This setup is used to dissipate the amount of rebound energy being transferred into the ground during loading and protects the facility from excessive ground motion and damage. Figure 3.5 shows a drawing of the generator mounted to the reaction structure.

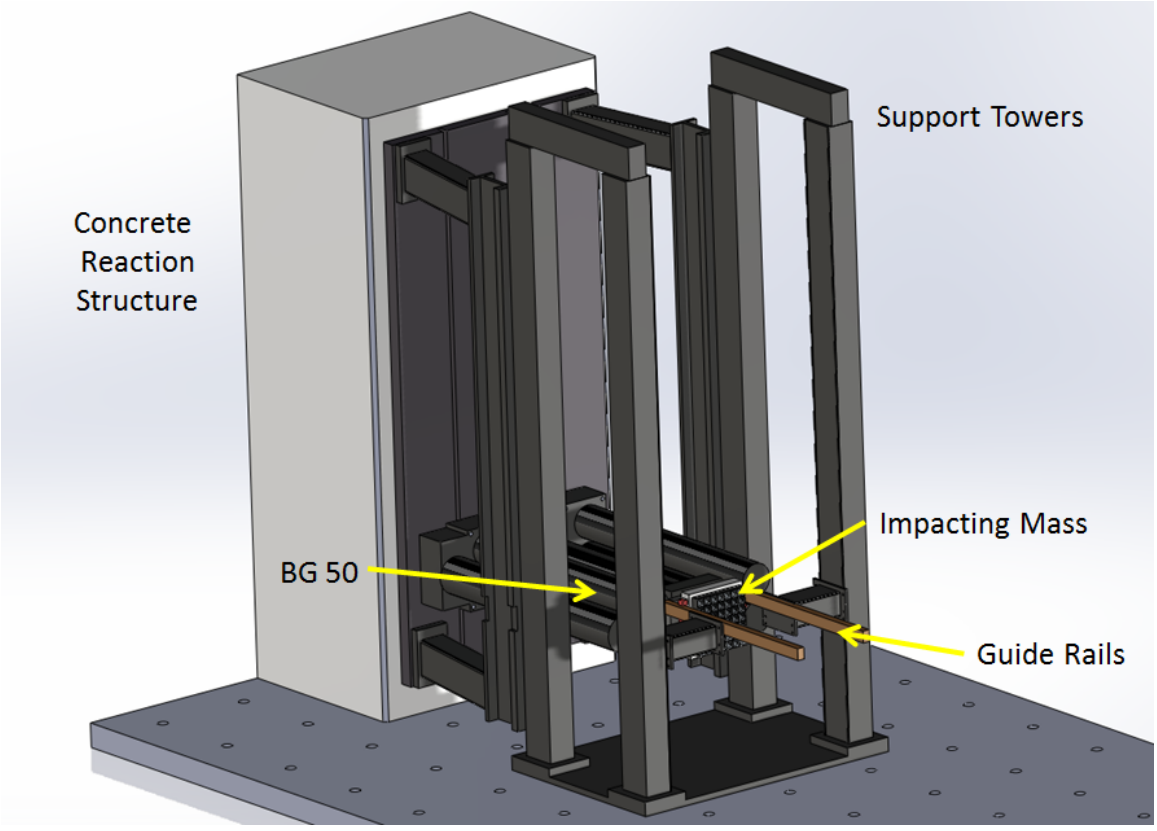

Figure 3.5: BG 50 Mounted to Reaction Structure

3.2 Previous Testing with the Blast Simulator

Important tests involving simulated blast loading of steel columns and CMU walls were conducted by Dr. Lauren Stewart [18] and Dr. Michael Oesterle [14]. The column tests were validated against field tests and showed the effectiveness of the simulator for applying blast-like impulses to load-bearing structural components. For the wall testing, the experiments involved loading of reinforced and unreinforced CMU sections as well as walls retrofitted with carbon fiber for strength and polyurea as a catchment system for spall. In addition to providing a thorough analysis of the response of the various wall systems, the series displayed the advantages of the simulator approach for conducting parametric studies and determining effective design options for future structural systems.

Figure 3.6: Steel Column Test with the Blast Simulator (taken directly from [18])

Figure 3.7: CMU Wall Test with the Blast Simulator (taken directly from [14])

It is worth noting that both of the test series used different programmer ar-

rangements than the configuration being used for the experimental testing described in this thesis. Different shape options provide the ability to apply the most effective load to the specimen under examination and allow for further adjustability in the test setup. Figure 3.8 shows a Blast Generator with several different programmer variations.

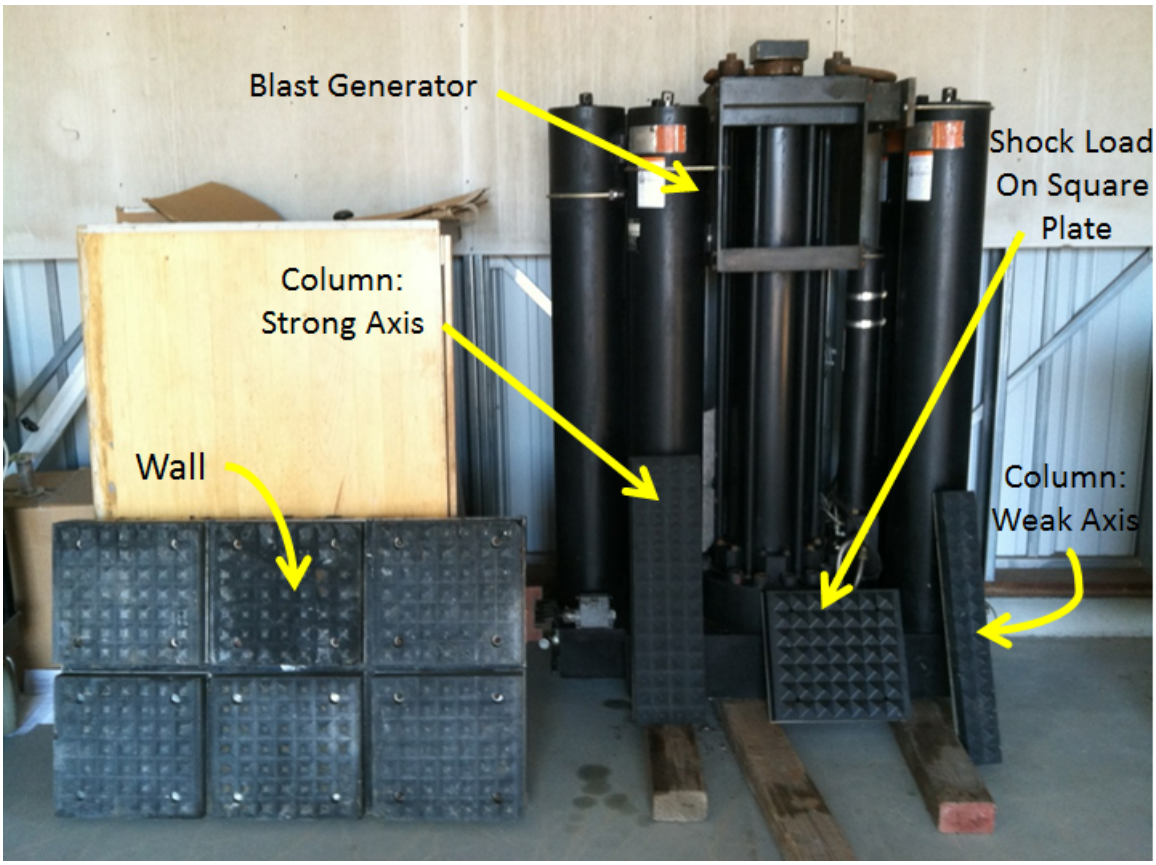

Figure 3.8: Programmer Variations

3.3 Shock Loading with the Blast Simulator

The types of impulsive loading delivered by the Blast Simulator in previous test series have proven to be effective representations of loads produced by blast events. Because a single-cycle shock pulse was desired for loading of the AFRL test article, it was clear that the simulator was also a plausible option for this type of experimental series. In order to move forward confidently with the approach of using the simulator as a shock device, a previous test series which involved shock-like loads was examined for reliability. Figure 3.9 shows the response of a steel specimen to a set of 3 different tests which had identical inputs. It is clear that, in addition to producing a significantly large peak acceleration across a clearly measurable pulse duration, the testing showed an impressive level of repeatability. The results were more than sufficient for displaying the effectiveness of the device for inducing shock loads in a steel specimen such as the AFRL test article being examined in this thesis.

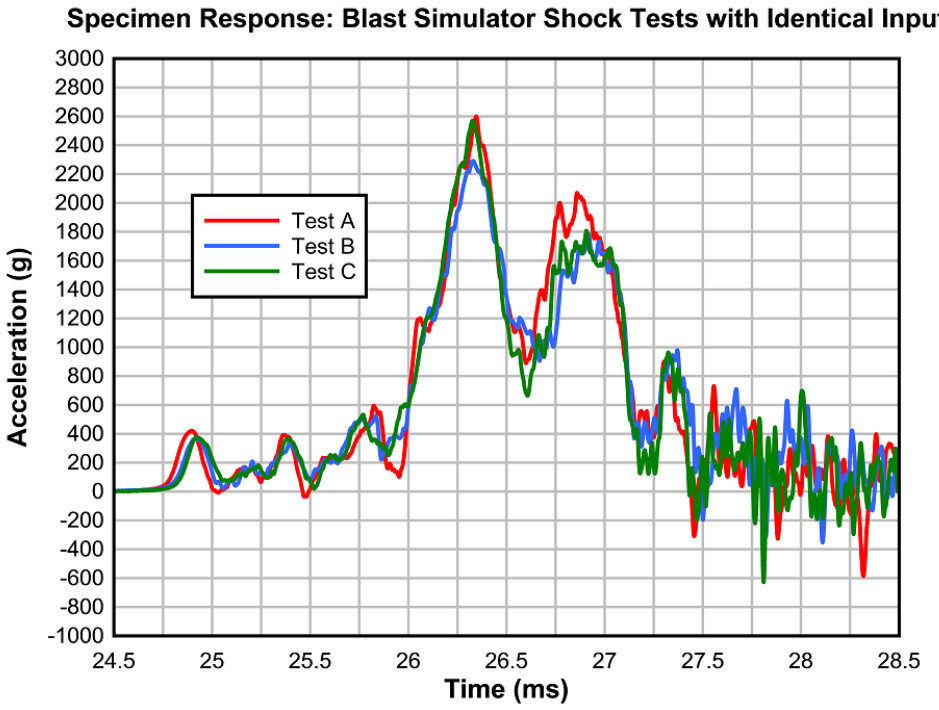

Figure 3.9: Repeatability of Blast Simulator for Shock Loading

Chapter 4

Experimental Shock Loading of Steel Cylinder

The experimental series for shock loading the AFRL test article using the Blast Simulator involved 24 tests with various loading configurations and impact velocities. The initial tests were conducted using a standard programmer as the impact medium. Subsequent tests included the use of polyurethane foam, leather, and sand as additions to the programmer configuration. The specified material was secured to the impact side of the programmer such that the specimen was loaded with the added material. In an attempt to compare data sets between tests with different impactor arrangements, a typical set of impact velocities was designated for each test series: 15 m/s, 30 m/s, and 40 m/s. As testing progressed, higher velocities were used for the most efficient loading mediums.

4.1 Test Setup

The specimen under examination was a hollow steel cylinder with a 16x16x1.5 in steel plate welded to the impact side (Figure 4.1). The back half (non-impact side) of the cylinder had a slight taper with increasing diameter towards the free end. Three custom steel pedestals were designed to support the specimen and allow it to fly freely away from its resting position upon impact. In order to insure that the specimen was located at the same height and resting at the same angle for each test, the pedestals were designed as threaded assemblies which could be adjusted to modify the position of the test article. A catcher pit (Figure 4.2) composed of four large concrete blocks and sand bags was used to stop the specimen during its flight and absorb the high amount of energy being carried away from the collision.

Figure 4.1: AFRL Test Article

In order to examine the effects of various loading mediums on the acceleration response of the specimen, several configurations were designed. Figure 4.3 shows the seven impacting mass arrangements which were used during the test series. The frames are described as follows: (a) single programmer, (b) double programmer, (c) polyurethane foam and programmer, (d) confined polyurethane foam and programmer, (e) layered leather and programmer, (f) confined sand and programmer, (g) confined sand and programmer covered with layered leather.

Figure 4.2: Specimen Catcher Pit

For specific tests which involved the use of softer impact materials such as foam or sand, a special steel confining box was designed. The box served the purposes of increasing the stiffening rate of the material by preventing lateral expansion and protecting the test area from ejecting particles. By attaching the box to the aluminum impact plate, the weight of the impacting mass assembly was increased by approximately 100 lbs. A drawing of the confining box is shown in Figure 4.4.

Because the impact surface of the specimen plate was 16x16 in, the inner dimensions of the box were set to 18x18 in to insure that the box would not contact the specimen and induce high-frequency ringing in the acceleration response as a result of metal-to-metal contact. Thus, only the specified impact material (sand or foam) collided with the test article, and the box effectively confined the material to a maximum lateral expansion of 18x18 in. Images for Test 16 and Test 17 show the specimen entering (but not contacting) the box as the sand compresses. The black components in the drawing are spacers which connect the box to the aluminum impact plate. The holes seen in the image were used as slots for attaching the box to the

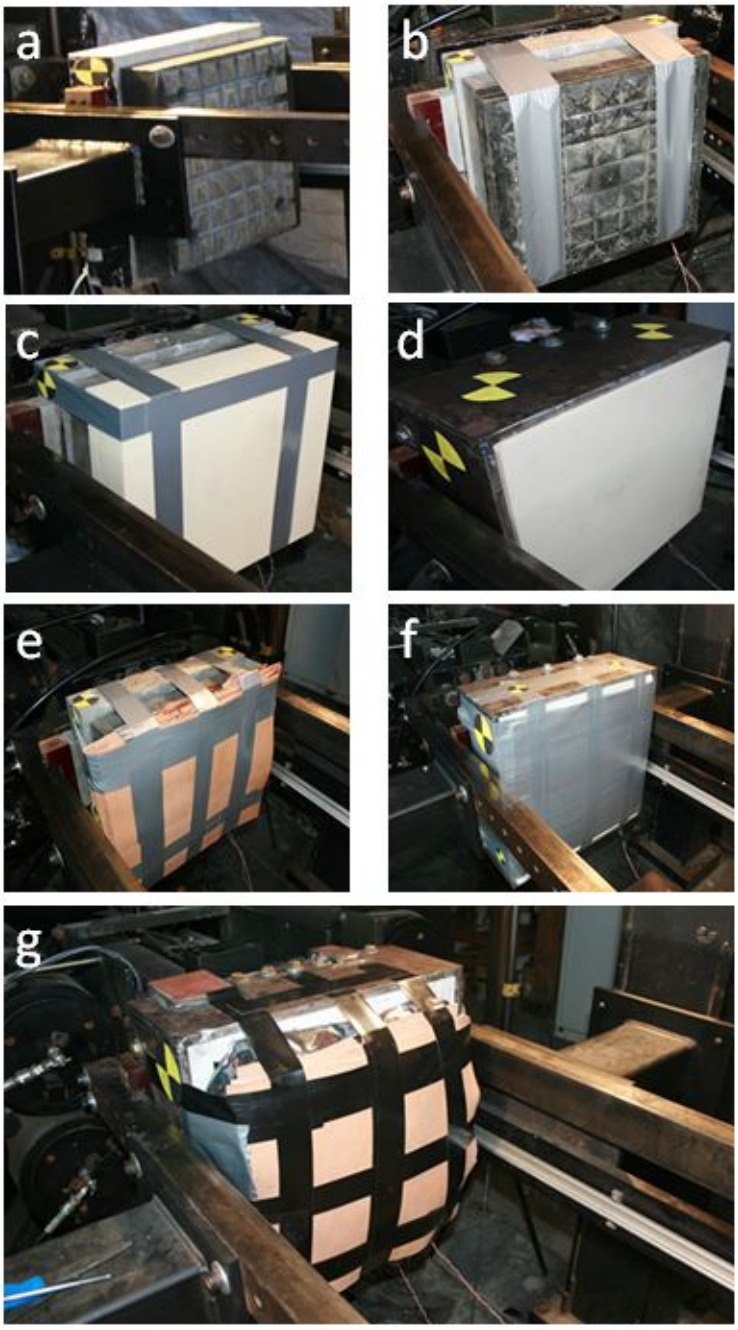

Figure 4.3: Loading Configurations for Experimental Series

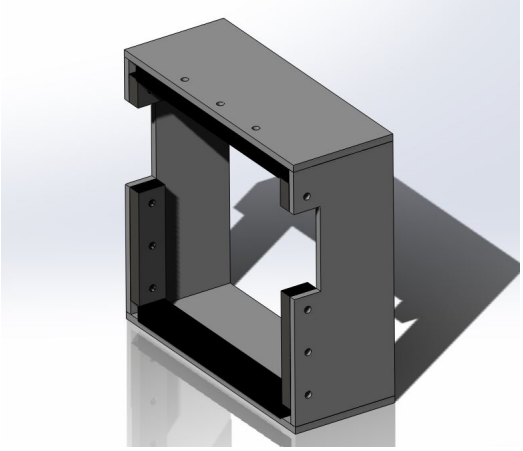

Figure 4.4: Drawing of Confining Box

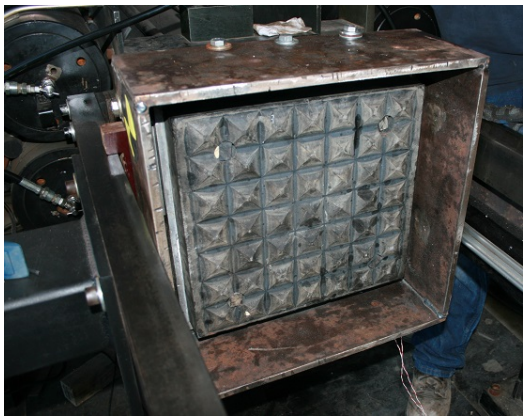

Figure 4.5: Confining Box with Programmer

aluminum plate with bolts, and the rectangular cutouts on the sides correspond to the locations of the phenolic rail guides. Figure 4.4 shows an image of the confining box with the aluminum plate and programmer attached before a softer impact material was added to the assembly.

4.2 Data Acquisition

Each test included two 10k g shock accelerometers (PCB 350B03) which were mounted to the non-impact side of the specimen in the locations seen in Figure 4.6. The sensors and wiring were protected by steel tabs, which were welded to the specimen, along with insulating foam to minimize losses during impact in the catcher pit. High-speed Phantom video cameras and tracking software were used to track the motion of the impacting mass and specimen for determining the changes in velocity experienced by the components as well as observe the progression of loading. The images in the Test Results section which display this progression were acquired with the high-speed cameras.

The data acquisition system was capable of simultaneous channel sampling at a rate of 1 MHz with an anti-aliasing low-pass filter at 500 kHz. As discussed in Chapter 2, this sampling rate allows for the shock responses shown in the results to be calculated to an upper-bound frequency of 100 kHz.

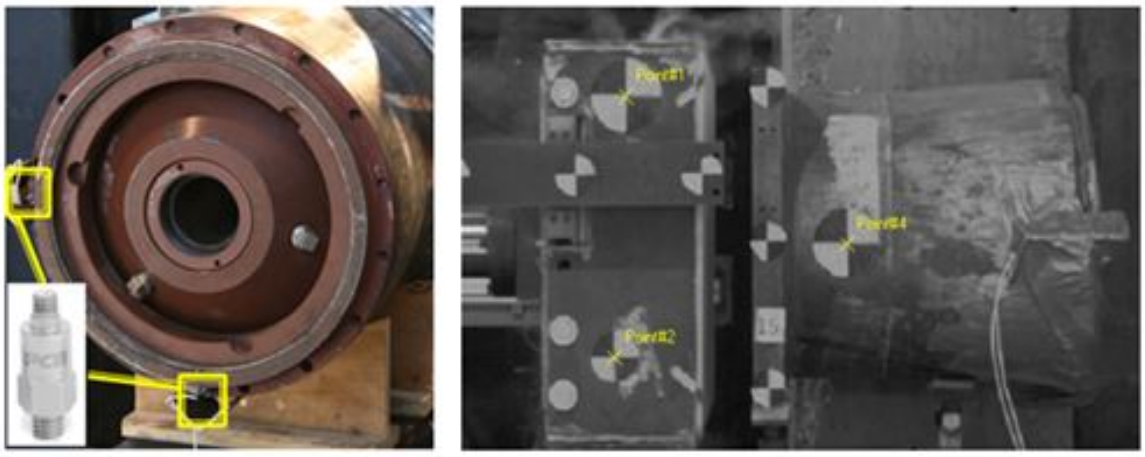

Figure 4.6: Data Acquisition - Left: Location of Accelerometers - Right: Video Tracking Software

4.3 Test Results

Analysis of each test includes a velocity-time history for the impacting mass and specimen, acceleration-time history for the specimen, and shock response spectrum. The velocity results are used in conjunction with the masses of the specimen and impactor to determine the amount of energy dissipated during the collision. Because the purpose of the energy method is to determine a correlation between the acceleration pulse duration and dissipated energy during the collision, the calculations are only run for tests which produced a reliable acceleration-time history for making comparisons. The equation describing the conservation of energy for the simulator impact events is given as:

$$\frac{1}{2}m_p{v_i}^2 + \frac{1}{2}m_m{v_i}^2 = \frac{1}{2}m_m{v_{o,m}}^2 + \frac{1}{2}m_s{v_{o,s}}^2 + E_d \tag{4.1}$$

with the variables defined as follows:

m_p - mass of piston
m_m - mass of impactor assembly
m_s - mass of specimen
v_i - impact velocity of piston and impactor assembly
$v_{o,m}$ - outgoing velocity of impactor assembly
$v_{o,s}$ - outgoing velocity of specimen
E_d - energy dissipated during collision

When examining the specimen accelerations and shock response, a major point of interest is the effects of the maximum acceleration and pulse duration of each acceleration-time history on the corresponding shock response spectrum. The peak acceleration seen in each shock response is given to show the natural frequency at which the greatest threat to the system under examination will be present. Chapter 2 provides discussion on the concepts which relate to the approaches used for the subsequent shock data analysis.

4.3.1 Single Programmer

The simplest loading configuration in the test series involved the use of a single programmer bolted to a 3 in thick aluminum plate as seen in Figure 4.7. Tracking targets were secured to one side of the aluminum plate to capture the velocity of the impactor assembly.

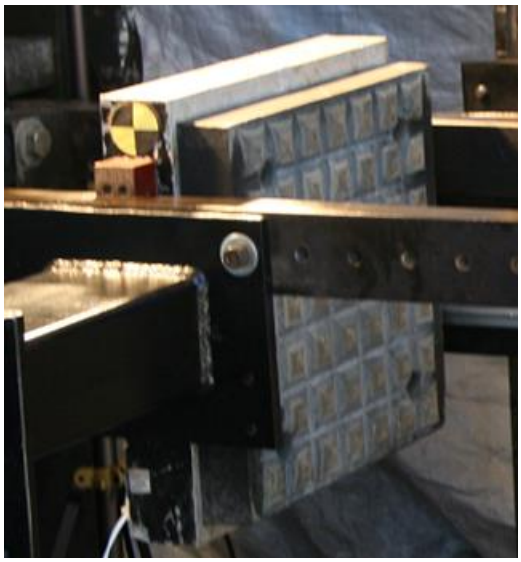

Figure 4.7: Single Programmer Impactor Configuration

Test 1

Test 1 was conducted with a target input velocity of 15 m/s (591 in/s) and a single programmer as the impacting medium (see Figure 4.7). The progression of loading is displayed in Figure 4.8. In frame (a), the impacting mass and specimen are shown before impact. The mass makes initial contact with the specimen in frame (b), and the programmer reaches maximum compression in frame (c). Rebounding of the specimen and the return of the programmer to its original state is shown in frame (d), and frame (e) shows the breaking away of the mass from the piston assembly. The free-flying states of the impacting mass and specimen are seen in frame (f).

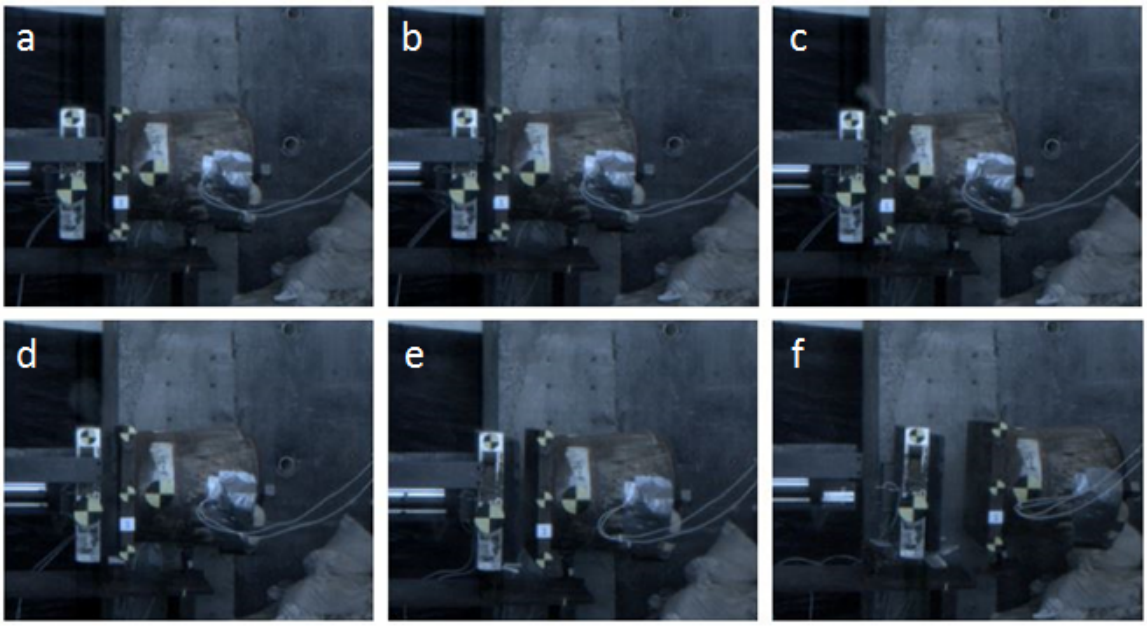

Figure 4.8: Test 1 - Progression of Shock Loading

The measured incoming mass velocity at impact was 16.9 m/s (665 in/s), and the outgoing specimen velocity was 9.9 m/s (390 in/s). The full velocity-time histories are shown in Figure 4.9. The energy dissipated during the collision was equal to 28.9% of the incoming kinetic energy.

The response seen in Figure 4.10 is characterized by the lowest peak acceleration (2,425 g) and largest pulse duration (1.03 ms) of the single programmer tests. Being the stiffest material applied to the specimen impact plate during the test series,

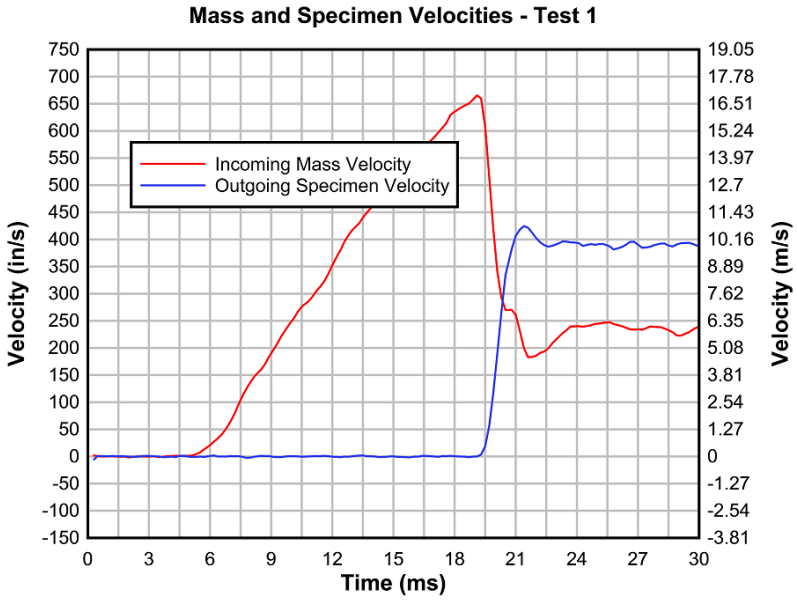

Figure 4.9: Test 1 - Impacting Mass and Specimen Velocities

the programmer produced the largest peak acceleration and shortest pulse duration of any 15 m/s test.

The resulting shock response spectrum is characterized by a peak acceleration of 3,500 g at 10 kHz. As expected, this is the largest response of any test conducted at 15 m/s.

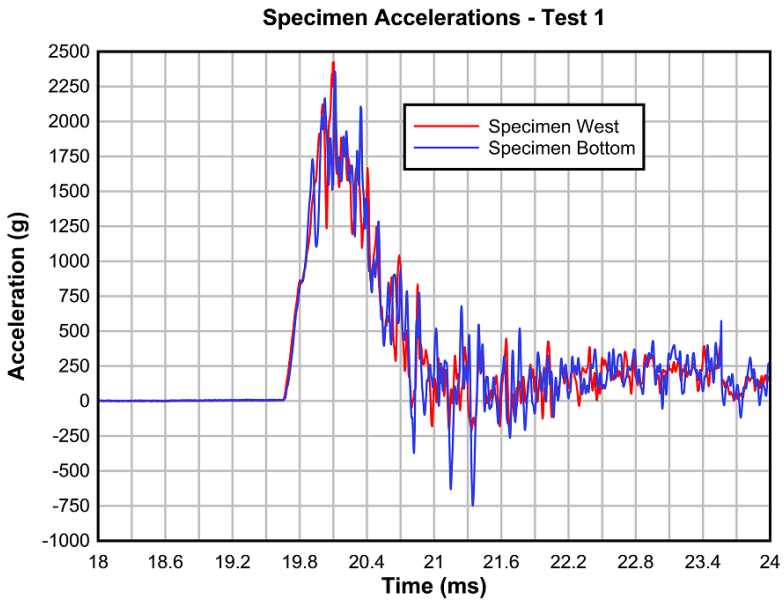

Figure 4.10: Test 1 - Specimen Accelerations

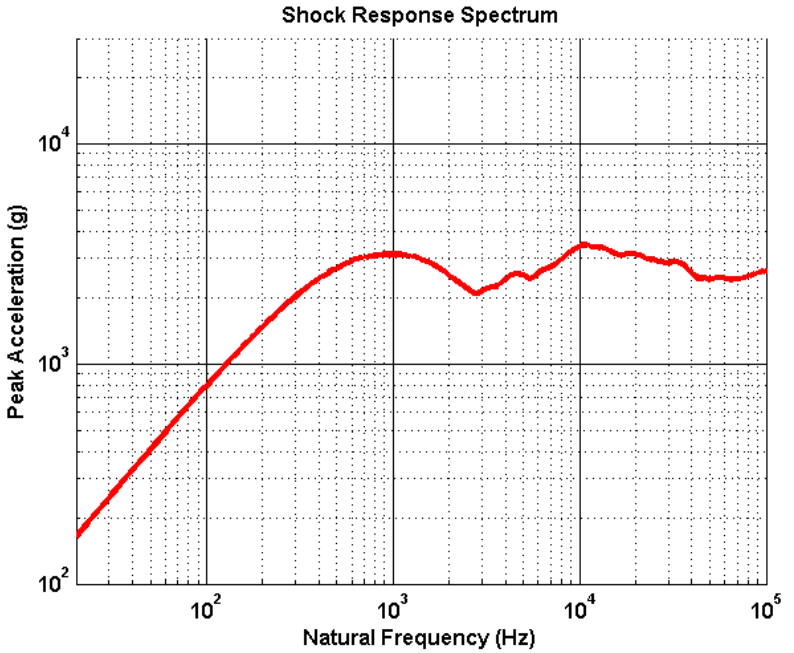

Figure 4.11: Test 1 - Shock Response Spectrum

Test 2

Test 2 was conducted with a target impact velocity of 30 m/s (1,181 in/s) and a single programmer as the impacting medium. The progression of loading is displayed in Figure 4.12. In frame (a), the impacting mass and specimen are shown before impact. The mass makes initial contact with the specimen in frame (b), and the programmer reaches maximum compression in frame (c). Rebounding of the specimen and the return of the programmer to its original state is shown in frame (d), and frame (e) shows the breaking away of the mass from the piston assembly. The free-flying states of the impacting mass and specimen are seen in frame (f).

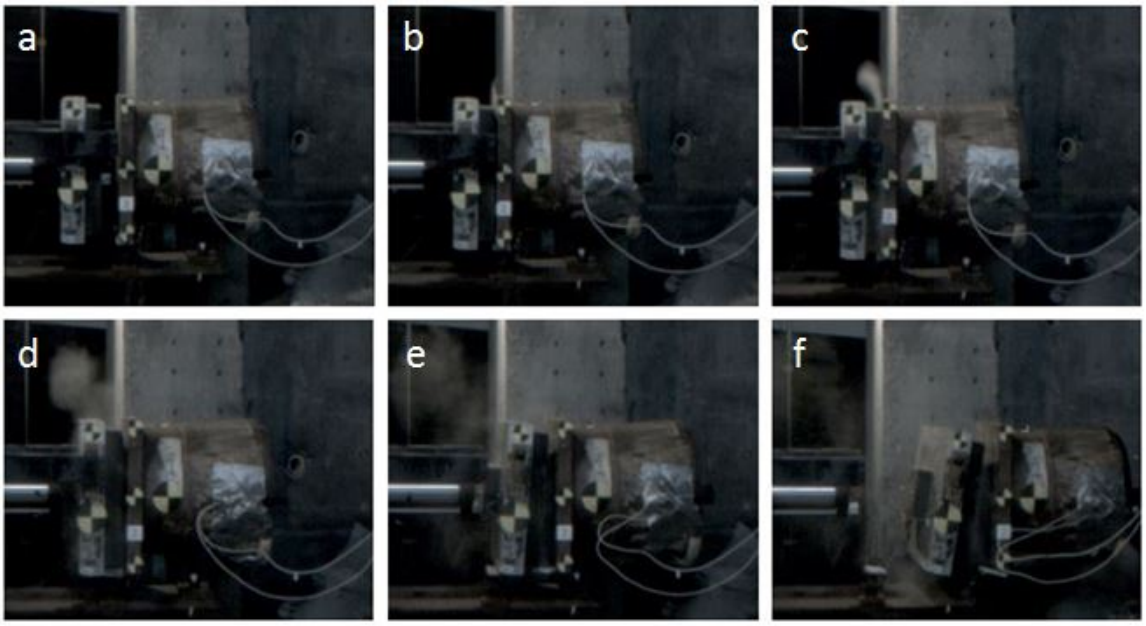

Figure 4.12: Test 2 - Progression of Shock Loading

The measured incoming mass velocity at impact was 30.2 m/s (1,189 in/s), and the outgoing specimen velocity was 17.1 m/s (673 in/s). The full velocity-time histories are shown in Figure 4.13. The energy dissipated during the collision was equal to 29.1% of the incoming kinetic energy.

The response seen in Figure 4.14 is characterized by a higher peak acceleration (4,865 g) and shorter pulse duration (0.62 ms) than Test 1. As with the test at 15 m/s, the programmer produced the largest peak acceleration and shortest pulse duration

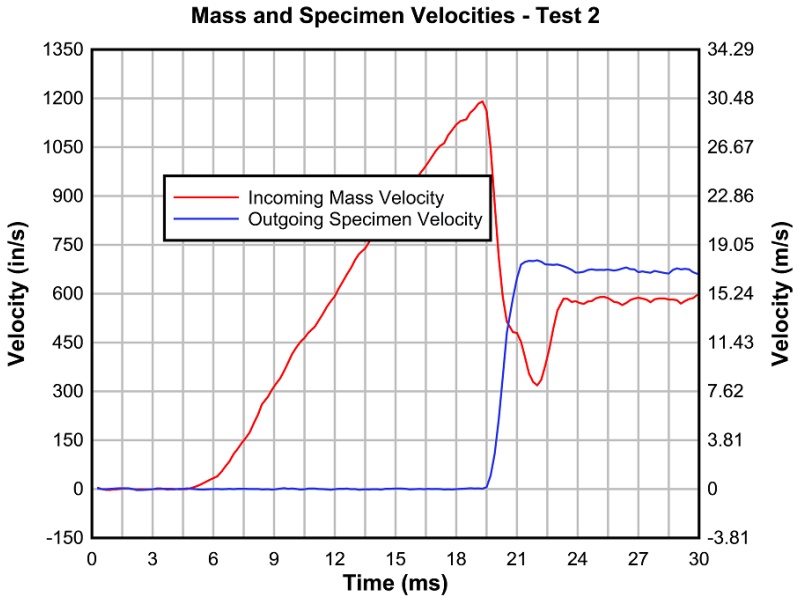

Figure 4.13: Test 2 - Impacting Mass and Specimen Velocities

of any 30 m/s test. While noticeable high-frequency content is present in the signal, the basic pulse shape and peak locations up to 20.6 ms are distinguishable.

The resulting shock response spectrum is characterized by a peak acceleration of approximately 17,000 g at 30 kHz, which was the largest response of any test conducted at 30 m/s.

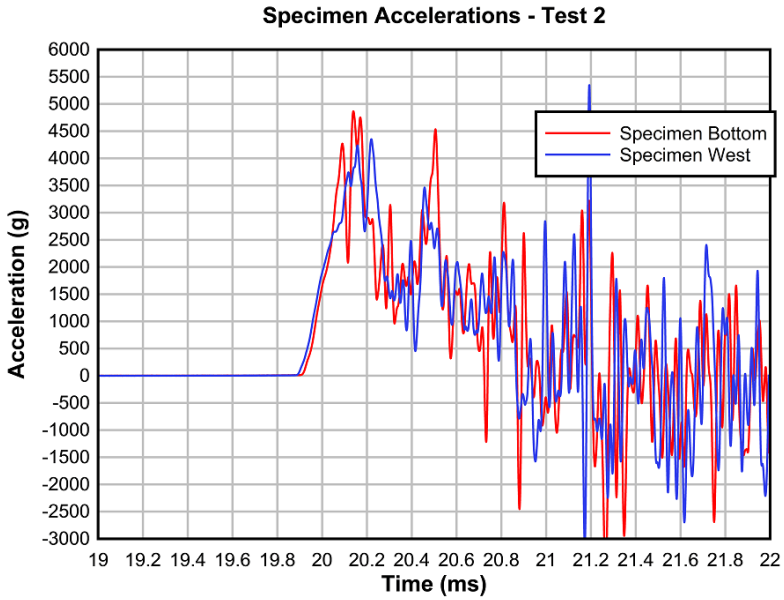

Figure 4.14: Test 2 - Specimen Accelerations

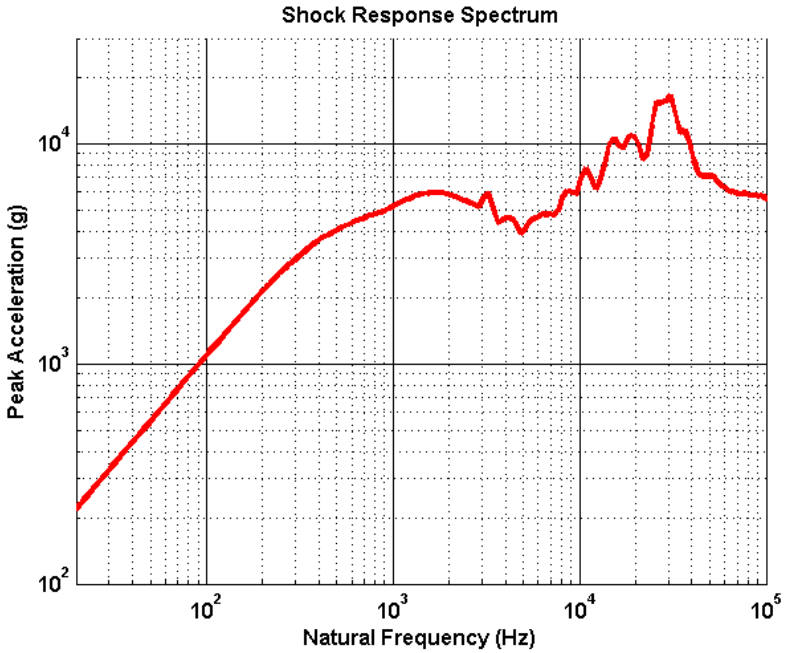

Figure 4.15: Test 2 - Shock Response Spectrum

Test 3

Test 3 was conducted with a target impact velocity of 40 m/s (1,575 in/s) and a single programmer as the impacting medium. The progression of loading is displayed in Figure 4.16. In frame (a), the impacting mass and specimen are shown before impact. The mass makes initial contact with the specimen in frame (b), and the programmer reaches maximum compression in frame (c). Rebounding of the specimen and the return of the programmer to its original state is shown in frame (d), and frame (e) shows the breaking away of the mass from the piston assembly. The free-flying states of the impacting mass and specimen are seen in frame (f).

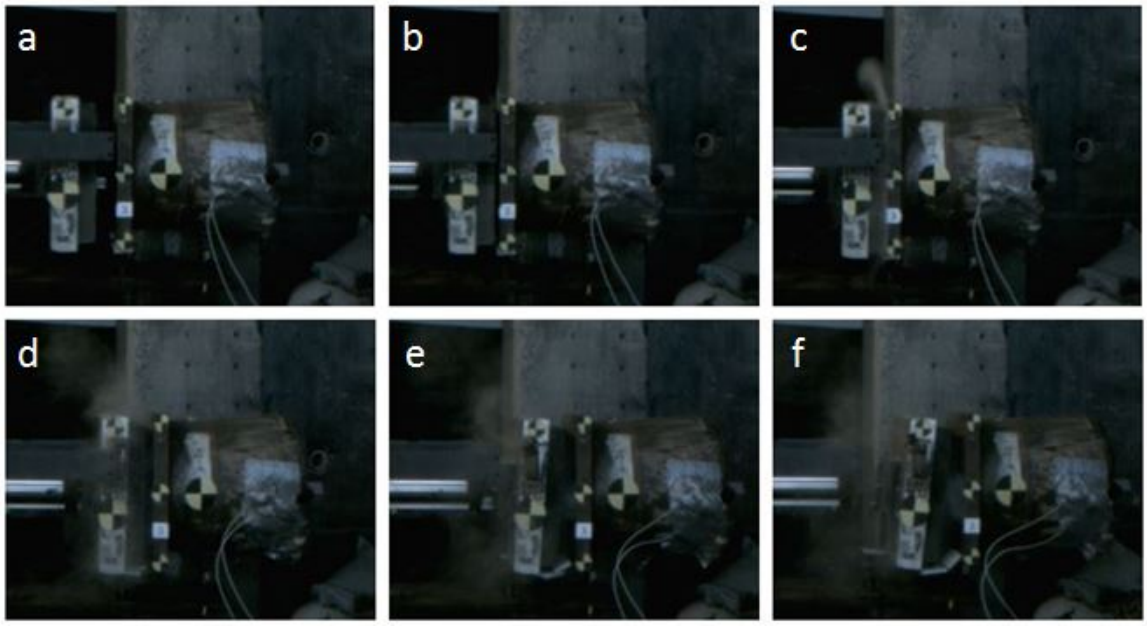

Figure 4.16: Test 3 - Progression of Shock Loading

The measured incoming mass velocity at impact was 41.5 m/s (1,634 in/s), and the outgoing specimen velocity was 22.1 m/s (870 in/s). The full velocity-time histories are shown in Figure 4.17. The energy dissipated during the collision was equal to 38.2% of the incoming kinetic energy.

The response seen in Figure 4.18 is characterized by both the highest peak acceleration (7,443 g) and shortest pulse duration (0.40 ms) of the entire test series. While noticeable high-frequency content is present in the signal, the basic pulse shape

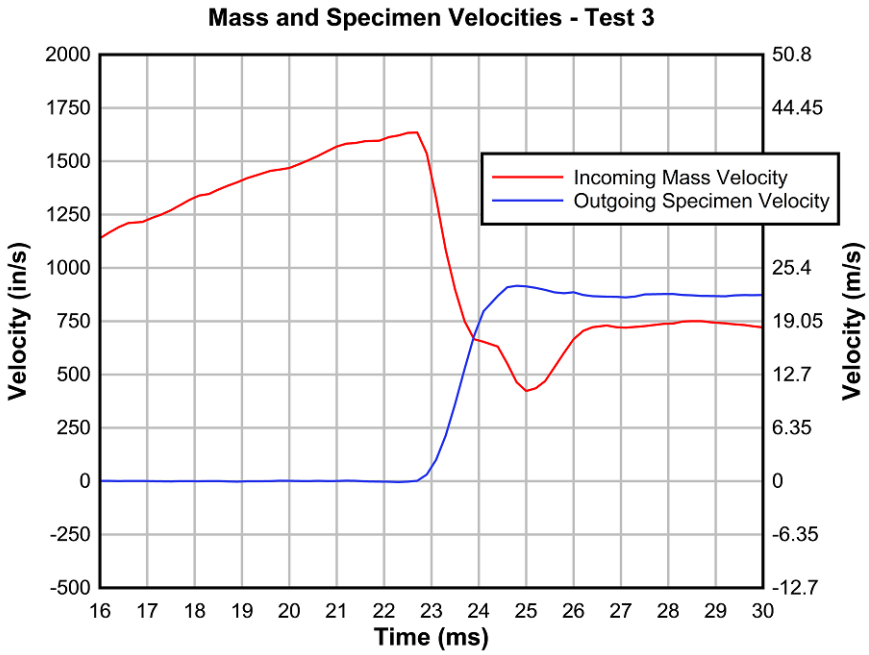

Figure 4.17: Test 3 - Impacting Mass and Specimen Velocities

and peak locations up to 23.6 ms are distinguishable.

The resulting shock response spectrum is characterized by a peak acceleration of approximately 16,000 g at 20 kHz, which was the largest response of any test conducted at 40 m/s.

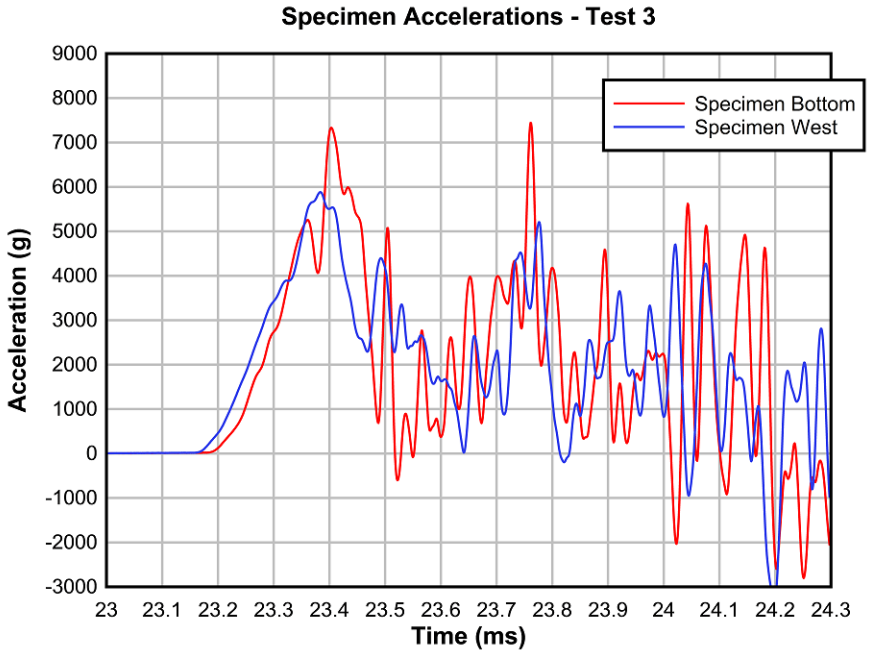

Figure 4.18: Test 3 - Specimen Accelerations

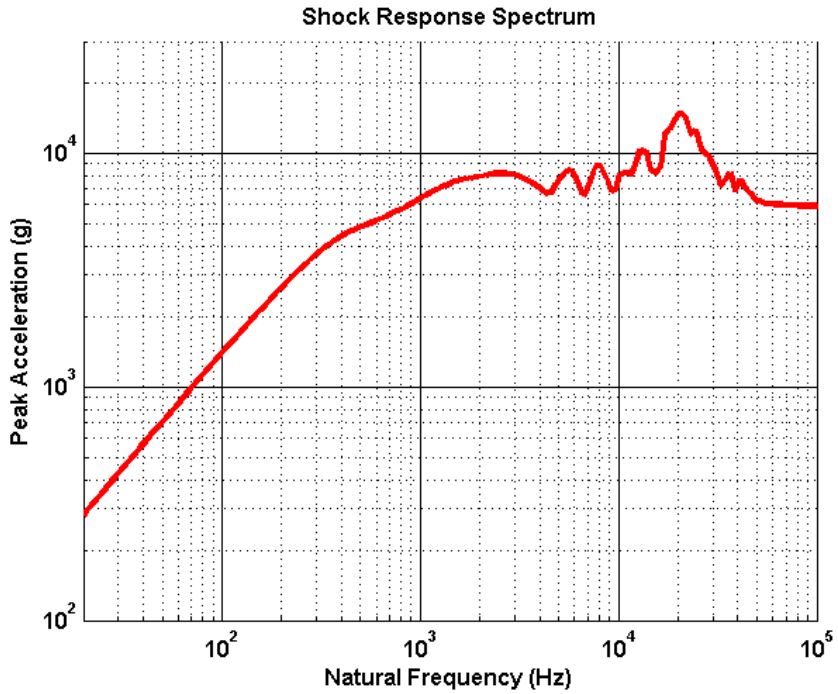

Figure 4.19: Test 3 - Shock Response Spectrum

Single Programmer Testing Summary

A summary of the single programmer testing is provided in Table 4.1 (P: Programmer).

Table 4.1: Single Programmer Testing Summary

Test	Loading Medium	Target Impact Velocity (m/s)(in/s)	Energy Dissipation (%)	Peak Acceleration (g)	Duration (ms)
1	P	15 (591)	28.9	2,425	1.03
2	P	30 (1,191)	29.1	4,865	0.62
3	P	40 (1,575)	38.2	7,443	0.40

4.3.2 Double Programmer

For the double programmer configuration, the programmer on the non-impact side was bolted to the aluminum plate, and the impact programmer was taped to the entire assembly as seen in Figure 4.20. Because of the threat of inducing high-frequency content in the data with metal-to-metal contact, duct tape was used to secure the programmers together rather than bolts or clamps.

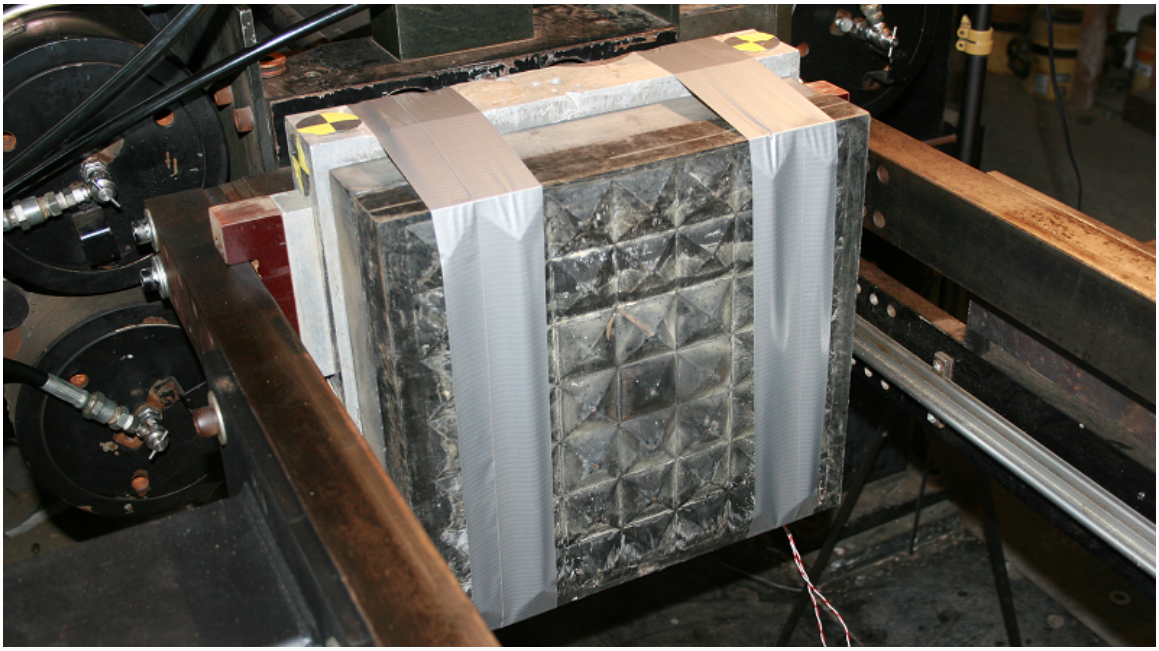

Figure 4.20: Double Programmer Impactor Configuration

Test 7

Test 7 was conducted with a target impact velocity of 30 m/s (1,181 m/s) and a double programmer as the impacting medium. The progression of loading is displayed in Figure 4.21. In frame (a), the impacting mass and specimen are shown before impact. The mass makes initial contact with the specimen in frame (b), and the double programmer assembly reaches maximum compression in frame (c). Rebounding of the specimen and the return of the programmer stack to its original state is shown in frame (d), and frame (e) shows the separation of programmer pads and breaking away of the mass from the piston assembly. The free-flying states of the impacting mass and specimen are seen in frame (f).

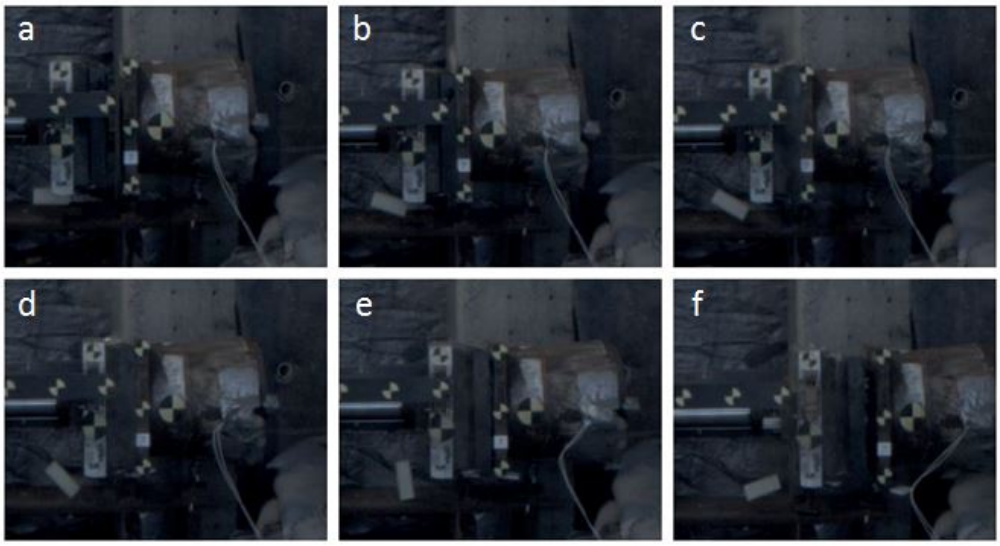

Figure 4.21: Test 7 - Progression of Shock Loading

The measured incoming mass velocity at impact was 31.1 m/s (1,224 in/s), and the outgoing specimen velocity was 17.0 m/s (669 in/s). The full velocity-time histories are shown in Figure 4.22.

The response seen in Figure 4.23 is characterized by significant high-frequency content. While a basic trend is observed in the acceleration-time history, the excessive ringing leads to a data set which is unreliable for comparison purposes with other loading configurations or shock response computation.

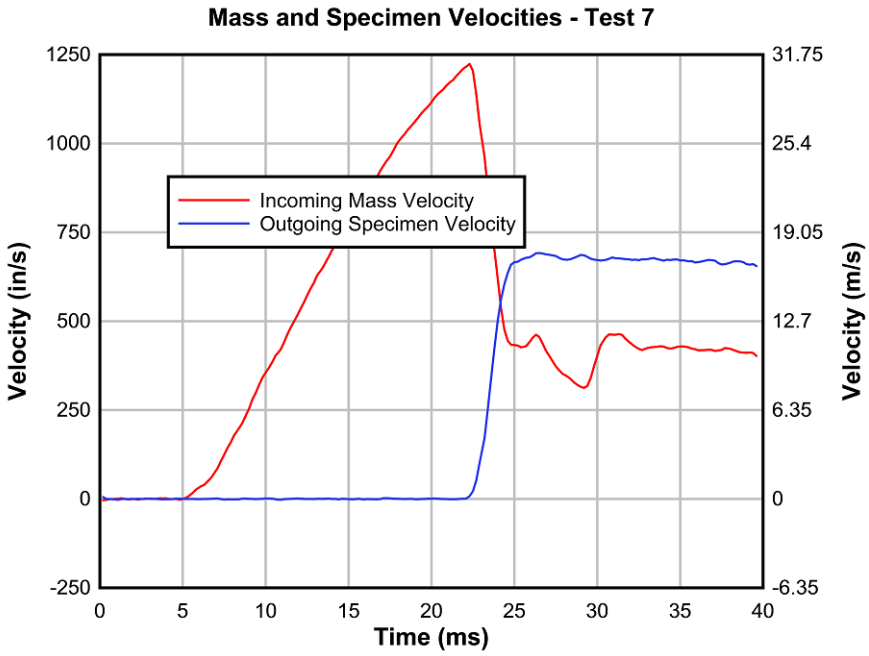

Figure 4.22: Test 7 - Impacting Mass and Specimen Velocities

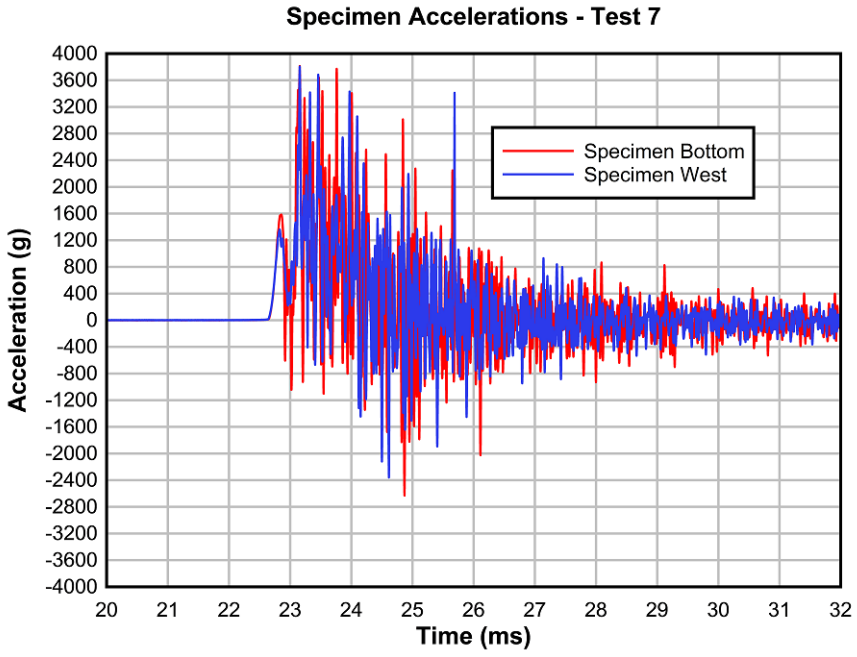

Figure 4.23: Test 7 - Specimen Accelerations

Test 8

Test 8 was conducted with a target impact velocity of 30 m/s (1,181 in/s) and a double programmer as the impacting medium. Because of the noisy data observed in Test 7, it was determined that a repeat test would be beneficial to determine if the problematic ringing could be eliminated. The results of this test are very similar to those of Test 7 and, thus, are not discussed in this section. The test images and data are provided in the appendices, but a shock response is not calculated because of the unreliable accelerometer results.

Test 11

Test 11 was conducted with a target impact velocity of 15 m/s (591 in/s) and a double programmer as the impacting medium. The progression of loading is displayed in Figure 4.24. In frame (a), the impacting mass and specimen are shown before impact. The mass makes initial contact with the specimen in frame (b), and the double programmer assembly reaches maximum compression in frame (c). Rebounding of the specimen and the return of the programmer stack to its original state is shown in frame (d), and frame (e) shows the separation of programmer pads and breaking away of the mass from the piston assembly. The free-flying states of the impacting mass and specimen are seen in frame (f).

The measured incoming mass velocity at impact was 16.8 m/s (663 in/s), and the outgoing specimen velocity was 9.9 m/s (389 in/s). The full velocity-time histories are shown in Figure 4.25.

Similar to the double programmer tests at 30 m/s, the response seen in Figure 4.26 is characterized by significant high frequency content. While a basic trend is observed in the acceleration-time history, the excessive ringing leads to a data set which is unreliable for comparison purposes with other loading configurations or shock response computation.

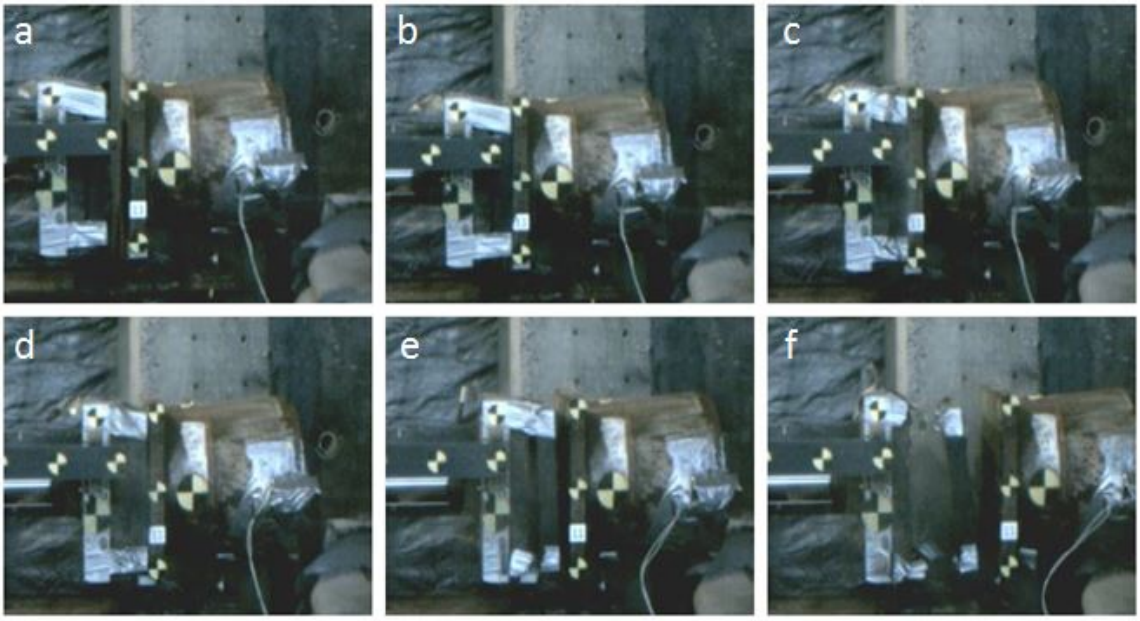

Figure 4.24: Test 11 - Progression of Shock Loading

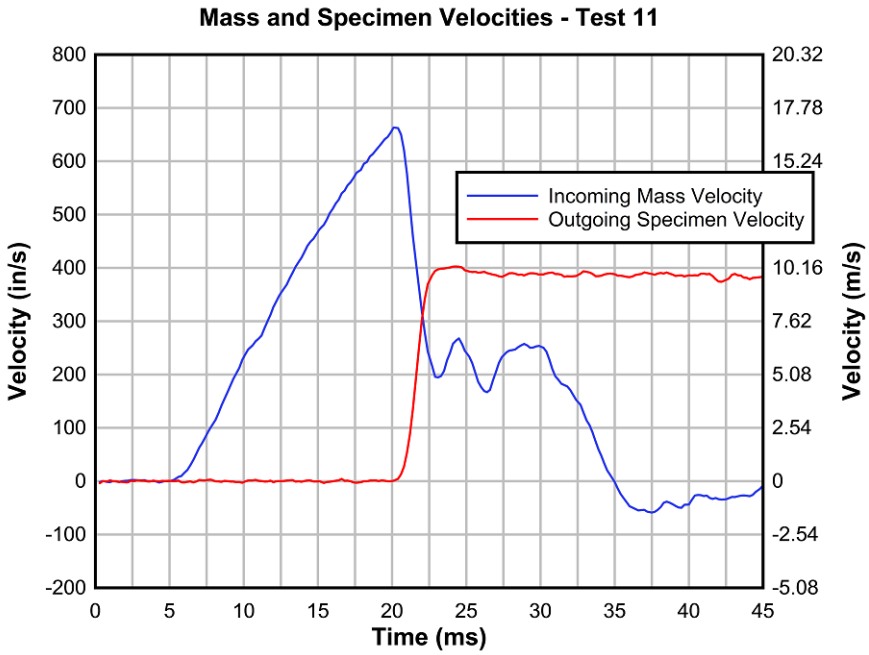

Figure 4.25: Test 11 - Impacting Mass and Specimen Velocities

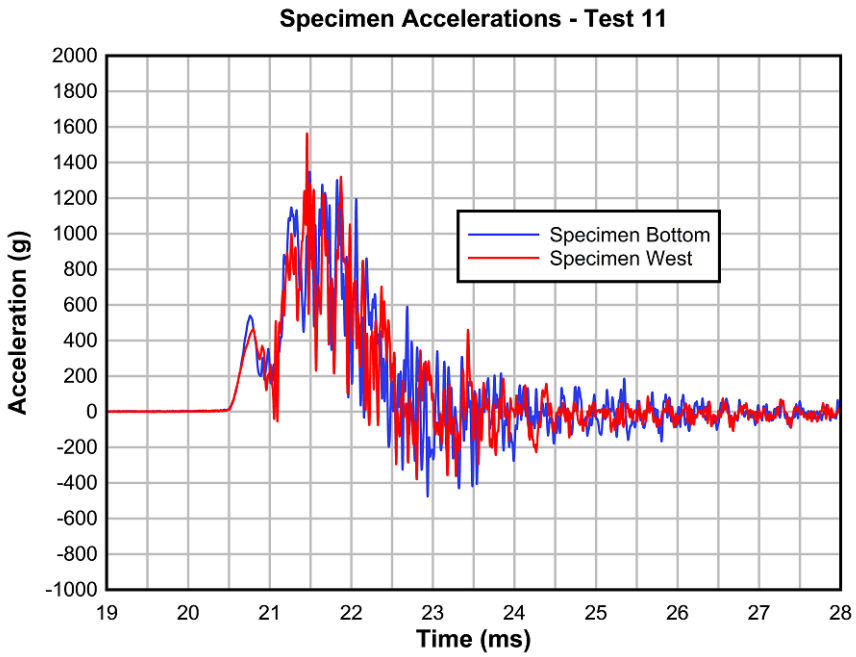

Figure 4.26: Test 11 - Specimen Accelerations

4.3.3 Polyurethane Foam

Tests involving the use of foam as an impact medium were characterized by one of two configurations. For Tests 4-6, a 3 in thick closed-cell polyurethane foam sheet was secured to the programmer on the loading face. The foam was characterized by the material properties obtained from the manufacturer shown in Table 4.2.

Table 4.2: Foam Material Properties

Material Property	Value
Density	15 pcf
Poisson's Ratio	0.3
Compressive Strength	728 psi
Compressive Modulus	20,371 psi
Shear Strength	490 psi
Shear Modulus	5,141 psi
Flexural Strength	851 psi
Flexural Modulus	25,991 psi

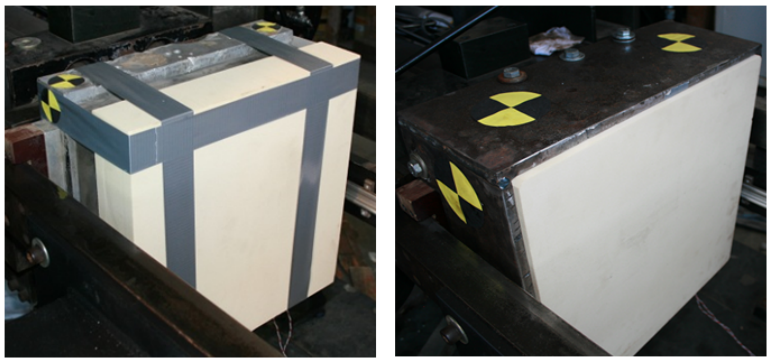

Figure 4.27: Unconfined Foam (Left) and Confined Foam (Right) as Impactor Materials

Test 4

Test 4 was conducted with a target impact velocity of 15 m/s (591 in/s) and a 3 in layer of polyurethane foam as the impacting medium. The progression of loading is displayed in Figure 4.28. In frame (a), the impacting mass and specimen are shown before impact. The mass makes initial contact with the specimen in frame (b), and the foam reaches maximum compression in frame (c). Rebounding of the specimen is shown in frame (d), and frame (e) shows the separation of foam from the programmer and breaking away of the mass from the piston assembly. The free-flying states of the impacting mass and specimen are seen in frame (f).

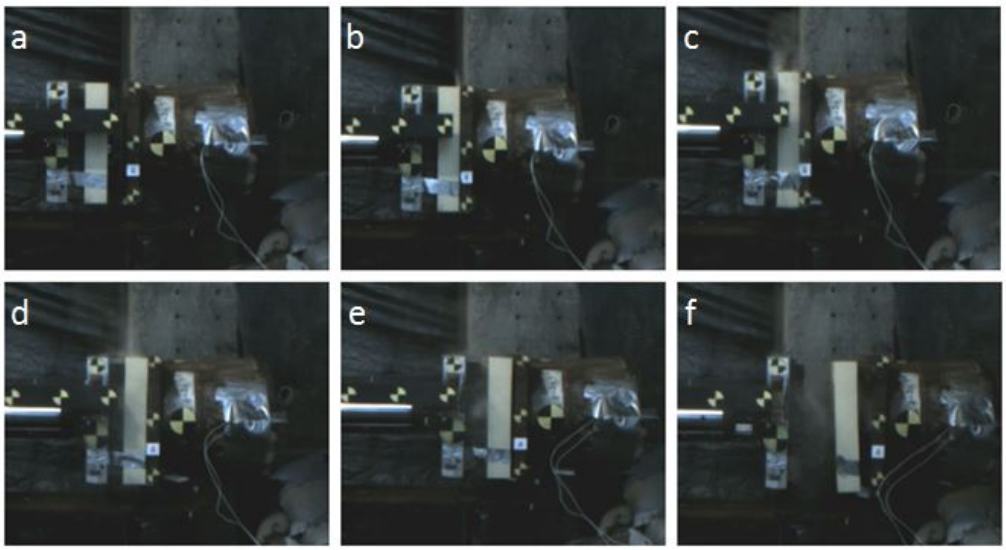

Figure 4.28: Test 4 - Progression of Shock Loading

The measured incoming mass velocity at impact was 14.2 m/s (559 in/s), and the outgoing specimen velocity was 8.9 m/s (350 in/s). The full velocity-time histories are shown in Figure 4.29.

As with the other unconfined foam tests, the response seen in Figure 4.30 is characterized by significant high frequency content. While a basic trend is observed in the acceleration-time history, the excessive ringing leads to a data set which is unreliable for comparison purposes with other loading configurations or shock response computation.

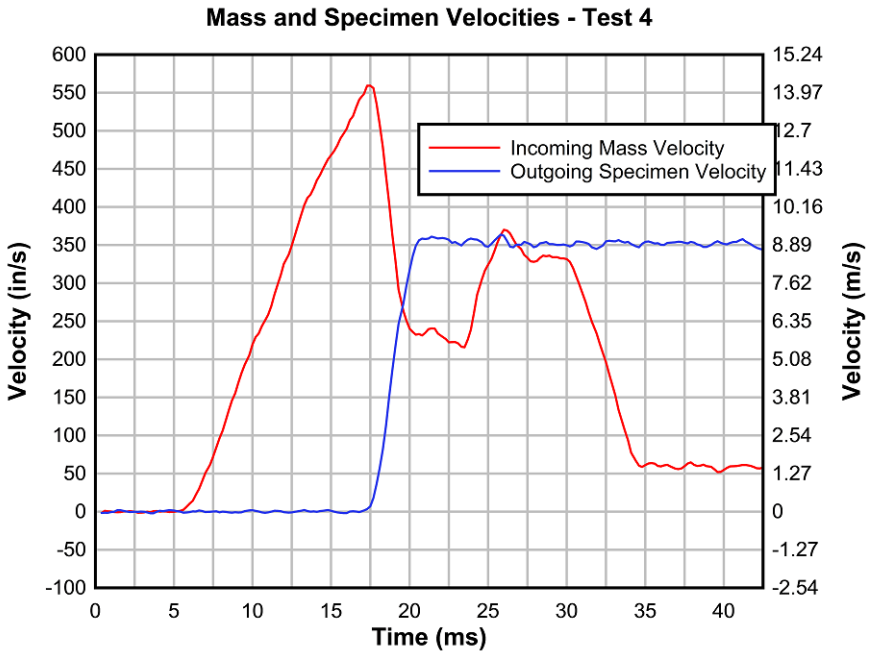

Figure 4.29: Test 4 - Impacting Mass and Specimen Velocities

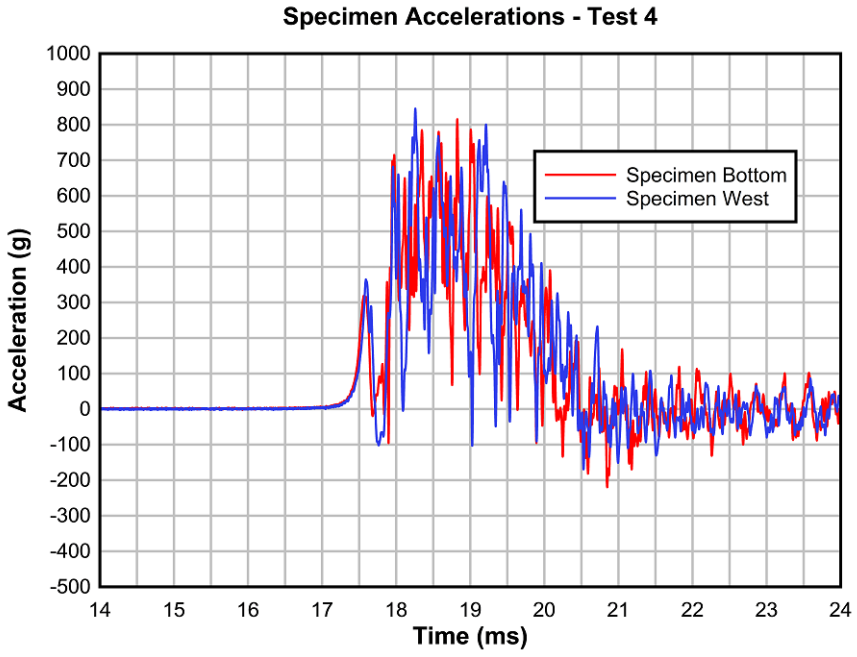

Figure 4.30: Test 4 - Specimen Accelerations

Tests 5-6

Tests 5-6 were conducted with target impact velocities of 30 m/s (1,181 in/s) and 40 m/s (1,575 in/s) respectively and a 3 in layer of foam as impact medium. As in Test 4, the accelerometer data was unreliable and deemed unsuitable for shock response calculation. A summary of the data is provided in Appendix B.

Test 12

Test 12 was conducted with a target impact velocity of 15 m/s (591 in/s) and a 3 in layer of confined foam as the impacting medium. The edges of the material were flush against the internal walls of the confining box as seen in frame (d) of Figure 4.3. The progression of loading is displayed in Figure 4.31. In frame (a), the impacting mass and specimen are shown before impact. The mass makes initial contact with the specimen in frame (b), and the foam reaches maximum compression in frame (c). Rebounding of the specimen and a cloud of foam particulates is shown in frame (d), and frame (e) shows the breaking away of the mass from the piston assembly. The free-flying states of the impacting mass and specimen are seen in frame (f).

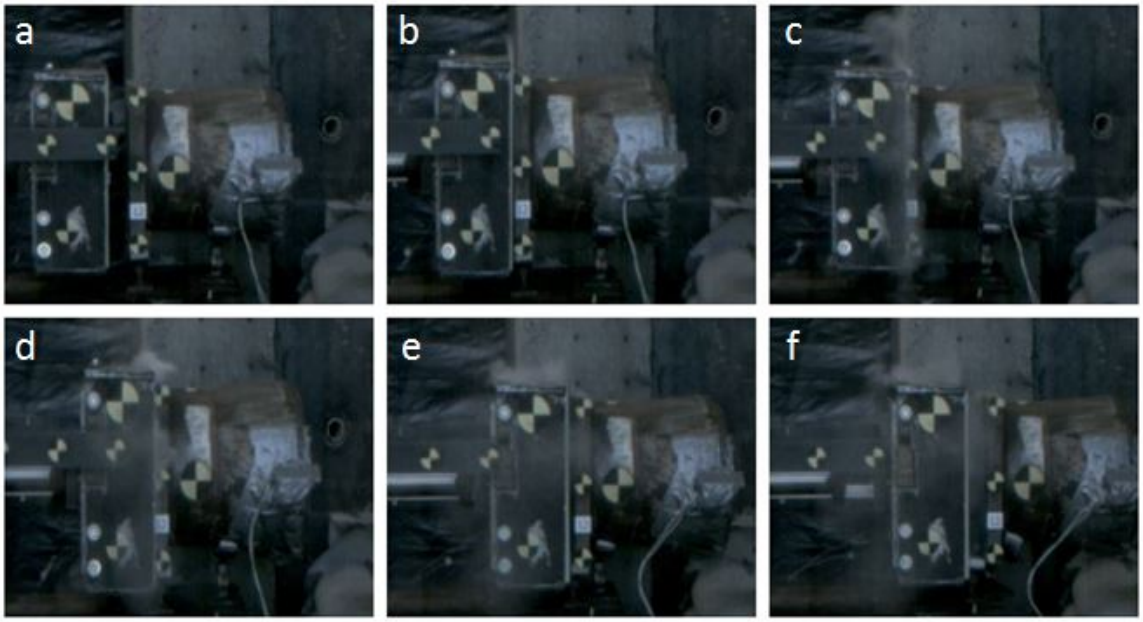

Figure 4.31: Test 12 - Progression of Shock Loading

The measured incoming mass velocity at impact was 15.0 m/s (591 in/s), and the outgoing specimen velocity was 9.5 m/s (374 in/s). The full velocity-time histories are shown in Figure 4.32.

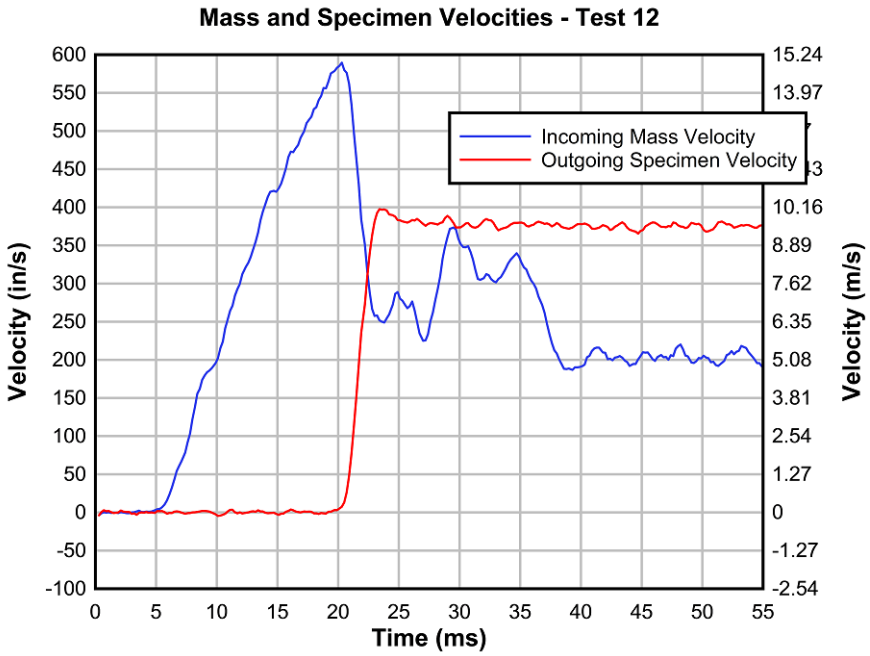

Figure 4.32: Test 12 - Impacting Mass and Specimen Velocities

The response seen in Figure 4.33 was the cleanest acceleration-time history obtained for both the confined and unconfined foam testing.

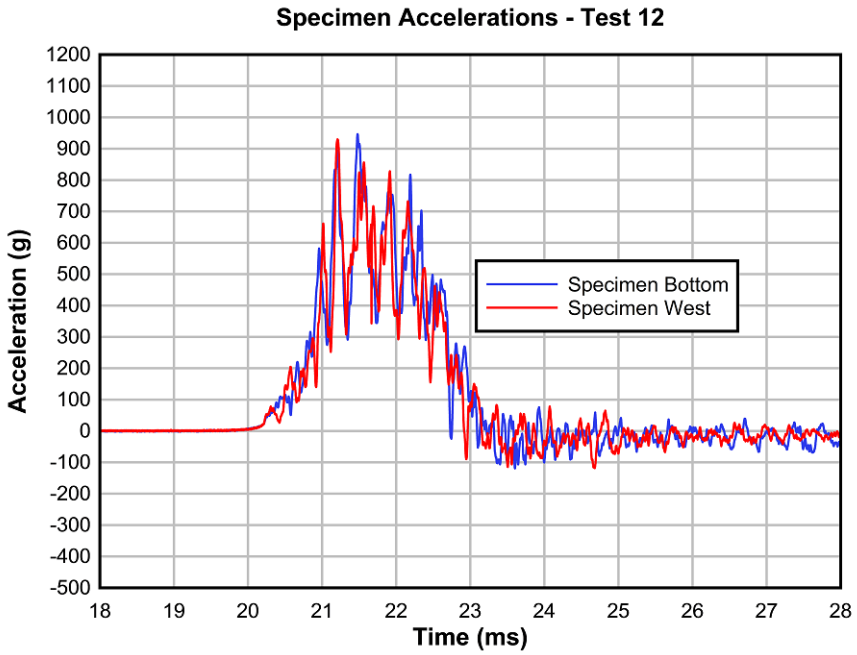

Figure 4.33: Test 12 - Specimen Accelerations

Tests 13-15

Test 13 was a repeat of Test 12 but produced a noisy and undesirable specimen acceleration response. Tests 14-15 were characterized by the same inputs as Tests 12-13 but an impact velocity of 30 m/s (1,181 in/s). These tests also produced noisy acceleration-time histories. The data for these three tests is summarized in Appendix B. As a result of the consistently poor data obtained using polyurethane foam, the material was discontinued as an impacting medium in the test series.

4.3.4 Leather

For Tests 9, 10, and 19, layered leather was placed on top of a programmer and secured to the impacting mass with tape as shown in Figure 4.34. The material was obtained from a bulk manufacturer and cut into approximately 16x16x1/8 in sections to match the impact surface of the specimen plate.

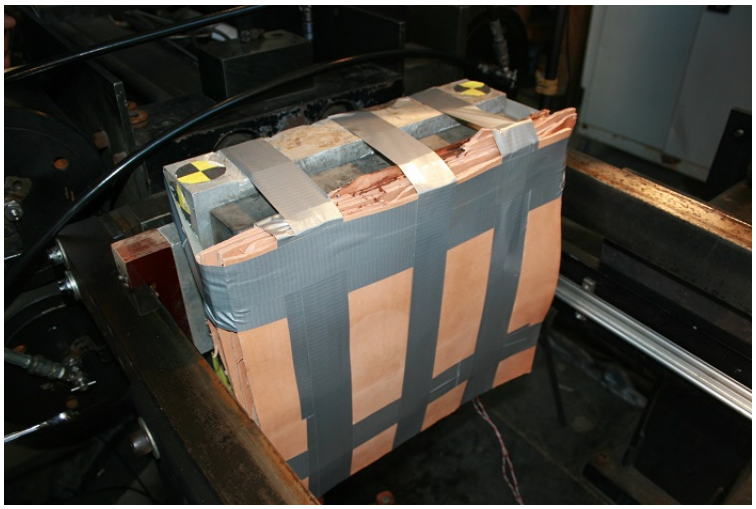

Figure 4.34: Impacting Mass Assembly with Layered Leather

Test 9

Test 9 was conducted with a target velocity of 15 m/s (591 in/s) and a 1.25 in stack of layered leather sections. The progression of loading is displayed in Figure 4.35. In frame (a), the impacting mass and specimen are shown before impact. The mass makes initial contact with the specimen in frame (b), and the leather reaches maximum compression in frame (c). Rebounding of the specimen and expansion of the leather stack is shown in frame (d), and frame (e) shows the initial separation of leather from the programmer and breaking away of the mass from the piston assembly. The free-flying states of the impacting mass and specimen are seen in frame (f).

The measured incoming mass velocity at impact was 17.2 m/s (677 in/s), and the outgoing specimen velocity was 9.4 m/s (371 in/s). The full velocity-time

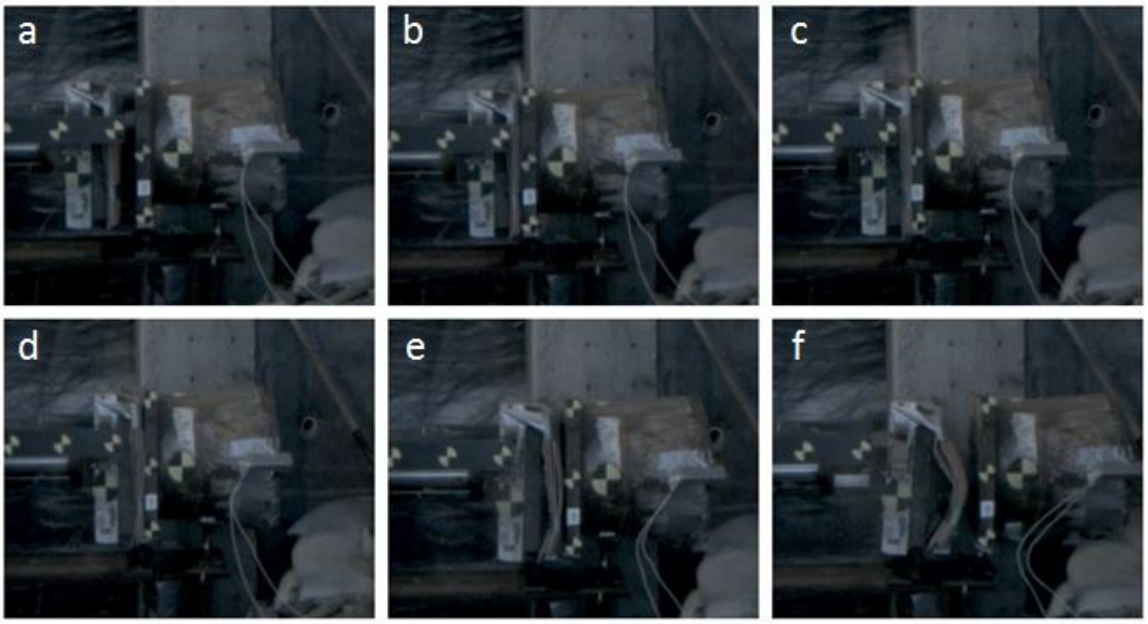

Figure 4.35: Test 9 - Progression of Shock Loading

histories are shown in Figure 4.36. The energy dissipated during the collision was equal to 40.6% of the incoming kinetic energy.

The first test using layered leather produced an excellent pulse shape (Figure 4.37) and a duration (1.25 ms) which was noticeably longer than that of Test 1, which used the same input velocity but only a programmer. However, the recorded peak acceleration (1,644 g) was also significantly lower.

The resulting shock response spectrum is characterized by a peak acceleration of 2,100 g at 600 Hz. The response is noticeably level throughout the high frequency range when compared to the responses seen in the programmer tests.

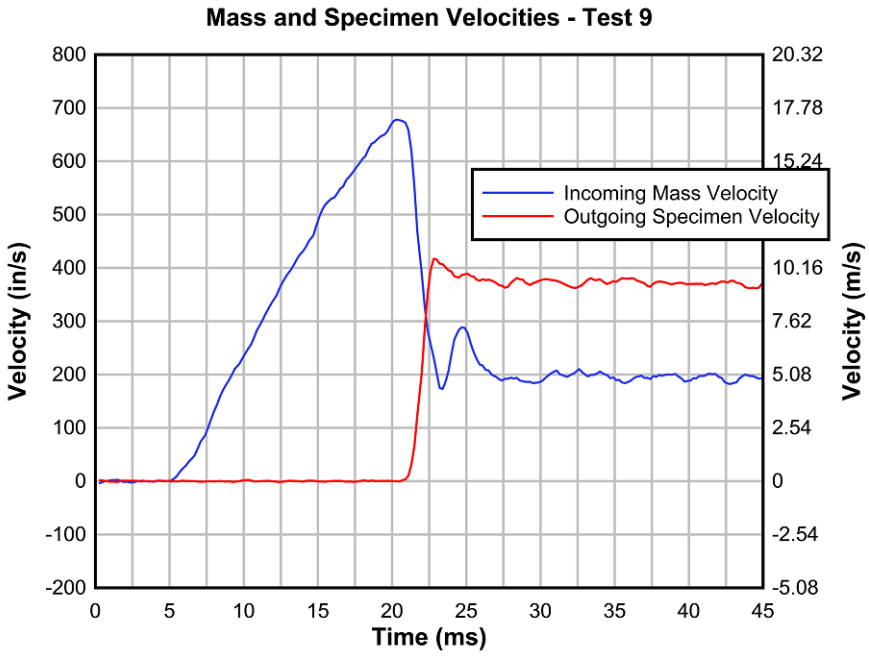

Figure 4.36: Test 9 - Impacting Mass and Specimen Velocities

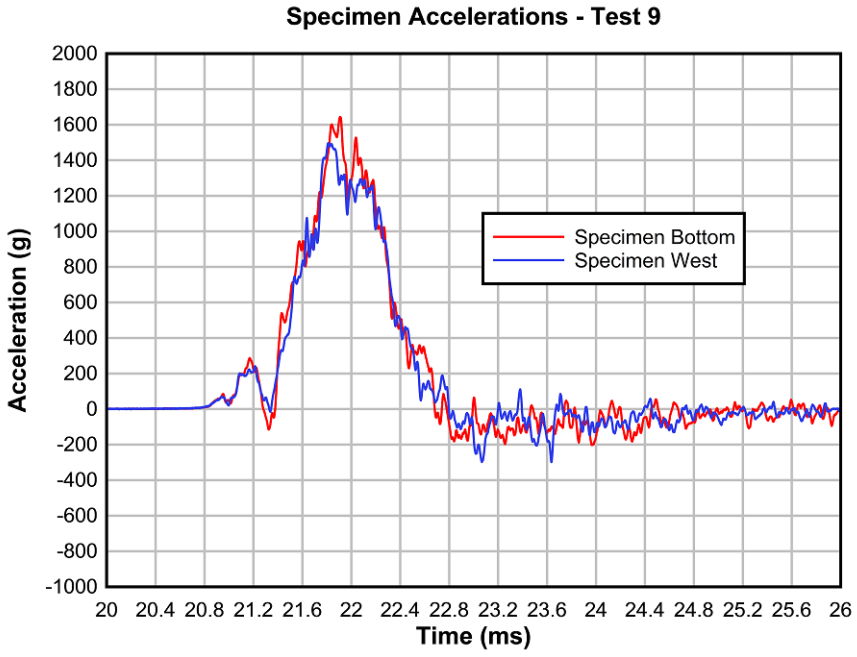

Figure 4.37: Test 9 - Specimen Accelerations

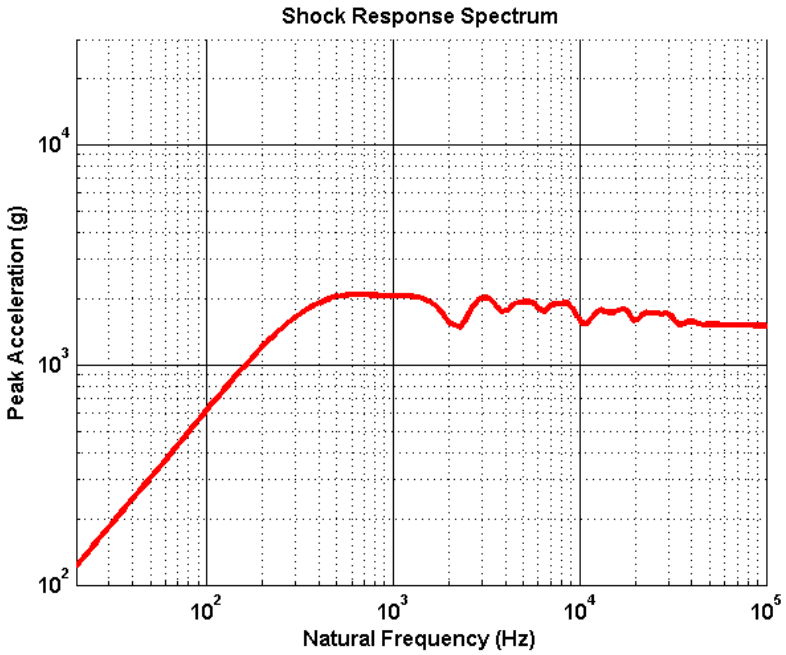

Figure 4.38: Test 9 - Shock Response Spectrum

Test 10

Test 10 was conducted with a target impact velocity of 30 m/s (591 in/s) and a 2.5 in stack of layered leather sections. The progression of loading is displayed in Figure 4.39. In frame (a), the impacting mass and specimen are shown before impact. The mass makes initial contact with the specimen in frame (b), and the leather reaches maximum compression in frame (c). Rebounding of the specimen and expansion of the leather stack is shown in frame (d), and frame (e) shows the initial separation of leather from the programmer and breaking away of the mass from the piston assembly. The free-flying states of the impacting mass and specimen are seen in frame (f).

The measured incoming mass velocity at impact was 30.4 m/s (1,197 in/s), and the outgoing specimen velocity was 16.9 m/s (665 in/s). The full velocity-time histories are shown in Figure 4.40. The energy dissipated during the collision was equal to 39.4% of the incoming kinetic energy.

The second test using layered leather produced a reasonably good pulse shape (Figure 4.41) and a duration (1.03 ms) which was noticeably longer than that of

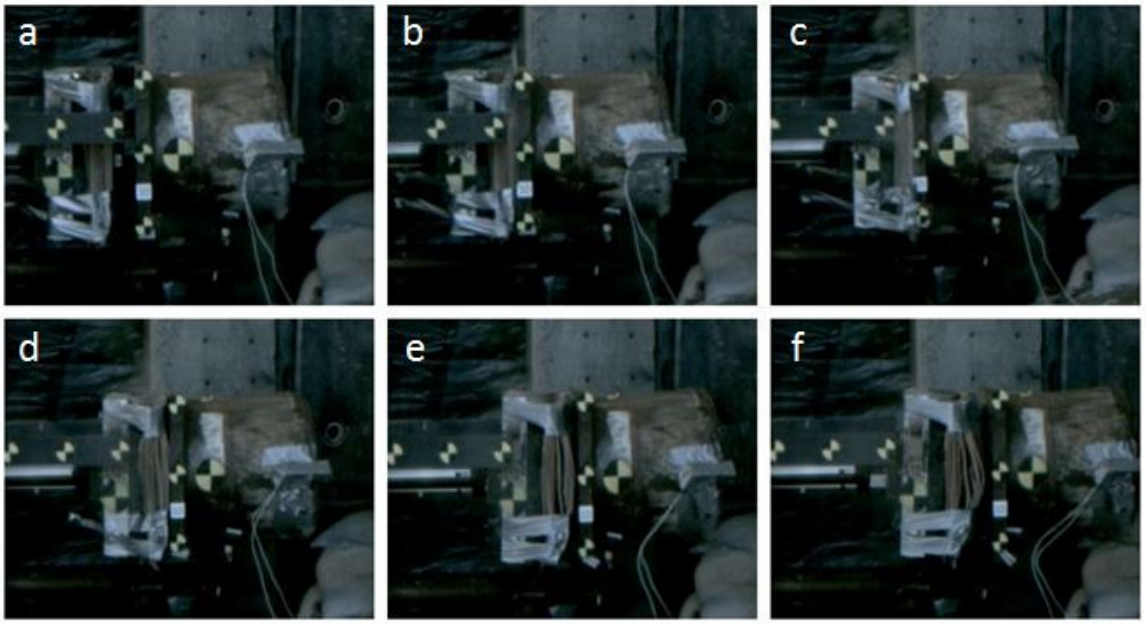

Figure 4.39: Test 10 - Progression of Shock Loading

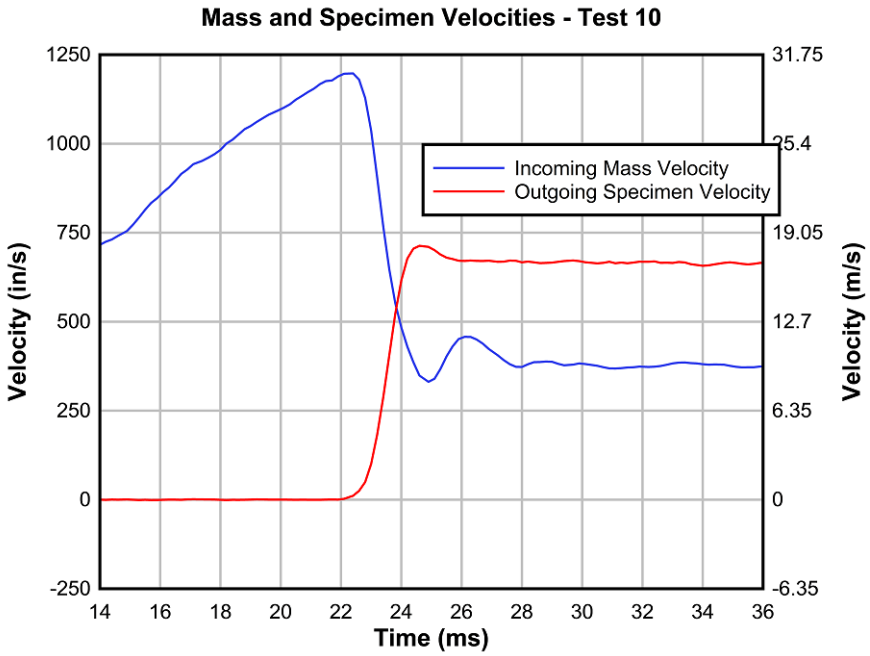

Figure 4.40: Test 10 - Impacting Mass and Specimen Velocities

Test 2, which used the same input velocity but only a programmer. However, the recorded peak acceleration (3,068 g) was also significantly lower. Compared to the acceleration-time history from Test 9 (15 m/s impact velocity), the response had a much larger peak acceleration but shorter loading duration.

The initial response seen up to 23 ms is most likely a result of the leather making initial impact with the specimen but carrying minimal stress as the layers (which were not all perfectly flat) were forced into a more compact stack before being truly compressed. The impacting mass begins to more fully load the specimen after 23 ms.

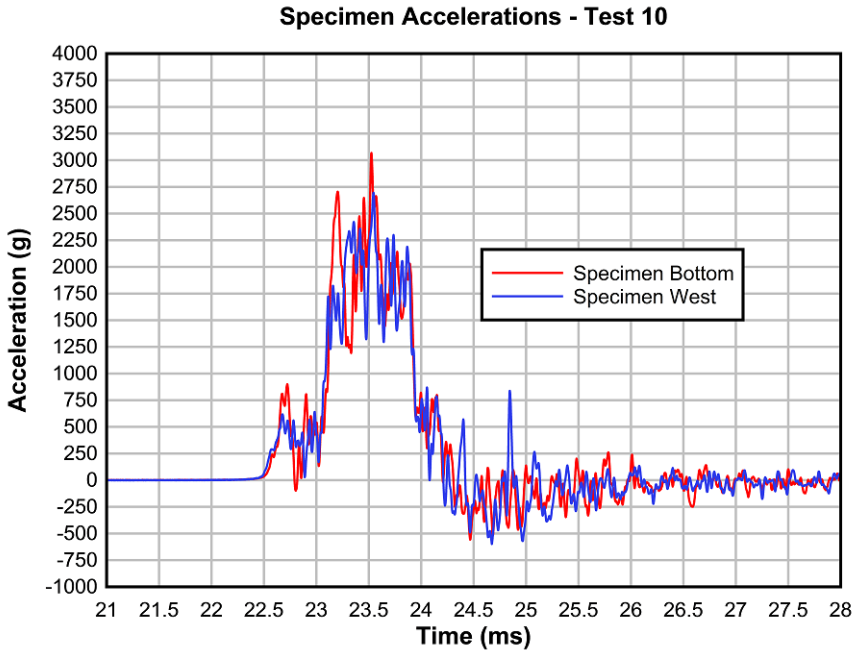

Figure 4.41: Test 10 - Specimen Accelerations

The resulting shock response spectrum is characterized by a peak acceleration of 4,200 g at 9 kHz. An average response of 3,000 g is observed across the high-frequency range.

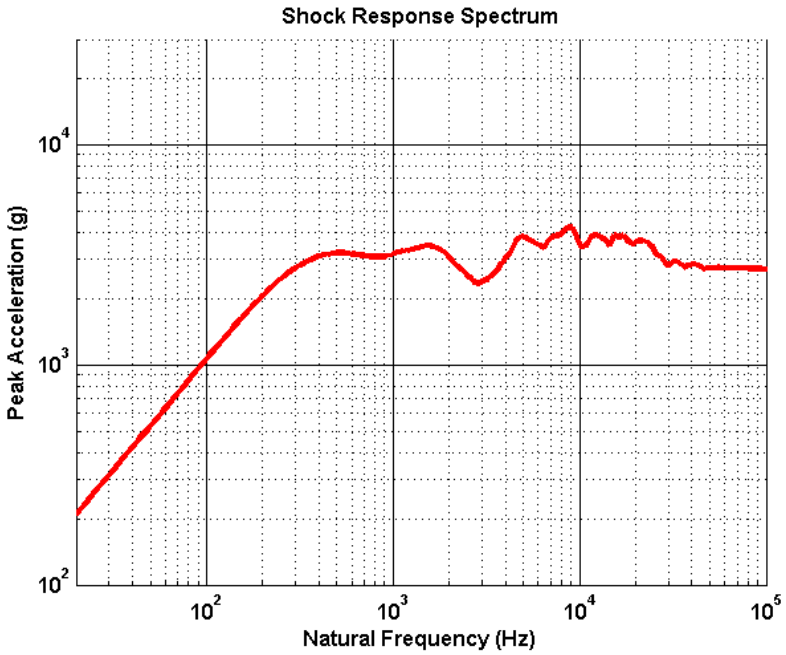

Figure 4.42: Test 10 - Shock Response Spectrum

Test 19

Test 19 was conducted with a target impact velocity of 40 m/s (1,575 in/s) and a 5 in stack of layered leather sections. Because of the thickness of the stack, the confining box was implemented as part of assembly to simply hold the leather in place (no confining effects). The progression of loading is displayed in Figure 4.43. In frame (a), the impacting mass and specimen are shown before impact. The mass makes initial contact with the specimen in frame (b), and the leather reaches maximum compression in frame (c). Rebounding of the specimen and expansion of the leather stack is shown in frame (d), and frame (e) shows the initial separation of leather from the programmer and breaking away of the mass from the piston assembly. The free-flying states of the impacting mass and specimen are seen in frame (f).

The measured incoming mass velocity at impact was 39.2 m/s (1,543 in/s), and the outgoing specimen velocity was 21.1 m/s (831 in/s). The full velocity-time histories are shown in Figure 4.44. The energy dissipated during the collision was equal to 58.4% of the incoming kinetic energy.

The response in Figure 4.45 shows both the highest peak acceleration and

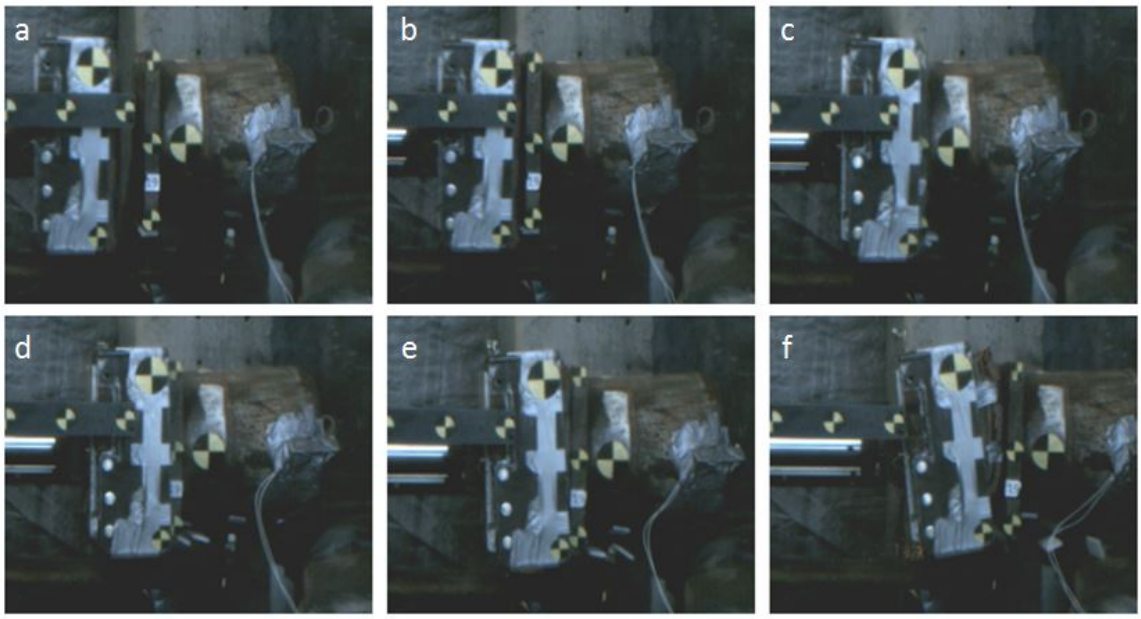

Figure 4.43: Test 19 - Progression of Shock Loading

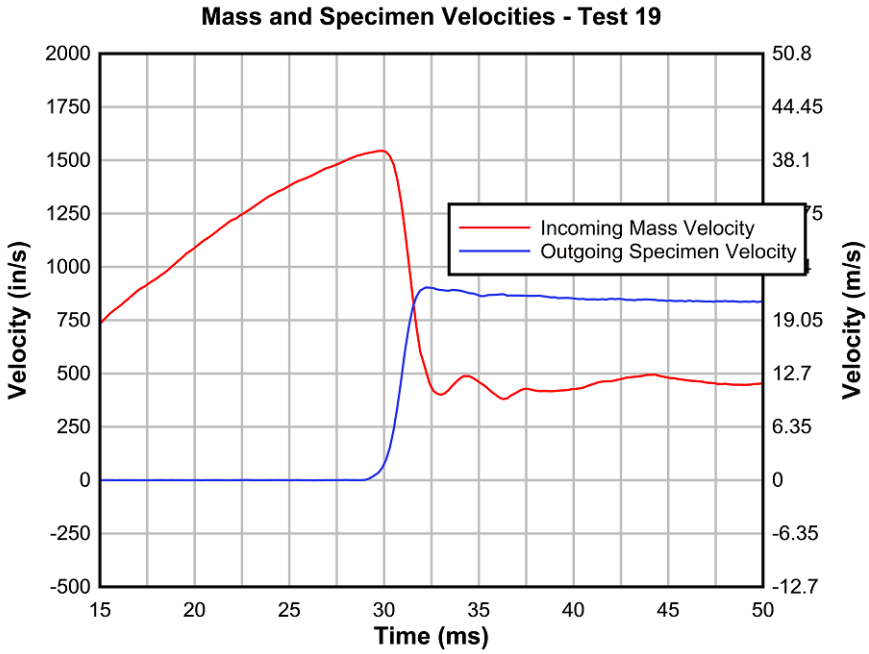

Figure 4.44: Test 19 - Impacting Mass and Specimen Velocities

longest loading duration (1.34 ms) of any leather test. While the peak acceleration (3,168 g) was less than half of the response seen in Test 3, which had the same target impact velocity but only a programmer, the duration was more than 3 times longer.

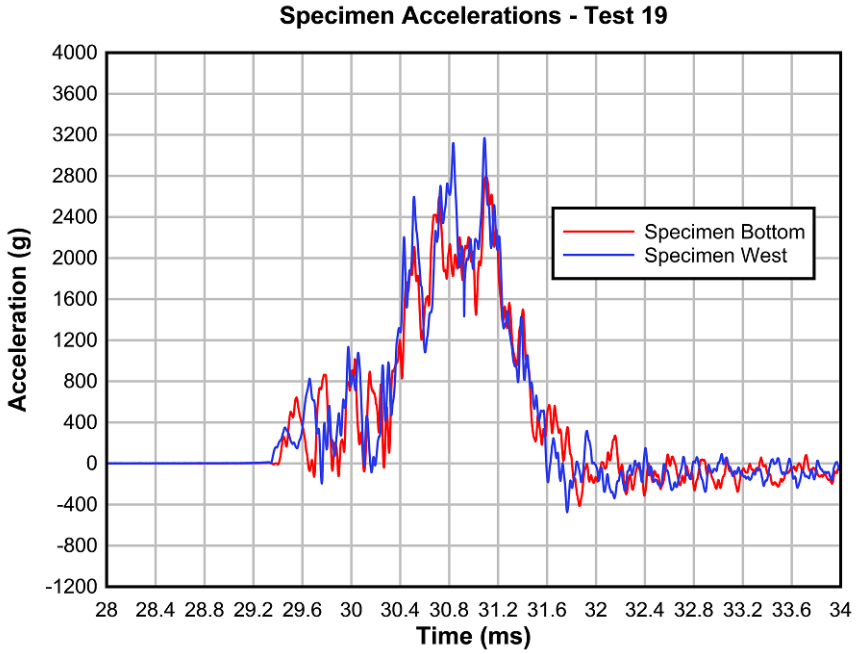

Figure 4.45: Test 19 - Specimen Accelerations

The resulting shock response spectrum is characterized by a peak acceleration of 5,000 g at 3.5 kHz.

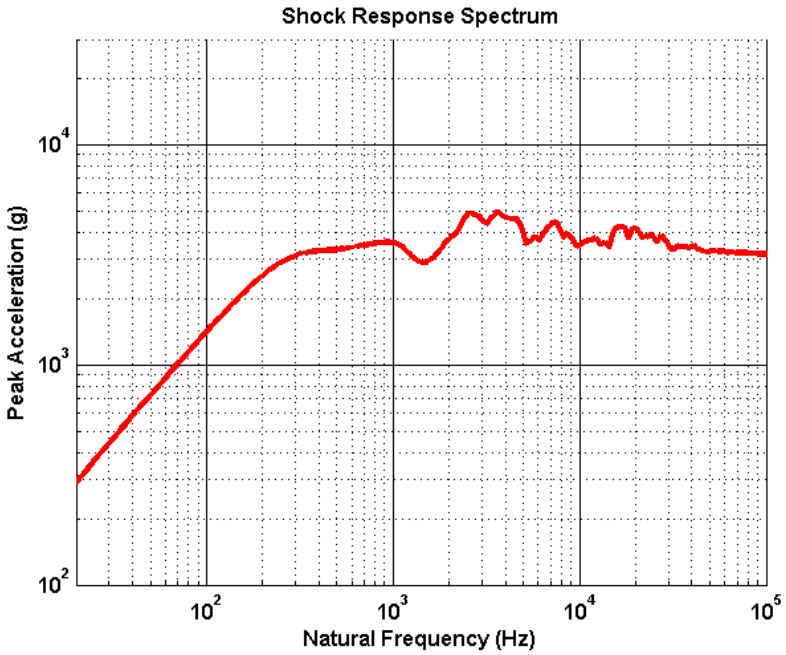

Figure 4.46: Test 19 - Shock Response Spectrum

Leather Testing Summary

A summary of the leather testing is provided in Table 4.3 (P: Programmer).

Table 4.3: Leather Testing Summary

Test	Loading Medium	Target Impact Velocity (m/s)(in/s)	Energy Dissipation (%)	Peak Acceleration (g)	Duration (ms)
9	P+1.25in Leather	15 (591)	40.6	1,644	1.25
10	P+2.5in Leather	30 (1,191)	39.5	3,068	1.03
19	P+5in Leather	40 (1,575)	58.4	3,168	1.34

4.3.5 Confined Sand

For Tests 16 and 17, 40 lbs. of sand was poured into a thin rubber bladder and placed on top of a programmer in the confining box. A layer of soft foam was placed around the inner perimeter of the box to keep the bladder centered in the assembly as shown in Figure 4.47. The bladder was enclosed in the box by sealing the impact side with tape as seen in Figure 4.48.

Figure 4.47: Confining Box with Sand Bladder

Test 16

Test 16 was characterized by a target impact velocity of 15 m/s (591 in/s) and 40 lbs. of confined sand as an impact medium as shown in 4.48. The progression of loading is displayed in Figure 4.49. In frame (a), the impacting mass and specimen are shown before impact. The mass makes initial contact with the specimen in frame (b), and the sand reaches maximum compression in frame (c). Rebounding of the specimen is shown in frame (d), and frame (e) shows the breaking away of the mass from the piston assembly. The free-flying states of the impacting mass and specimen are seen in frame (f).

The measured incoming mass velocity at impact was 17.6 m/s (693 in/s), and the outgoing specimen velocity was 9.1 m/s (358 in/s). The full velocity-time histories

Figure 4.48: Impacting Mass Assembly with Confined Sand

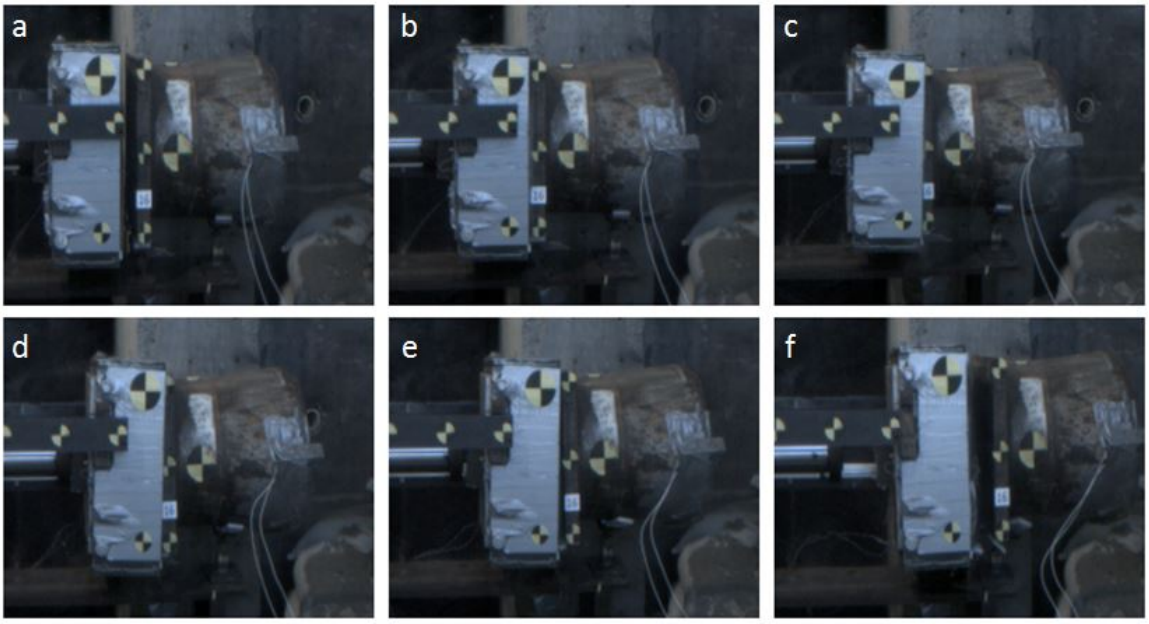

Figure 4.49: Test 16 - Progression of Shock Loading

are shown in Figure 4.50. The energy absorbed during the collision was equal to 63.2% of the incoming kinetic energy.

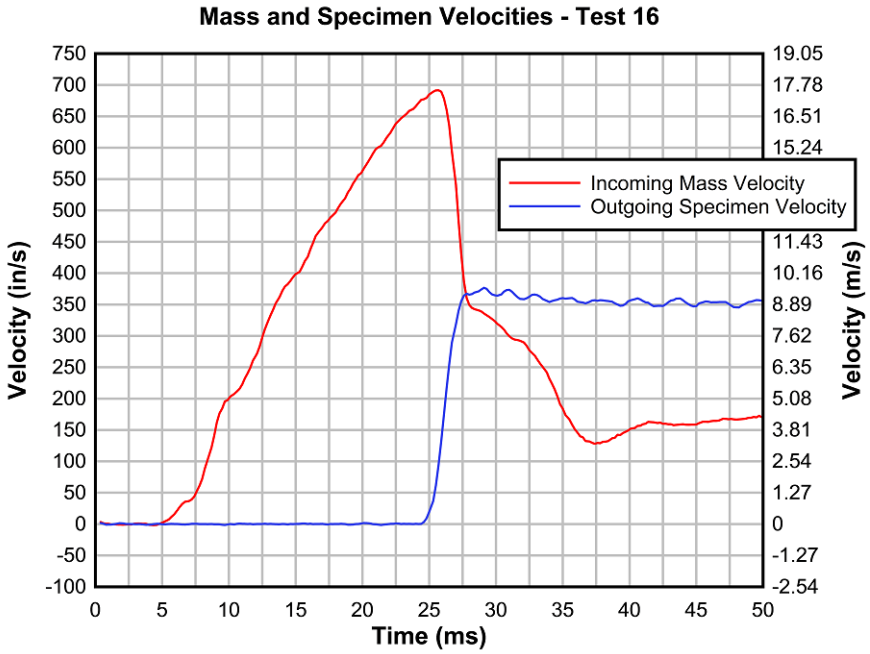

Figure 4.50: Test 16 - Impacting Mass and Specimen Velocities

While the response seen in Figure 4.51 has a significant amount of high-frequency noise, the pulse shape is much more distinguishable than the signals seen in many of the foam and double programmer tests. Because the duration is calculated at 10 percent of the peak acceleration on each end of the pulse as explained in Chapter 2, the random spikes cause the value to be very small. Thus, a duration value is not included for this test. The peak acceleration was 1,148 g.

The resulting shock response spectrum is characterized by a peak acceleration of 2,700 g at 4.5 kHz. A distinct and sudden rise in response is observed at 1.5 kHz, which is not observed in other tests with stiffer impactor materials.

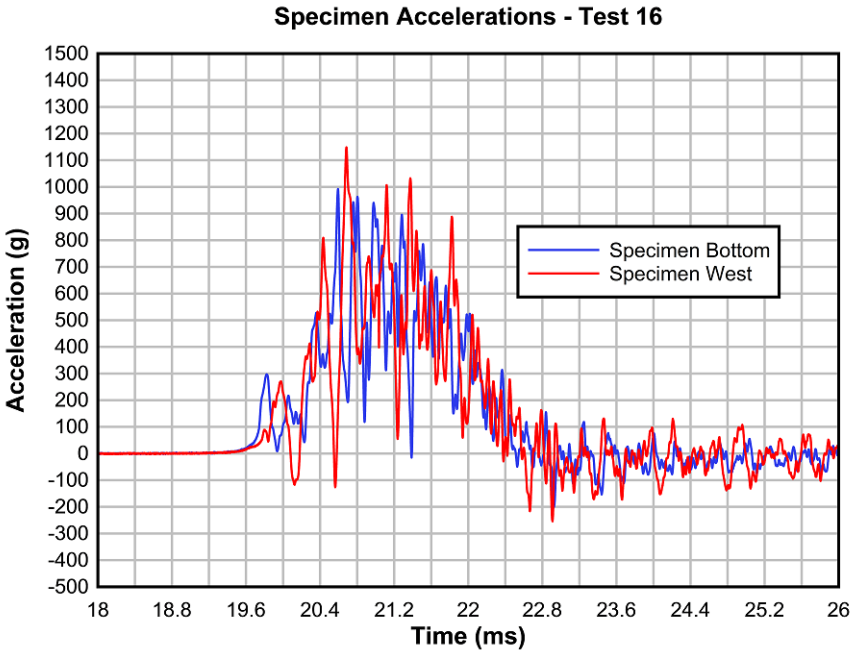

Figure 4.51: Test 16 - Specimen Accelerations

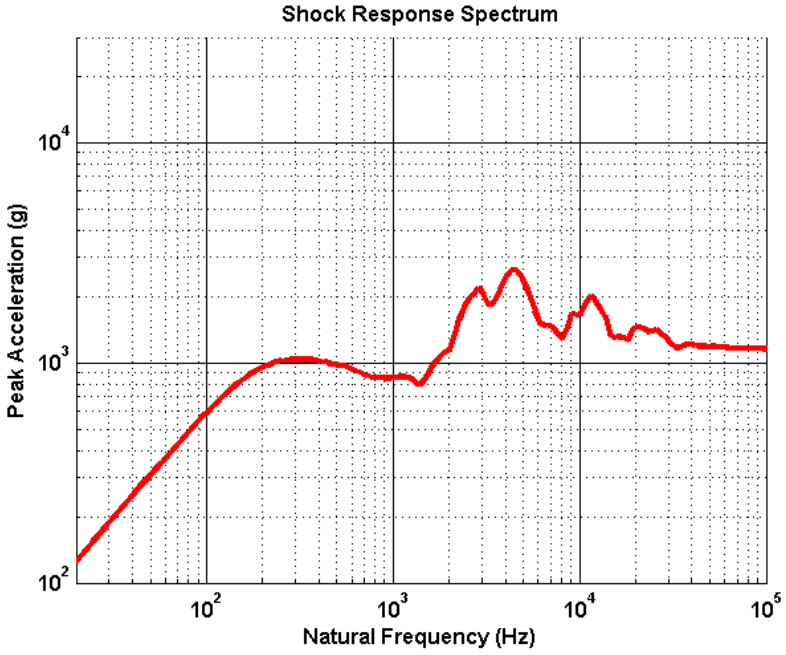

Figure 4.52: Test 16 - Shock Response Spectrum

Test 17

Test 17 was characterized by a target impact velocity of 30 m/s and 40 lbs. of confined sand as an impact medium. The progression of loading is displayed in Figure 4.53. In frame (a), the impacting mass and specimen are shown before impact. The mass makes initial contact with the specimen in frame (b), and the sand reaches maximum compression in frame (c). Rebounding of the specimen is shown in frame (d), and frame (e) shows the breaking away of the mass from the piston assembly. The free-flying states of the impacting mass and specimen are seen in frame (f).

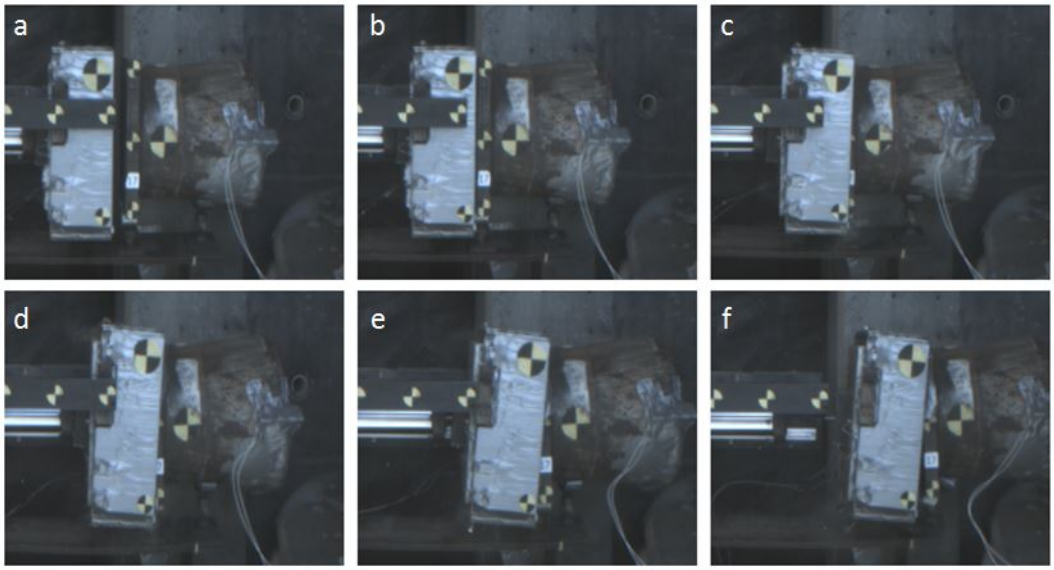

Figure 4.53: Test 17 - Progression of Shock Loading

The measured incoming mass velocity at impact was 31.2 m/s (1,228 in/s), and the outgoing specimen velocity was 14.7 m/s (579 in/s). The full velocity-time histories are shown in Figure 4.54. The energy dissipated during the collision was equal to 63.2% of the incoming kinetic energy.

With the same amount of sand as Test 16 but an increased velocity at impact, the resulting higher peak acceleration was expected. The duration was distinctly longer than the results seen from the programmer and leather tests at 30 m/s, but the peak response was lower.

The resulting shock response spectrum is characterized by a peak acceleration

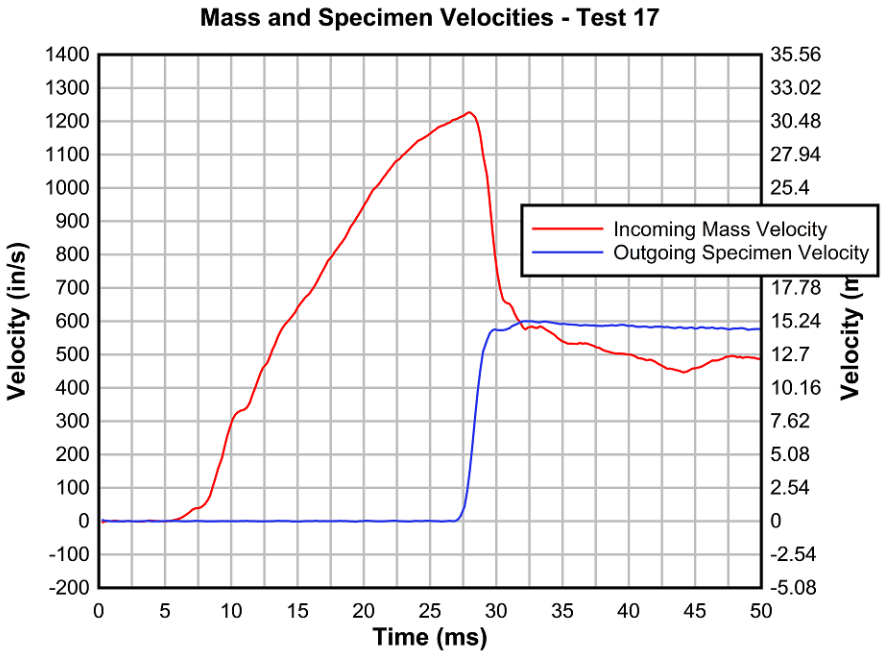

Figure 4.54: Test 17 - Impacting Mass and Specimen Velocities

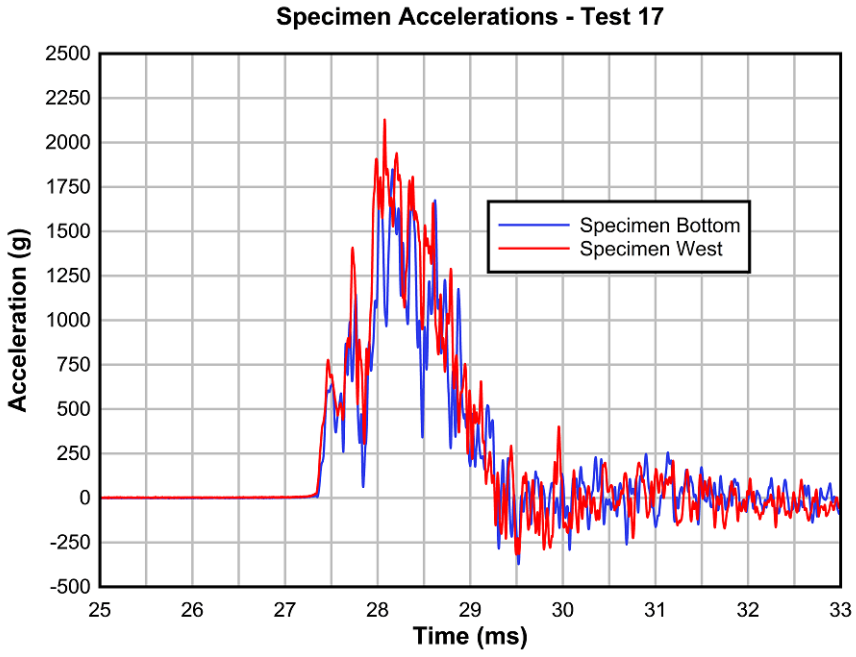

Figure 4.55: Test 17 - Specimen Accelerations

of 3,800 g at 3.8 kHz. Unlike Test 16, the response is fairly consistent through the high-frequency range.

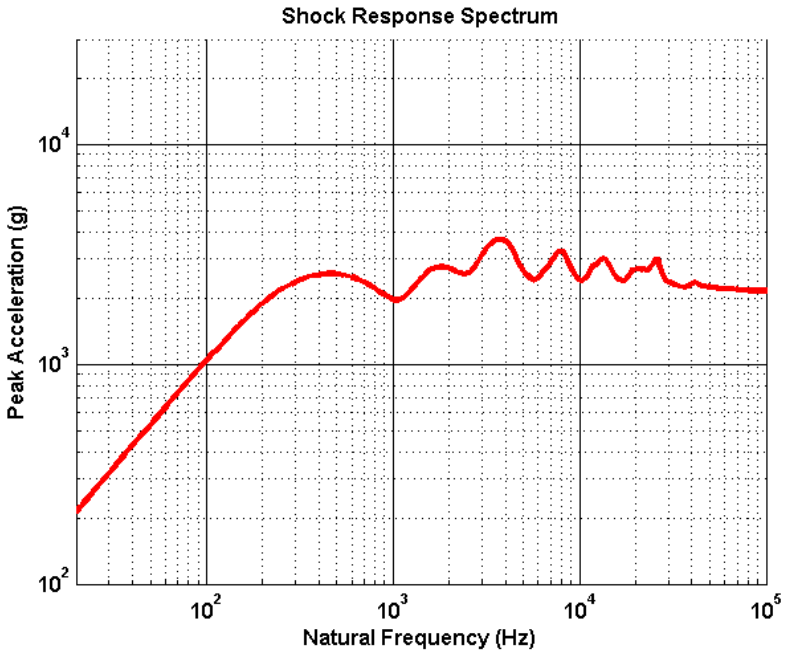

Figure 4.56: Test 17 - Shock Response Spectrum

Sand Testing Summary

A summary of the sand testing is provided in Table 4.4 (P: Programmer). The exclusion of a duration calculation is explained previously in the Test 16 section.

Table 4.4: Sand Testing Summary

Test	Loading Medium	Target Impact Velocity (m/s)(in/s)	Energy Dissipation (%)	Peak Acceleration (g)	Duration (ms)
16	P+40lbs Sand	15 (591)	63.2	1,148	–
17	P+40lbs Sand	30 (1,191)	63.2	2,129	1.80

4.3.6 Confined Sand and Leather

Tests 18-24 used a combination of confined sand and leather as an impact medium. The leather layers explained previously were secured to a sand bladder which was placed on top of a programmer as shown in Figure 4.57. Before attaching the impacting mass assembly to the blast generator piston, the leather was stretched with double-curvature over the sand to create a surface which would load the specimen more gradually than would be possible with a flat impact surface. The purpose of this approach was to produce a longer acceleration pulse duration in the specimen.

Figure 4.57: Leather and Sand Combination as Impact Medium

Test 18

Test 18 was characterized by a target impact velocity of 40 m/s (1,575 in/s) and 60 lbs of confined sand covered with 2.5 in of layered leather as an impact medium. The progression of loading is displayed in Figure 4.58. In frame (a), the impacting mass and specimen are shown before impact. The mass makes initial contact with the specimen in frame (b), and the sand-leather combination reaches maximum compression in frame (c). Rebounding of the specimen is shown in frame (d), and frame (e) shows the breaking away of the mass from the piston assembly.

The free-flying states of the impacting mass and specimen are seen in frame (f). The tipping of the mass and specimen observed in frames (d)-(f) was due to the shifting of the sand towards the bottom of the confining box before testing. The slightly asymmetric loading caused a noticeable slant in the specimen and mass during and after impact but did not disturb the data acquisition at the free end of the test article. This phenomenon is also observed in various degrees in Tests 22-24.

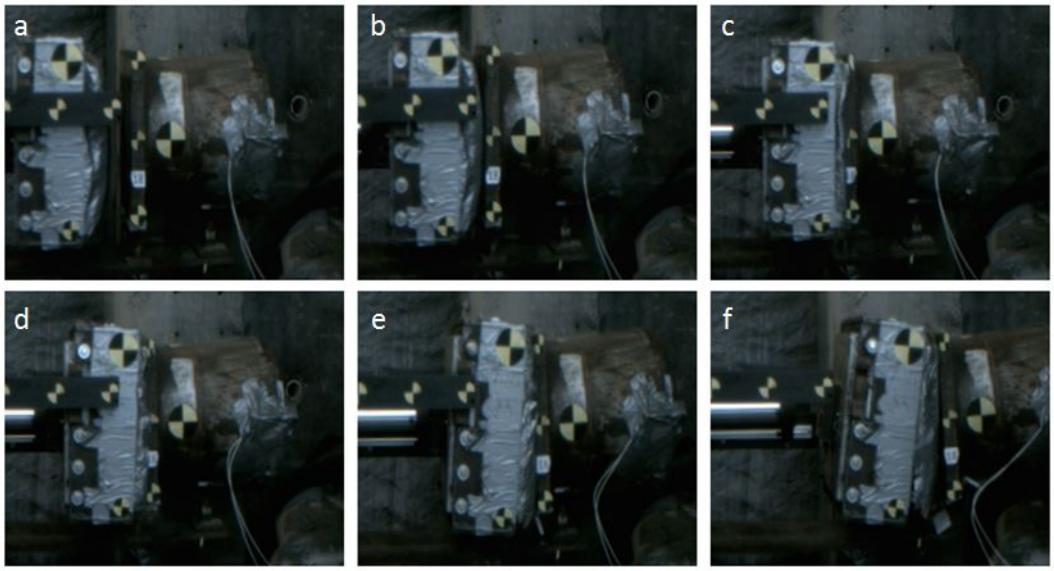

Figure 4.58: Test 18 - Progression of Shock Loading

The measured incoming mass velocity at impact was 39.5 m/s (1,555 in/s), and the outgoing specimen velocity was 21.24 m/s (836 in/s). The full velocity-time histories are shown in Figure 4.59. The energy dissipated during the collision was equal to 55.0% of the incoming kinetic energy.

The first test with the combination of leather and sand produced an excellent pulse shape with the longest loading duration of any test up to that point. The peak acceleration was comparable to that of Test 17, which had only sand and a lower impact velocity.

The resulting shock response spectrum is characterized by a peak acceleration of 3,300 g at 5.5 kHz. Due to the long duration of the acceleration pulse, we see a large response in the low-frequency range when compared to other tests with similar peak accelerations.

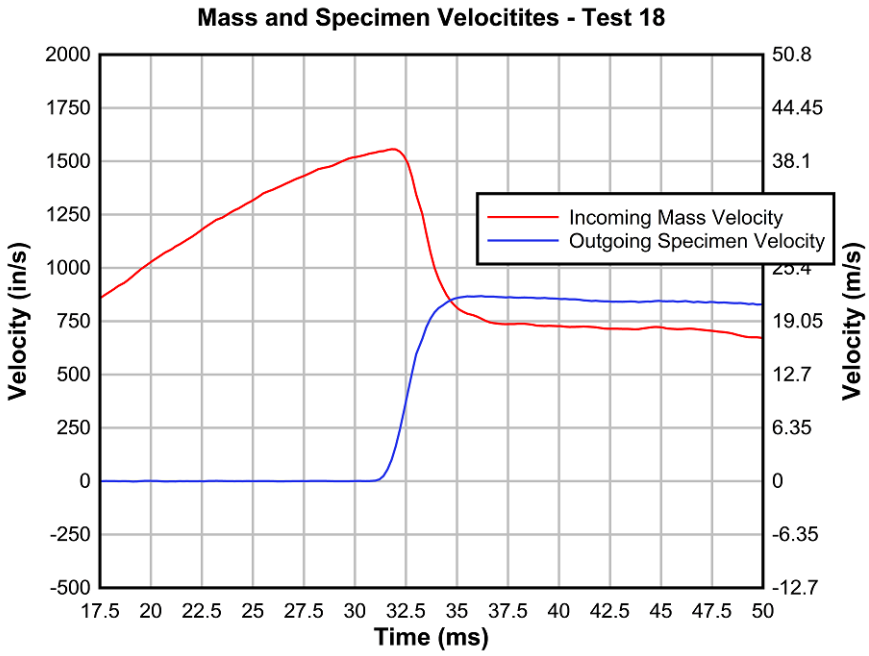

Figure 4.59: Test 18 - Impacting Mass and Specimen Velocities

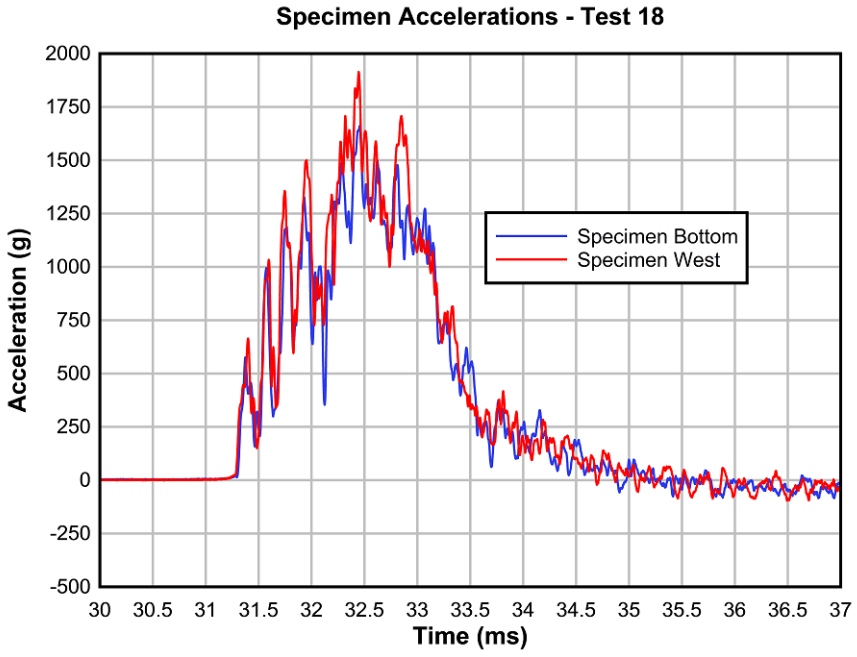

Figure 4.60: Test 18 - Specimen Accelerations

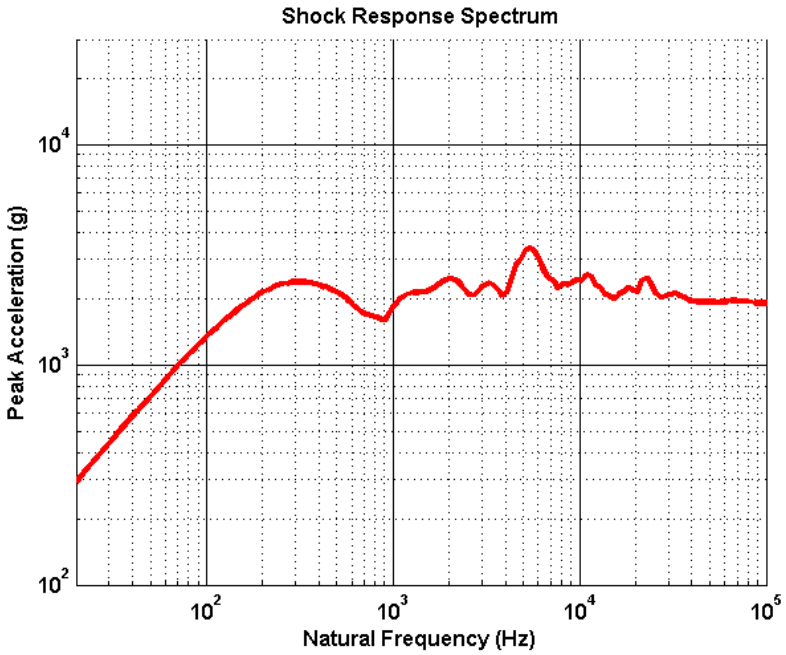

Figure 4.61: Test 18 - Shock Response Spectrum

Test 20

Test 20 was characterized by a target impact velocity of 45 m/s (1,772 in/s) and 80 lbs of confined sand covered with 1.25 in of layered leather as an impact medium. Due to its similarities to Test 18, the test will not be discussed in the results section, but a summary of the data is provided in Appendix B.

Test 21

Test 21 was characterized by a target impact velocity of 55 m/s (2,165 in/s) and 60 lbs of confined sand covered with 2 in of layered leather as an impact medium. The progression of loading is displayed in Figure 4.62. In frame (a), the impacting mass and specimen are shown before impact. The mass makes initial contact with the specimen in frame (b), and the sand-leather combination reaches maximum compression in frame (c). Rebounding of the specimen is shown in frame (d), and frame (e) shows the breaking away of the mass from the piston assembly. The free-flying states of the impacting mass and specimen are seen in frame (f).

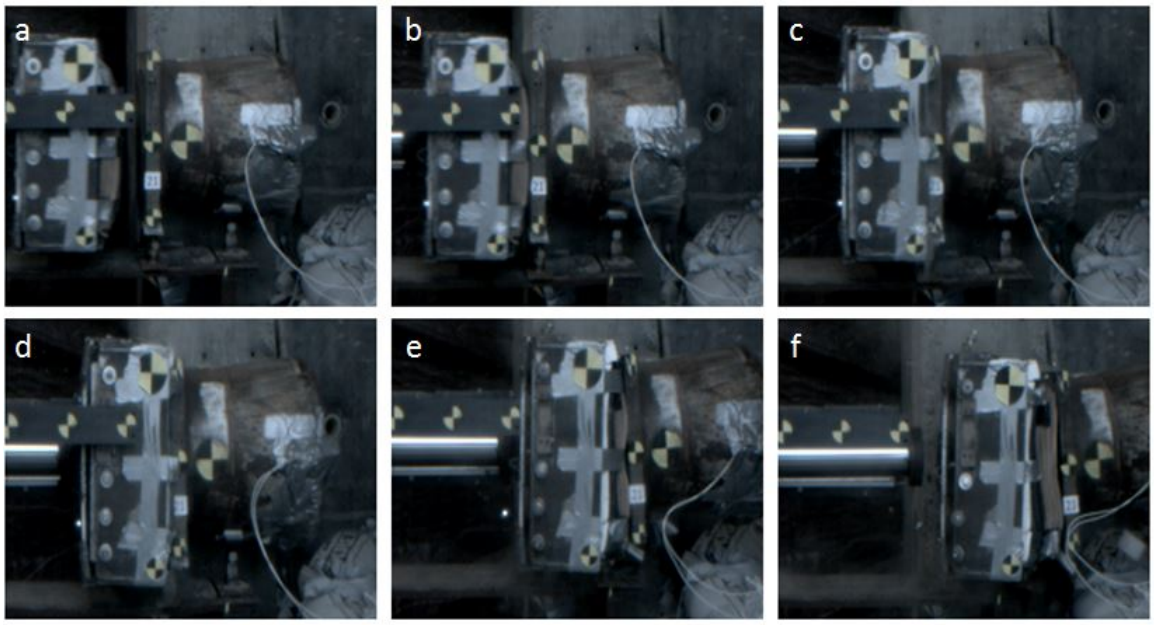

Figure 4.62: Test 21 - Progression of Shock Loading

The measured incoming mass velocity at impact was 52.2 m/s (2,055 in/s), and the outgoing specimen velocity was 29.9 m/s (1,177 in/s). The full velocity-time histories are shown in Figure 4.63. The energy dissipated during the collision was equal to 49.5% of the incoming kinetic energy.

Test 21 produced arguably the cleanest response curve in the experimental series. With one of the longest loading durations, minimal high frequency noise or random spikes, and one of the highest peak accelerations in the test series, the results showed the effectiveness of the leather-sand combination as a long-duration shock-loading configuration.

The resulting shock response spectrum is characterized by a peak acceleration of 4,800 g at 4.5 kHz. Due to the long duration of the acceleration pulse, we see a large response in the low-frequency range when compared to other tests with similar peak accelerations.

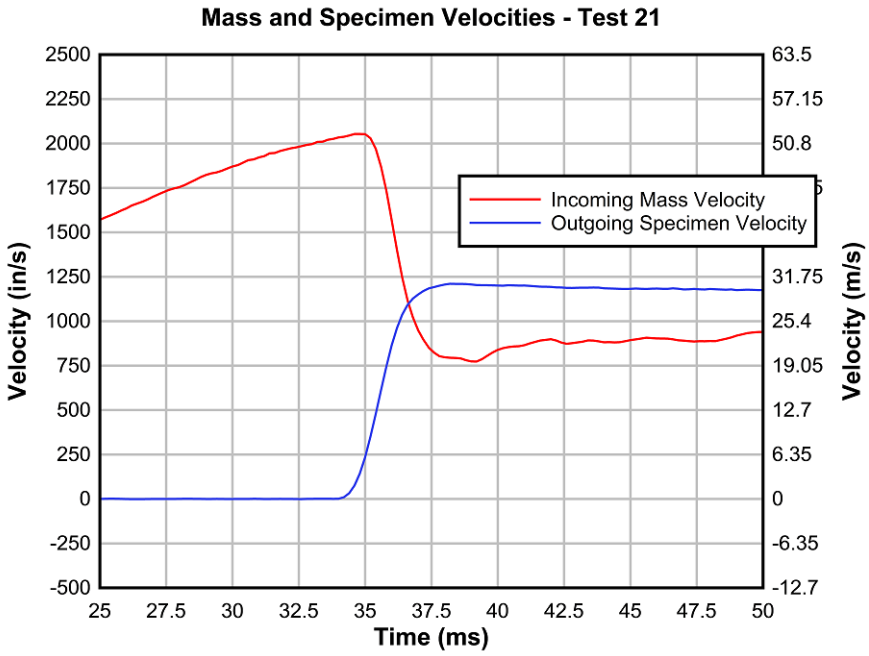

Figure 4.63: Test 21 - Impacting Mass and Specimen Velocities

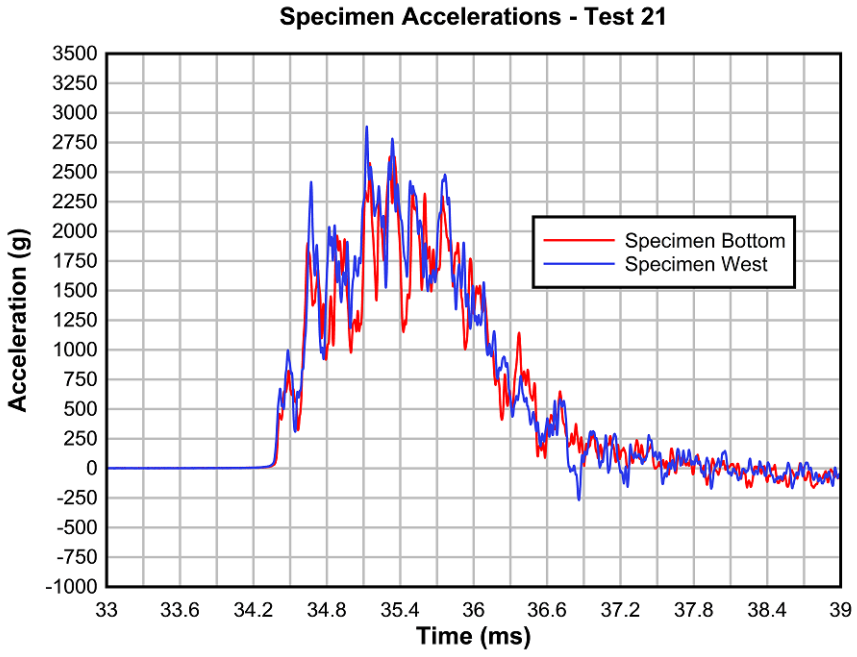

Figure 4.64: Test 21 - Specimen Accelerations

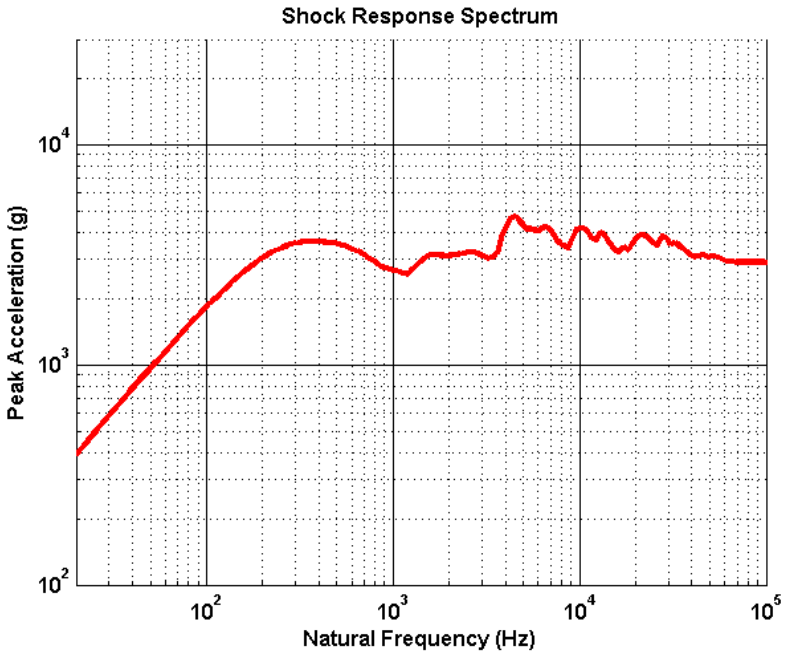

Figure 4.65: Test 21 - Shock Response Spectrum

Test 22

Test 22 was characterized by a target impact velocity of 45 m/s and 60 lbs. of confined sand covered with 2 in of layered leather as an impact medium. The test will not be discussed in the results section, but a summary of the data is provided in Appendix B.

Test 23

Test 23 was characterized by a target impact velocity of 50 m/s (1,969 in/s) and 50 lbs. of confined sand covered with 2 in of layered leather as an impact medium. The standard aluminum impacting plate was replaced with a steel plate, effectively increasing the mass of the impactor by 73 lbs. The progression of loading is displayed in Figure 4.66. In frame (a), the impacting mass and specimen are shown before impact. The mass makes initial contact with the specimen in frame (b), and the sand-leather combination reaches maximum compression in frame (c). Rebounding of the specimen is shown in frame (d), and frame (e) shows the breaking away of

the mass from the piston assembly. The free-flying states of the impacting mass and specimen are seen in frame (f).

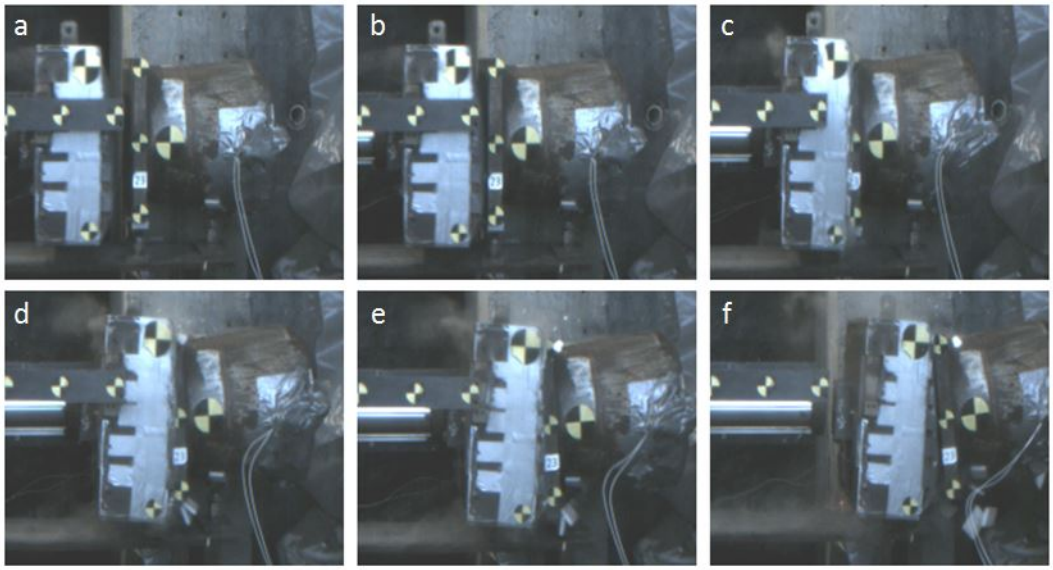

Figure 4.66: Test 23 - Progression of Shock Loading

The measured incoming mass velocity at impact was 49.1 m/s (1,933 in/s), and the outgoing specimen velocity was 28.6 m/s (1,126 in/s). The full velocity-time histories are shown in Figure 4.67. The energy dissipated during the collision was equal to 49.8% of the incoming kinetic energy.

The response of Test 23 had the highest peak acceleration of any test which had impacting materials other than the programmer alone. It also had the second longest loading duration and, despite the somewhat inconsistent data produced between the two specimen accelerometers, a relatively smooth pulse shape. Because of the clear random spike observed in the middle of the signal, the effective peak acceleration is considered to be 3,000 g.

The resulting shock response spectrum is characterized by a peak acceleration of 5,000 g at 4.5 kHz and again at 26 kHz. Due to the long duration of the acceleration pulse, we see a large response in the low-frequency range when compared to other tests with similar peak accelerations.

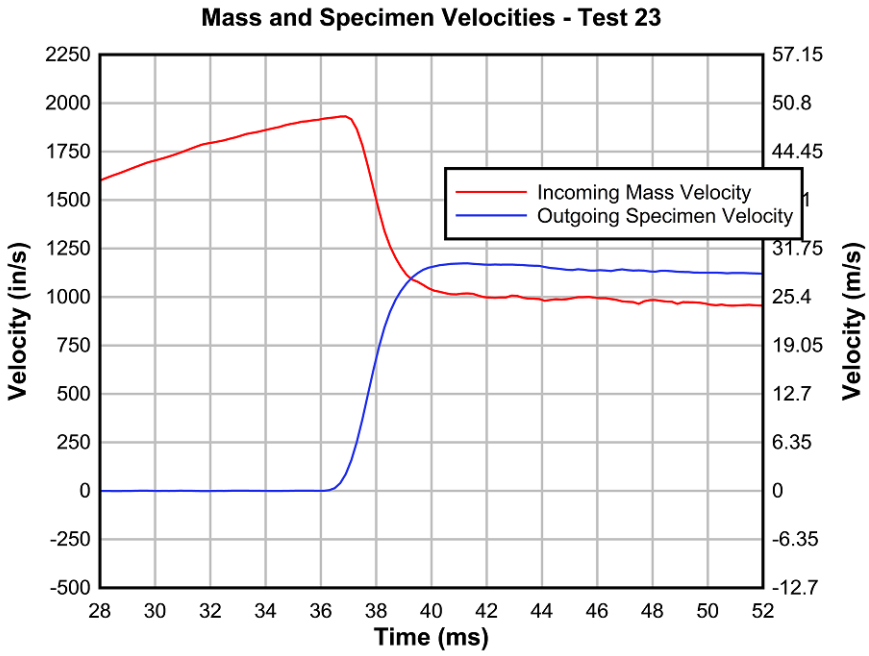

Figure 4.67: Test 23 - Impacting Mass and Specimen Velocities

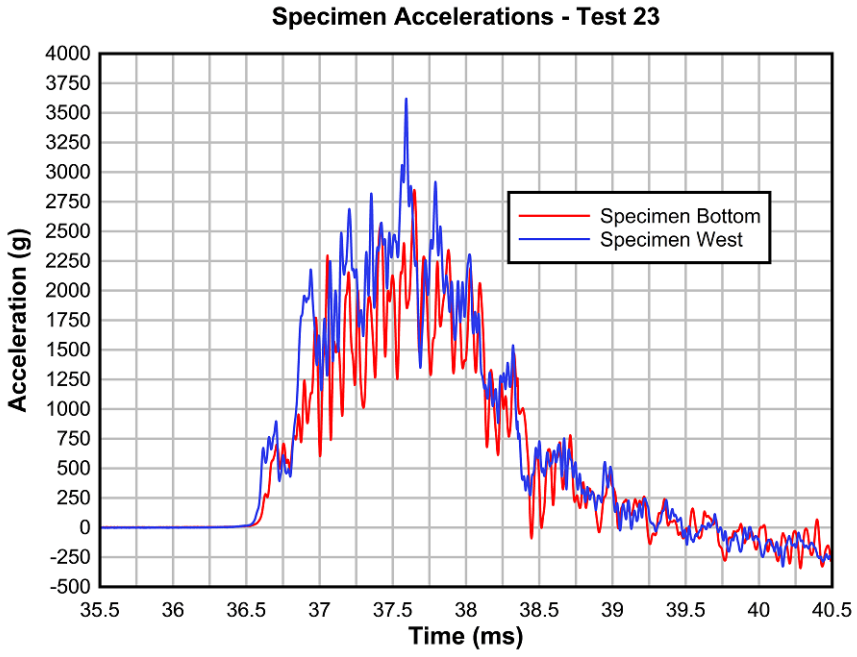

Figure 4.68: Test 23 - Specimen Accelerations

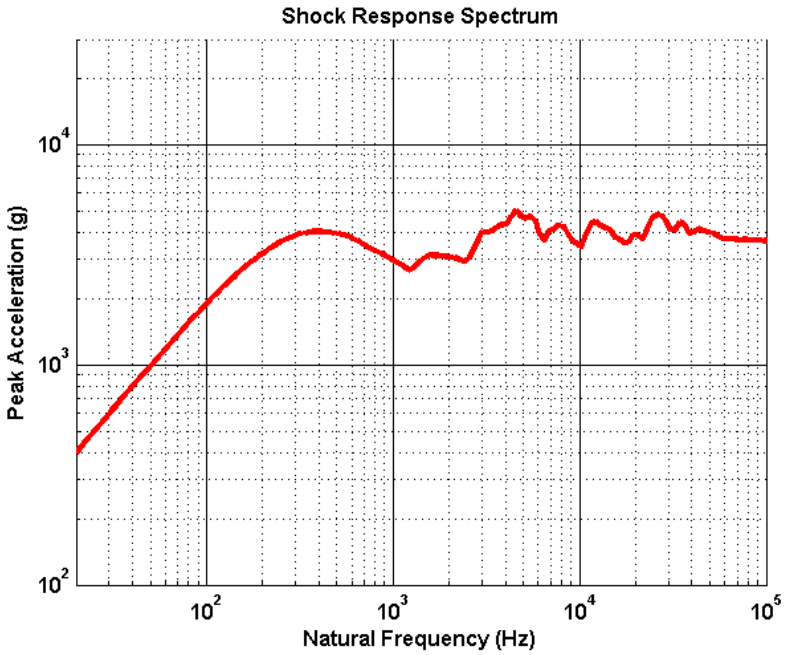

Figure 4.69: Test 23 - Shock Response Spectrum

Test 24

Test 24 was characterized by a target impact velocity of 50 m/s (1,969 in/s) and 35 lbs. of confined sand covered with 2 in of layered leather as an impact medium. The shape of the acceleration-time history was somewhat inconsistent with previous tests and will not be discussed in the results section. A summary of the data is provided in Appendix B.

Sand-leather Testing Summary

A summary of the sand-leather combination testing is provided in Table 4.5 (P: Programmer).

Table 4.5: Sand-leather Testing Summary

Test	Loading Medium	Target Impact Velocity (m/s)(in/s)	Energy Dissipation (%)	Peak Acceleration (g)	Duration (ms)
18	P+2.5in Leather+60 lbs Sand	40 (1,575)	55.0	1,944	2.15
20	P+1.25in Leather+80 lbs Sand	45 (1,772)	59.6	1,800	2.73
21	P+2in Leather+60 lbs Sand	55 (2,165)	49.5	2,885	2.20
22	P+2in Leather+60 lbs Sand	45 (1,772)	47.3	2,533	1.58
23	P+2in Leather+50 lbs Sand	50 (1,969)	49.8	3,000	2.30
24	P+2in Leather+35 lbs Sand	50 (1,969)	50.3	3,356	1.90

4.4 Summary

A full description of the experimental series for tests with reliable acceleration-time histories is given in Table 4.6 (P: Programmer).

Table 4.6: Experimental Testing Summary

Test	Loading Medium	Target Impact Velocity (m/s)(in/s)	Energy Dissipation (%)	Peak Acceleration (g)	Duration (ms)
1	P	15 (591)	28.9	2,425	1.03
2	P	30 (1,191)	29.1	4,865	0.62
3	P	40 (1,575)	38.2	7,443	0.40
9	P+1.25in Leather	15 (591)	40.6	1,644	1.25
10	P+2.5in Leather	30 (1,191)	39.5	3,068	1.03
17	P+40lbs Sand	30 (1,191)	63.2	2,129	1.80
18	P+2.5in Leather+60 lbs Sand	40 (1,575)	55.0	1,944	2.15
19	P+5in Leather	40 (1,575)	58.4	3,168	1.34
20	P+1.25in Leather+80 lbs Sand	45 (1,772)	59.6	1,800	2.73
21	P+2in Leather+60 lbs Sand	55 (2,165)	49.5	2,885	2.20
22	P+2in Leather+60 lbs Sand	45 (1,772)	47.3	2,533	1.58
23	P+2in Leather+50 lbs Sand	50 (1,969)	49.8	3,000	2.30
24	P+2in Leather+35 lbs Sand	50 (1,969)	50.3	3,356	1.90

A correlation between energy dissipation during each collision and the corresponding acceleration pulse duration for tests with reliable data is shown in Figure 4.70. Equation (4.1) provides the method for determining the amount of dissipated energy. The trend shows an approximately linear increase in pulse duration with increase in the percentage of original energy absorbed. Due to the complexity of the impact scenarios, it is difficult to determine the reason for the presence of the outliers seen on the right side of the plot (Tests 17 and 19). However, it can be shown in general that higher levels of energy dissipation will lead to increased pulse durations. Intuitively, one would expect that softer materials with greater damping would produce a longer loading time and, thus, a longer acceleration response pulse duration. The data shows that this assumption is a reasonable approach for designing impact events which call for specific pulse durations.

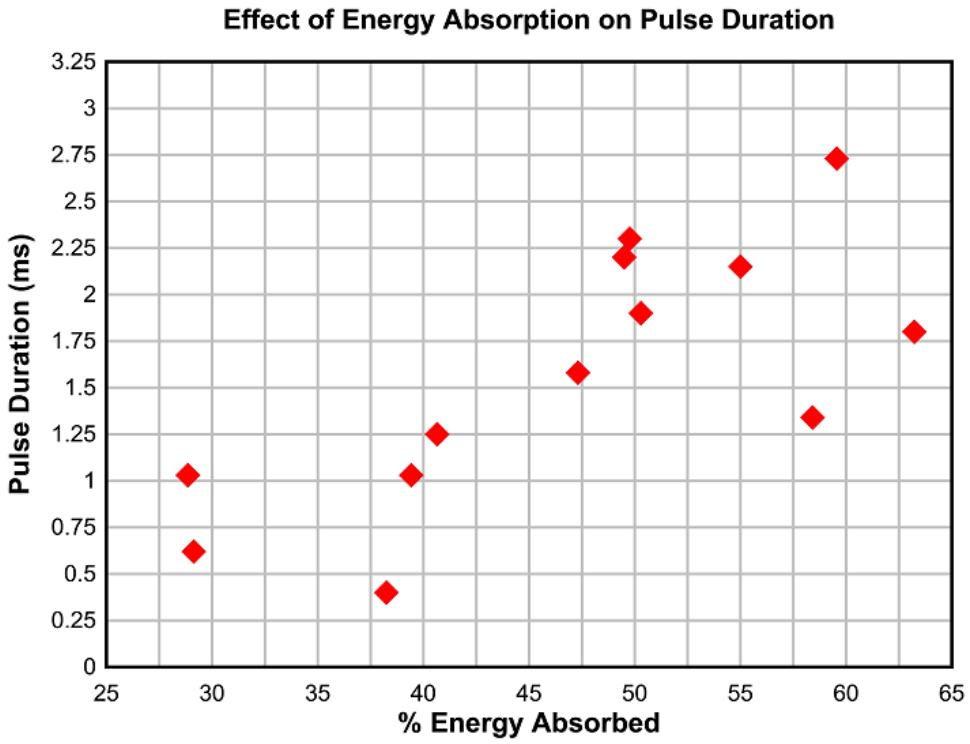

Figure 4.70: Correlation Between Energy Absorption During Impact and Specimen Acceleration Pulse Duration

Shock response spectrum comparisons are provided to display the differences in test results across the specified range of spectrum frequencies. Because the tests were conducted with very different impact mediums, the plots provide useful comparisons for examining how the loading durations and peak accelerations induced by the various materials affect the response spectrum. For the purposes of this analysis and discussion, the "low-frequency" region spans from 0 to 100 Hz, the "mid-frequency" region from 100 to 1,000 Hz, and the "high-frequency" region from 1,000 to 100,000 Hz.

Figure 4.71 shows a comparison of the shock response spectrums for tests which were run with a target impact velocity of 15 m/s. Test 1, which used only a single programmer, had the highest peak acceleration of the three tests and, consequently, the highest response in the high-frequency range of the spectrum plot. Test 16 (confined sand), although it was characterized by a lower peak acceleration than Test 9 (leather), clearly matched the spectrum response in the low-frequency range. This result is indicative of the fact that an increase in pulse duration will lead to a greater spectrum response in the low-frequency range for an identical peak in the acceleration-time history.

A comparison for tests run with a 30 m/s impact velocity is shown in Figure 4.72. While all of these tests had different pulse durations and peak accelerations in the specimen response, each of them behaved similarly in the low-frequency range. This result is explained by the fact that the data shows the highest peak acceleration (Test 2) corresponding to the shortest duration, and the lowest peak acceleration (Test 16) corresponding to the longest duration. The high-frequency region of the spectrum shows that Test 2 should have a significantly larger peak acceleration than the other tests, which is clearly displayed in the acceleration-time histories shown in Section 4.3.

Figure 4.73 shows a comparison of the shock response spectrums for tests which were run with a target impact velocity of 40 m/s. Consistent with the previous comparisons, the test with only a programmer (Test 3) produced the largest peak response by far. While the leather and sand tests produced similar peak responses, there is a distinct difference in the low-frequency region of the spectrum due to the longer load duration seen in the acceleration-time history for the sand-leather test

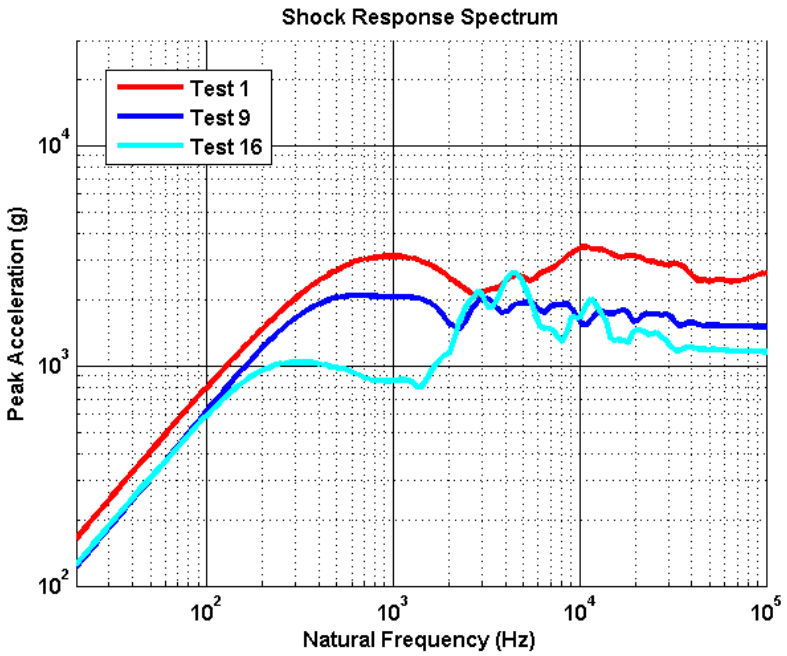

Figure 4.71: Shock Response Spectrum Comparison: Tests @ 15 m/s Impact Velocity

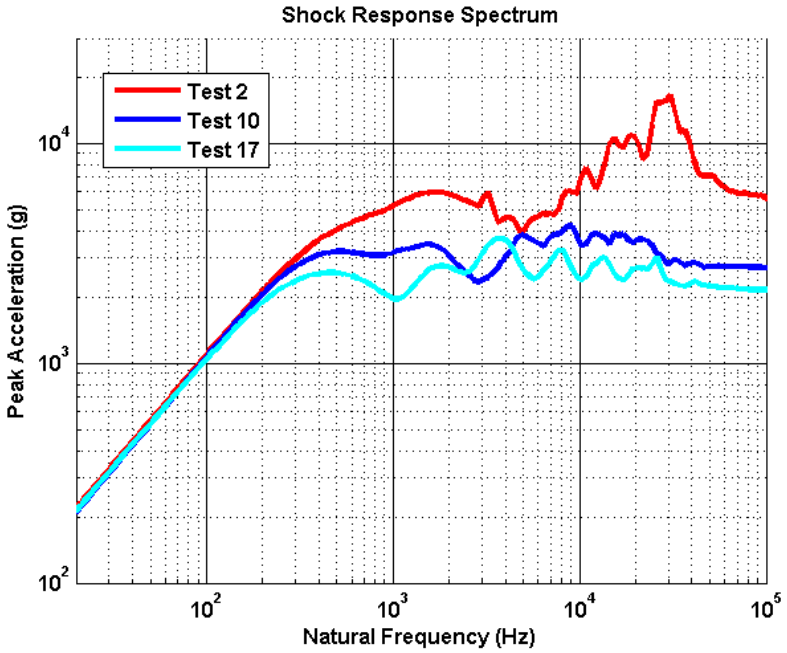

Figure 4.72: Shock Response Spectrum Comparison: Tests @ 30 m/s Impact Velocity

(Test 18). At the very lowest frequencies, we see the sand-leather response being slightly higher even than the programmer test.

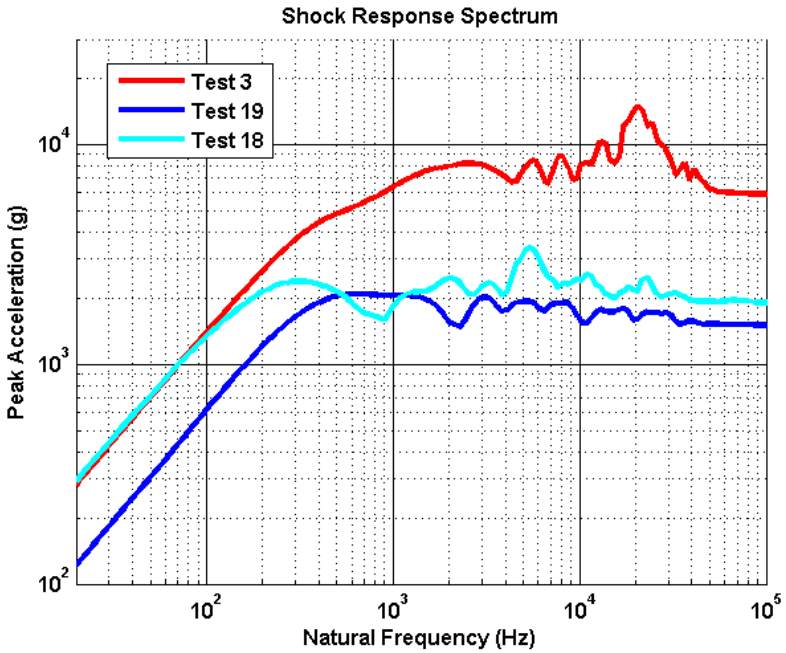

Figure 4.73: Shock Response Spectrum Comparison: Tests @ 40 m/s Impact Velocity

A comparison of tests which produced some of the highest peak accelerations in the series ("high-level tests") is shown in Figure 4.74. Although Test 3 had the largest peak response of any test, it produced smaller spectrum values in the low-frequency region than the two tests with leather and sand, which were run with 55 m/s (Test 21) and 50 m/s (Test 23) impact velocities. It would not be unreasonable to assume, however, that another programmer test at 50 m/s would be able to match or surpass the responses seen from the other tests in the low-frequency range because of the greatly increased peak accelerations which would be present in the data.

The results show that sand or a combination of leather and sand is the most effective method for increasing the spectrum response in the low-frequency range for a given peak acceleration. It is also clear that tests with programmer only produce the highest peak responses in the high-frequency region. For lower impact velocities, leather provides a response which is similar to sand for low frequencies but larger for

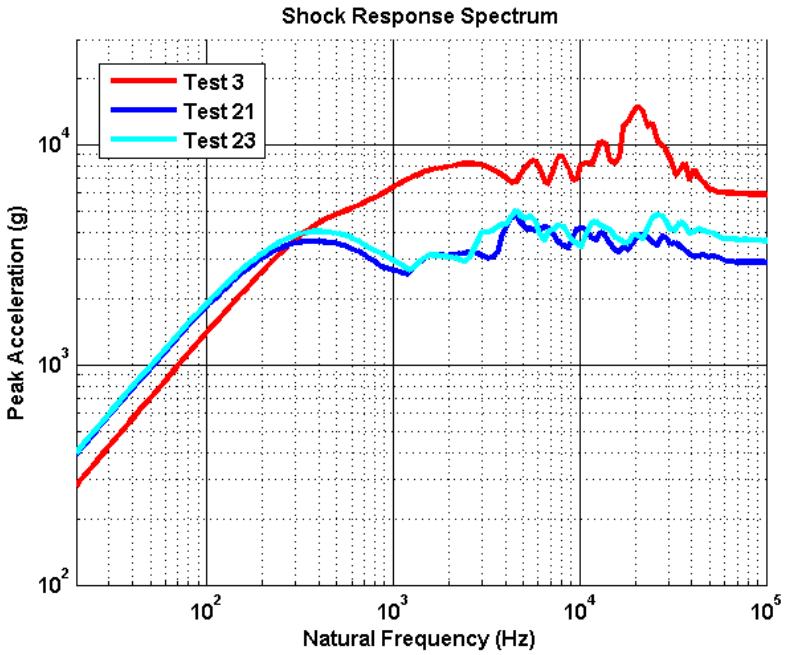

Figure 4.74: Shock Response Spectrum Comparison: High-level Tests

high frequencies.

Analysis of the shock response spectrums show that the Blast Simulator is capable of producing a wide variety of shock loads which can be tailored across the entire frequency range by adjusting the impact velocity and material. A study of the results may lead one to ask why any material other than programmer should be used because of its ability to produce the highest responses in both the low-frequency and high-frequency ranges. In response to this, it is important to consider the usefulness of being able to produce a response such as that of Test 23 in Figure 4.74, which has a relatively large response at lower frequencies and smaller response at high frequencies when compared to the programmer test (Test 3). While it would take little effort to run a programmer test which matched the response of Test 23 in either the low or high frequency ranges, it would not be realistic to conclude that both could be matched simultaneously. In the case that an impact event with a relatively high low-frequency response and relatively low high-frequency response should be simulated, sand and leather would clearly be a better option than programmer only. Thus, modifying the appropriate loading parameters is an effective method for designing an experimental

test which simulates a very specific shock scenario.

In an attempt to further show the usefulness of the results, a sample case is provided. Consider that a design team has acquired field data on the steel cylinder and has developed a shock response specification for two loading cases shown in Figure 4.75. The team would like to be able to approximately reproduce these shock levels in a laboratory environment in order to test with greater efficiency.

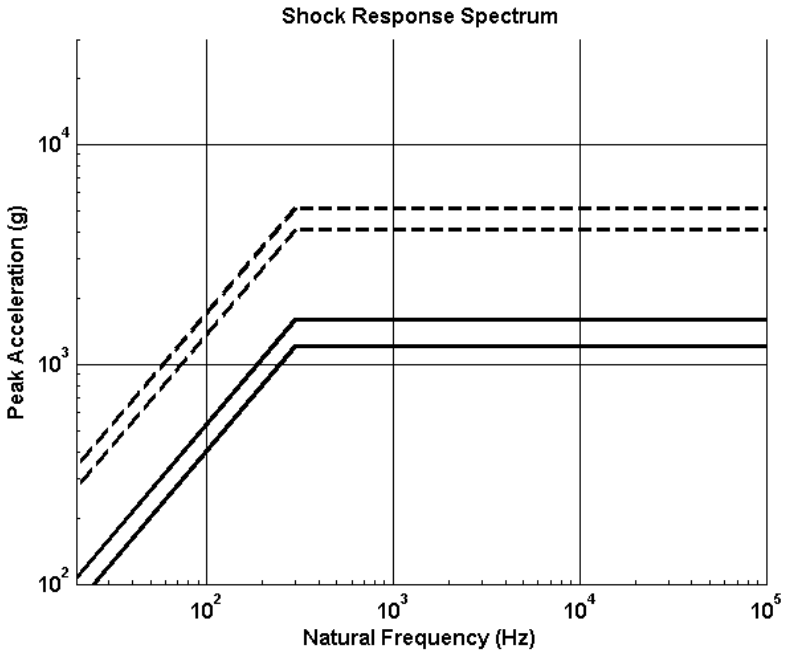

Figure 4.75: Examples of SRS Test Specifications

Based on the results from the experimental series shown in this chapter, some initial responses can be made. Displaying the shock response data from several tests (Figure 4.76), it can be shown that the bottom test specification (dashed lines) can be matched using leather with an impact velocity of 15 m/s (turquoise curve). Thus, this configuration would be used initially to attempt to match the provided limits in a new experimental series. However, the upper specification (solid lines) is not matched in the high-frequency region by any test in the original series. Considering that responses were produced which fall above and below these boundaries, it can be hypothesized that the specification could be matched if a sufficient number of tests were run with the Blast Simulator. This approach could potentially require

several tests and a significant amount of time and effort at the laboratory. If the shock response results from different impacting configurations which were not used in the original testing series could be predicted with a reasonable level of accuracy, an appropriate setup could be designed for use with the Blast Simulator to match the upper specification. As a result, the number of required experimental tests could be significantly decreased, reducing time and cost requirements. An effective method for making such predictions is to create numerical models which are representative of the experimental testing. The following chapter provides a thorough analysis of such an approach.

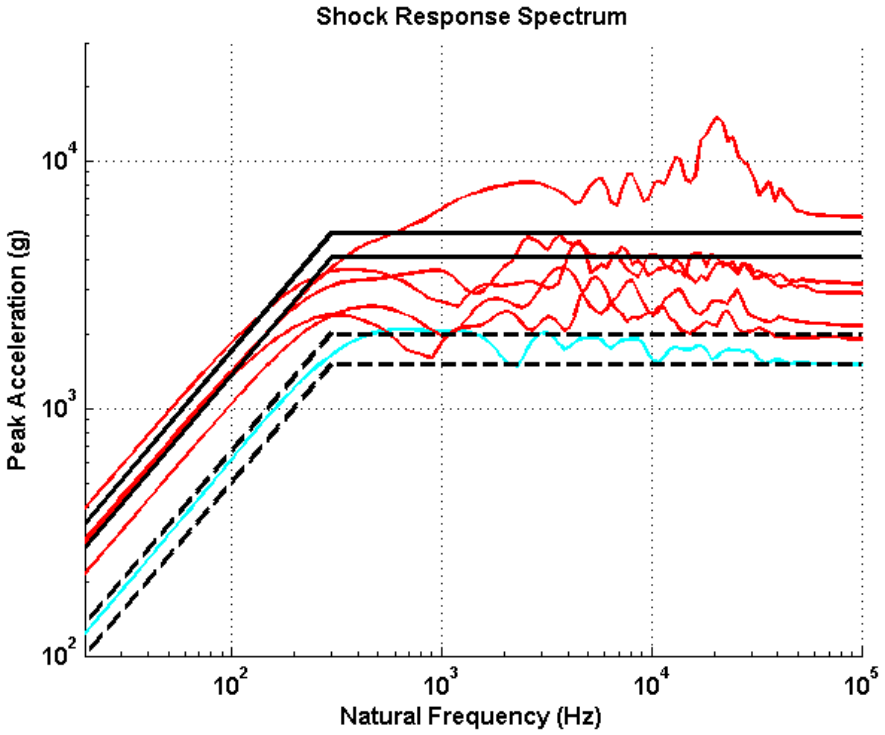

Figure 4.76: Experimental Test Results with Test Specifications

A portion of Chapter 4 is a reprint of the material as it appears in Blast Simulator Testing for High-g Shock Environment Characterization (2013). Durant, Brad, Stewart, Lauren, Wolfson, Janet, Hegemier, Gilbert. *Proceedings of the 83rd Shock and Vibration Symposium.* The thesis author was the primary investigator and author of this paper.

Chapter 5

Numerical Simulation of Experimental Testing

A set of numerical models was developed and calibrated with the advanced finite element tool, LS-DYNA, in order to provide the ability to predict the expected specimen responses from loading scenarios not examined in the experimental series. Because shock testing is often an iterative process, reliable models can save time, energy and money by providing insight into expectations for future work. If a specific shock is desired by the analyst during an experimental sequence, simulations can provide a good starting point for the designation of input parameters and reduce the number of tests required to produce a desired signal. The following models from 8 different experimental tests are calibrated to reasonable accuracy for loading conditions involving programmer, leather, sand, and a combination of leather and sand.

The experimental acceleration-time histories were characterized by noticeable high-frequency content which may have resulted from localized specimen behavior or the mounting configuration of the accelerometers. Because scenarios such as these cannot be realistically modeled, the high-frequency portions of signals were systematically removed for purposes of model calibration. In order to determine what frequency range to omit from the original signals, the specimen was impacted with a ball-peen hammer to induce the natural modes of vibration. A Fourier analysis of the resulting acceleration-time signal showed that the highest distinct resonant frequency was present at approximately 5300 Hz. Based on this analysis, a low-pass filter at 5300

Hz was applied to each of the experimental acceleration-time histories to eliminate resonance effects at and above this frequency value. Figure 5.1 shows the filtering scheme applied to the Test 1 signal as an example. It is clear that the basic trend of the curve is not affected to the point of discrediting the filtered data.

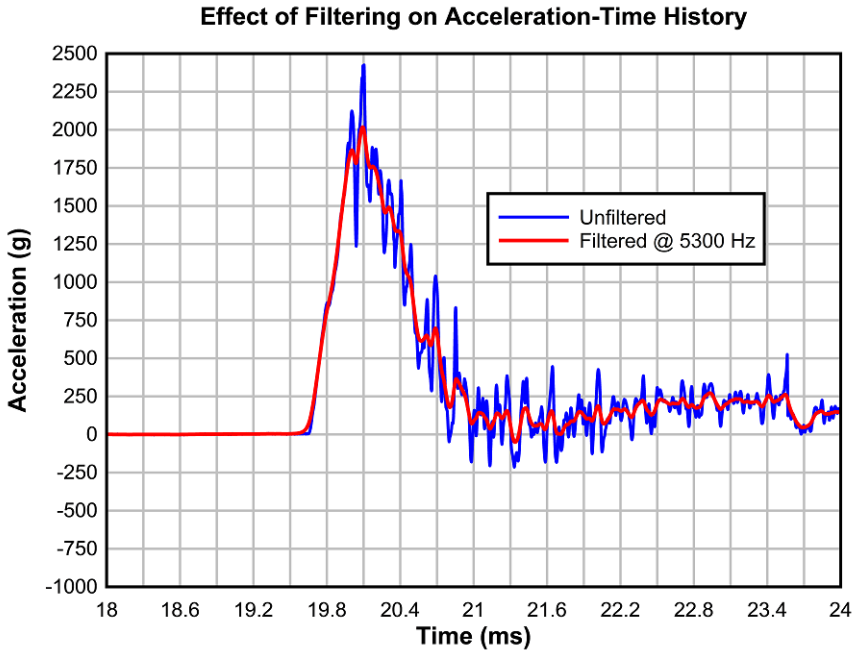

Figure 5.1: Test 1 - Comparison of Filtered and Unfiltered Data

The simulated specimen accelerations were recorded from nodes which corresponded to the locations of the accelerometers in the experimental tests as seen in Figure 5.2. Because the shock response from each actual test was calculated using the acceleration-time history with the highest peak value, the simulated specimen response curve which best represented the highest experimental peak was used for the comparisons seen in subsequent sections.

Motion for the impacting mass was simulated by simply applying an initial velocity to all components of the mass. To insure that the experimental scenario was being accurately reproduced, the assigned velocity for each model was set equal to the value recorded with TEMA in the experimental results. Because the input settings for the Blast Simulator for each test specify that the acceleration at impact is zero, it is a safe assumption to assign an initial velocity rather than simulate the entire

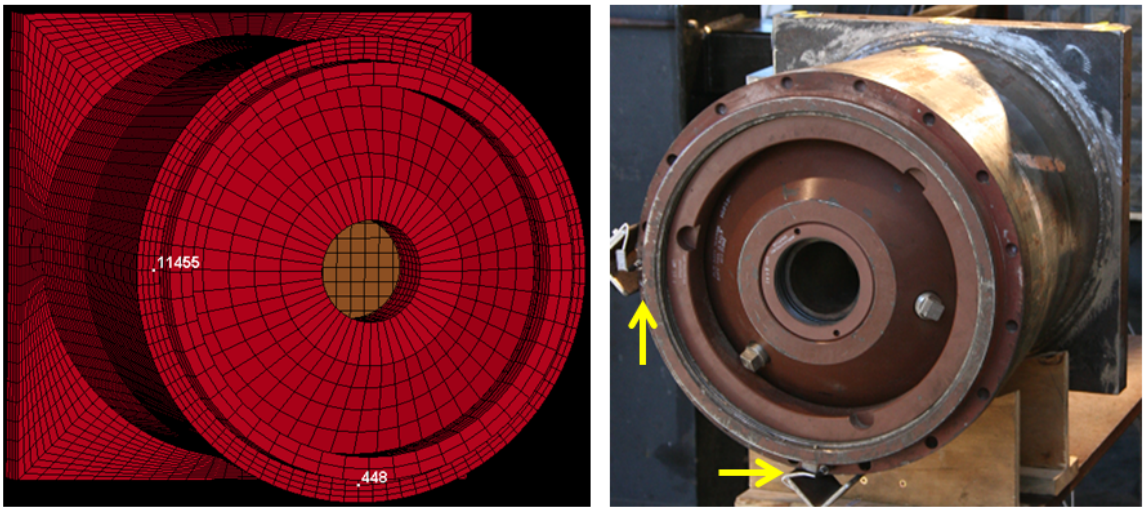

Figure 5.2: Acceleration Acquisition Locations: Numerical and Experimental

approach time of the mass.

The models were developed using the explicit function of LS-DYNA, which is designed for efficient calculations for dynamic loading events. The software automatically calculates the maximum time step based on the Courant-Friedrichs-Lewy Characteristic Length (Courant condition), which considers the ratio of smallest element thickness to sound speed in each material. If a wave can pass through an element in a time which is smaller than the set timestep, the step must be reduced to avoid instabilities.

All of the parts are modeled with fully integrated, 8-node solid elements. While being computationally more expensive than shell elements, solid elements are the better option for thick, soft elements such as those used for rubber, leather, and sand. The aspect ratio, which is the ratio between the largest and smallest dimension of an element, is no greater than 15 in any part. The majority of elements have very small ratios between 1 and 3. In LS-DYNA, the ideal aspect ratio is 1, but expecting to model complex parts with this value is unrealistic and not necessary for sufficiently accurate results. For the models being examined, the aspect ratios are low enough to produce beneficial results. Further explanation of all material models used in the simulations is provided in the LS-DYNA User's Manual [4].

5.1 Programmer

5.1.1 Material Models

The simulations for Tests 1-3 included an aluminum mass, programmer, and the test article. Four different material models were required to characterize the parts.

The aluminum mass was a standard 6061 aluminum plate with dimensions of 16x16x2.75 inches to match the geometry of the experimental mass and a weight of 60 lbs. Because the mass experienced very little deformation, rate effects were not included in the material model *MAT_PLASTIC_KINEMATIC which was used. Due to the fact that the numerical analysis needed to include the mass of the Blast Generator piston and connecting plate between the piston and impacting mass, the density of the aluminum was artificially increased to lump the entire weight of the three components in the plate. A simulation which included a geometrical model of the piston was performed but showed negligible difference from the lumped mass approach.

The parameters for the programmer material model (*MAT_SIMPLIFIED_RUBBER_WITH_DAMAGE) and geometry was provided by Aaron Freidenberg. In [6], he provides a thorough explanation and validation of the model. The only adjustment made for the following simulations was an increase of the bulk unloading modulus to 360 ksi, which is a reasonable value for adiprene as seen in [7]. The plate and programmer mesh is shown in Figure 5.3.

The test article model is composed of a metal shell for the specimen and a simple foam to represent the added mass of the internal sand mentioned in Section 4.1. While the exact material of the specimen is unknown, using high-strength steel properties with the *MAT_PLASTIC_KINEMATIC model is sufficiently close for the developed simulations. Because the response of the specimen was essentially a rigid translation in space with very minimal deformation, rate effects were not included. A density of 0.3 lbs/in^3, modulus of elasticity of 29x10^6 psi, yield stress of 60,000 psi, and poisson's ratio of 0.3 were used. The complex geometry of the specimen was carefully reproduced in order to insure accuracy of the simulated acceleration-time histories at different nodes in the part. Figure 5.4 shows the mesh of the test article

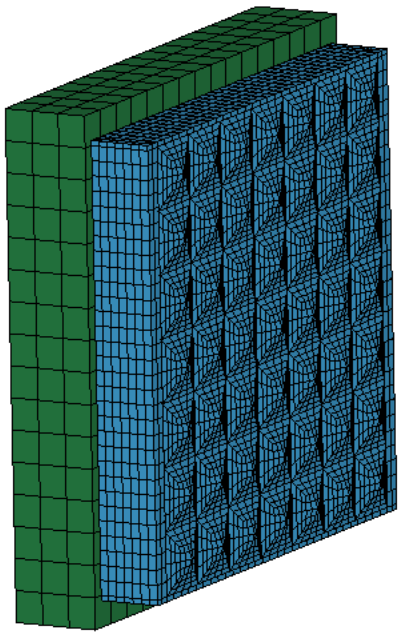

Figure 5.3: Aluminum Plate and Programmer Mesh

model which was used for all simulations. An image showing a comparison between the numerical and experimental test setups is also provided in Figure 5.5.

To model the boundary between the aluminum plate and programmer, *CONTACT_AUTOMATIC_SURFACE_TO_SURFACE_TIEBREAK was used. This contact fixes the parts together until a tension force between them exists which exceeds a set allowable limit. For all models, this limit was set to a very high value to insure that the programmer did not detach from the aluminum plate.

The impact between the programmer and specimen was modeled using *CONTACT_SURFACE_TO_SURFACE. For this contact type, slave nodes are restricted from penetrating through the surfaces of the master elements. Thus, with the programmer pyramids designated as the master surface, the specimen nodes could not pass through the impacting surface, and a proper collision occurred.

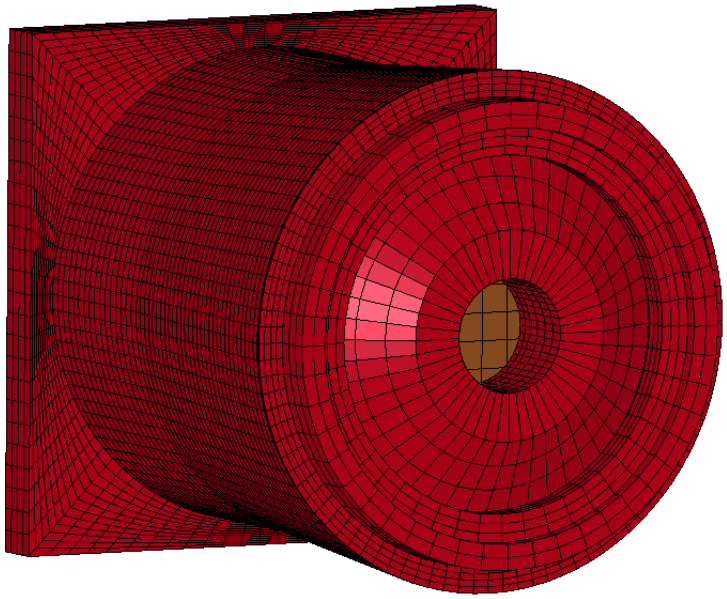

Figure 5.4: Specimen Mesh

5.1.2 Test 1

The simulation for Test 1 was able to capture the shape of the experimental acceleration-time history very well as seen in Figure 5.7. While the peak acceleration is somewhat low (83% of the true maximum value) and the duration is shorter, the basic response is clearly represented well. The simulated progression of loading displayed in Figure 5.6 shows the initial contact between programmer and specimen, full compression of the programmer, and rebound of the specimen.

With the understanding that the shock response spectrum levels off in the high frequency range at the peak acceleration value from the acceleration-time history, it is expected that the numerical result will show a lower response in this region. Also, because a longer duration for the same peak acceleration will produce a higher response in the low frequency range, it should also be expected that the numerical response will be lower in this region as well. The results in Figure 5.8 show that this is accurate. It is obvious, however, that the shape of the experimental shock response is captured well by the model.

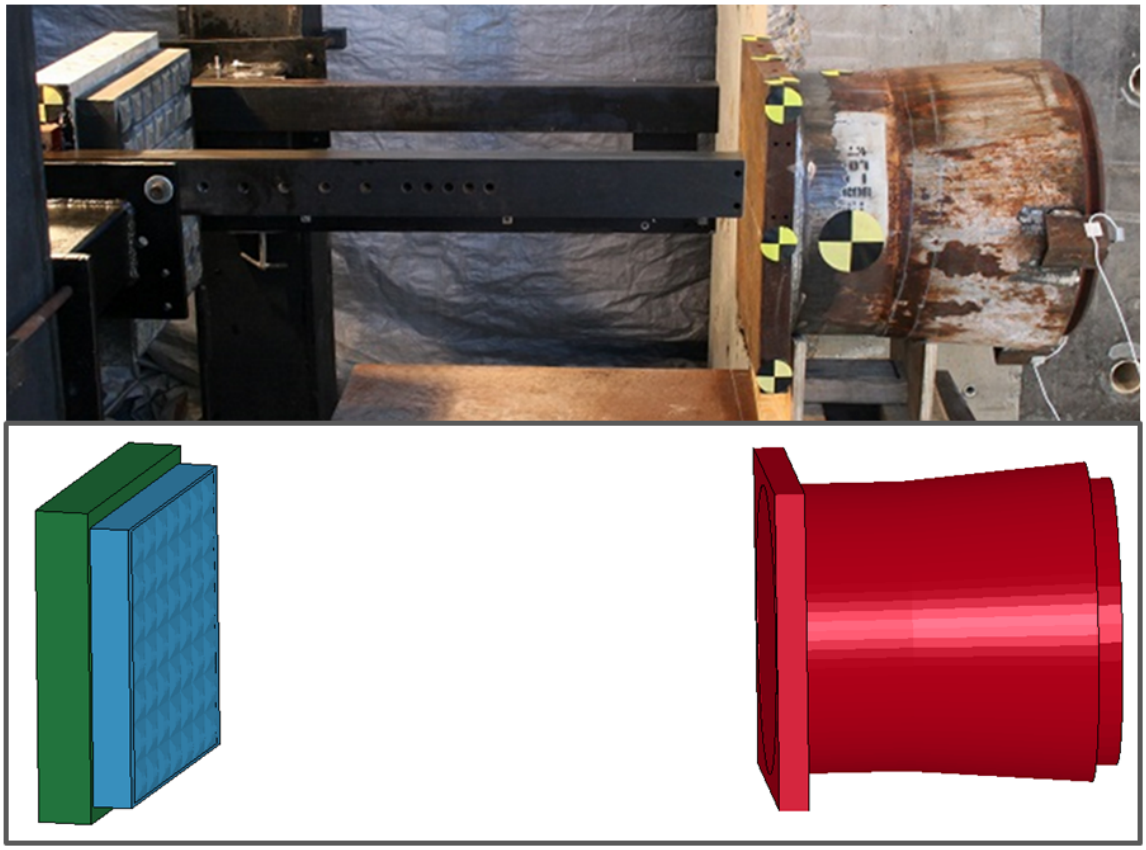

Figure 5.5: Comparison of Experimental and Numerical Setup

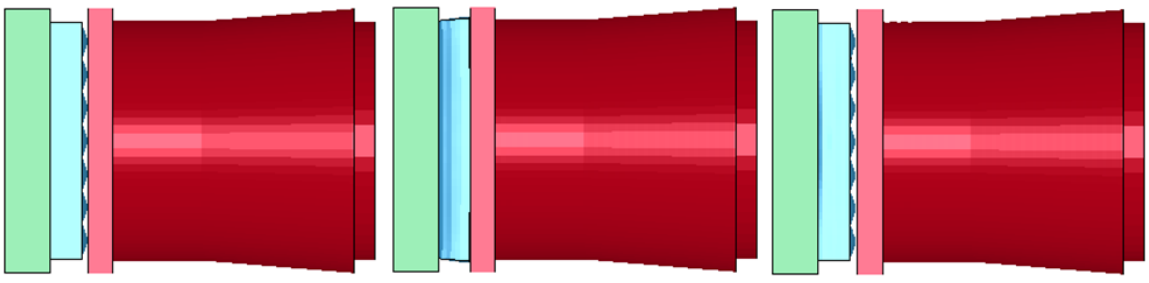

Figure 5.6: Test 1 - Simulated Progression of Loading

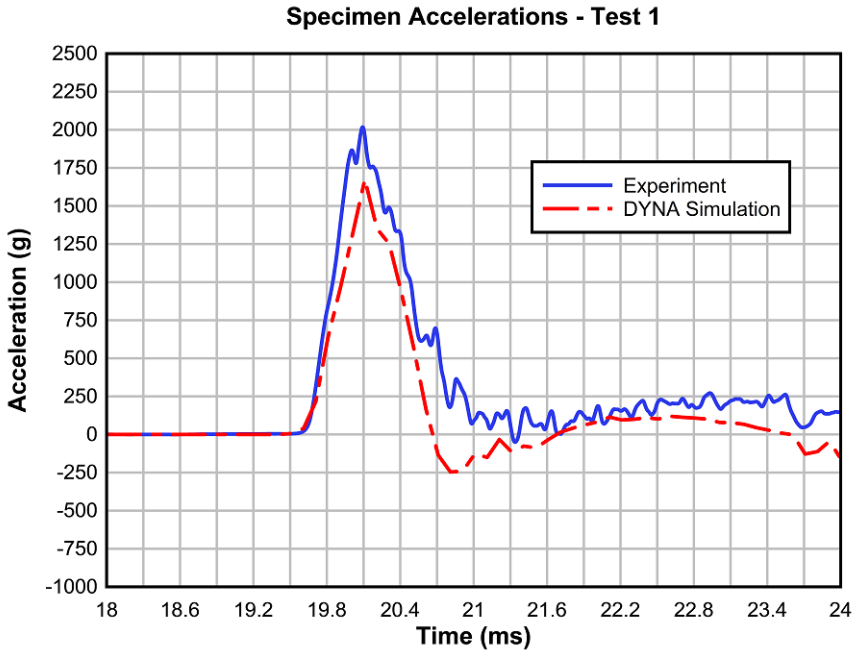

Figure 5.7: Test 1 - Comparison of Experimental and Simulation Results

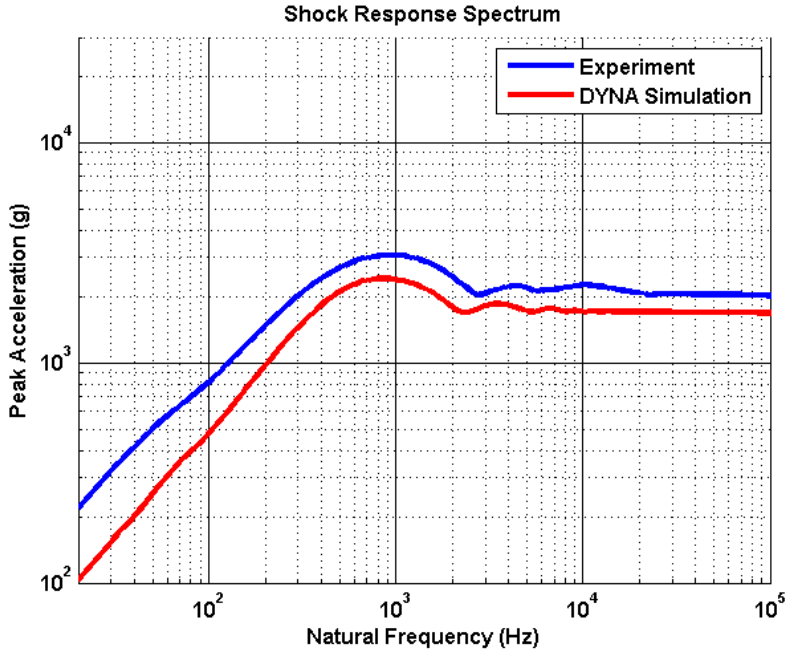

Figure 5.8: Test 1 - Comparison of Experimental and Simulation Shock Responses

5.1.3 Test 2

The simulation for Test 2 also captured the basic shape of the experimental acceleration-time history well as seen in Figure 5.10. While the peak acceleration is somewhat low (79% of the true maximum value) and the duration is slightly shorter as in Test 1, the basic response is represented well. The simulated progression of loading displayed in Figure 5.9 shows the initial contact between programmer and specimen, full compression of the programmer, and rebound of the specimen.

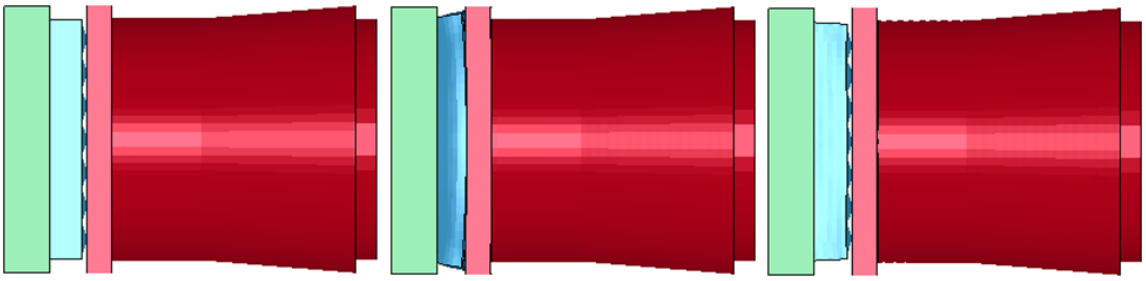

Figure 5.9: Test 2 - Simulated Progression of Loading

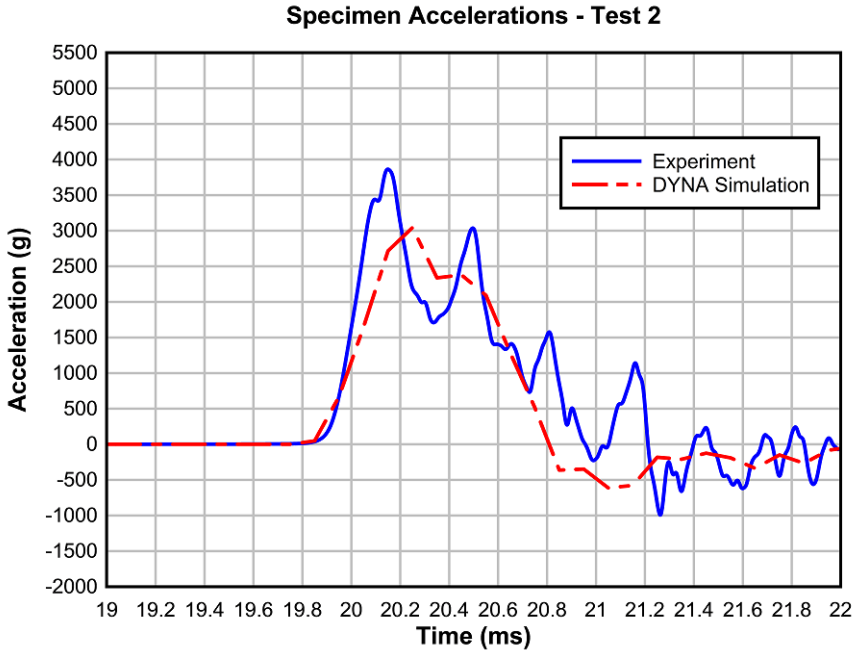

Figure 5.10: Test 2 - Comparison of Experimental and Simulation Results

As with Test 1, we see that the shock response spectrum (Figure 5.11) shows lower peak responses in both the low and high frequency ranges. However, because Test 2 did a slightly better job of capturing the loading duration, the low frequency values are relatively closer than those of Test 1.

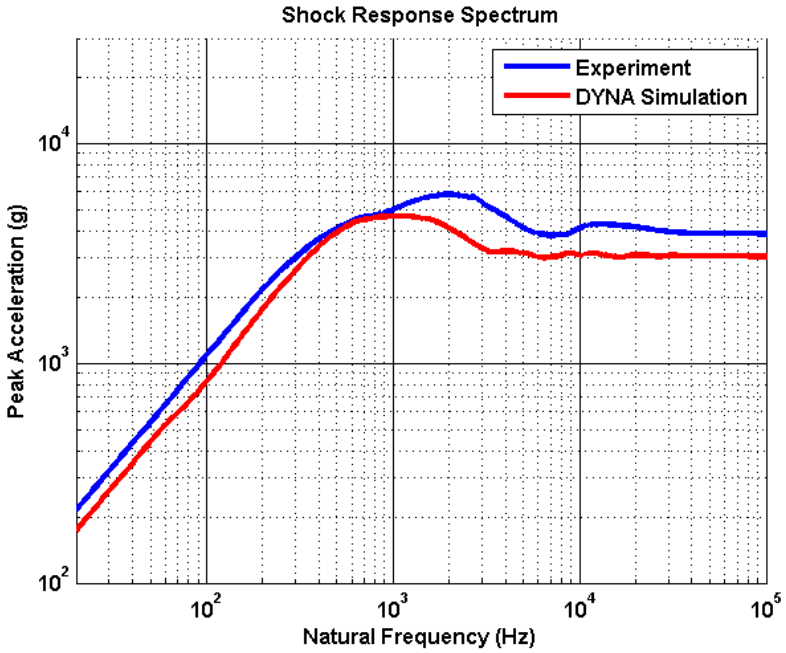

Figure 5.11: Test 2 - Comparison of Experimental and Simulation Shock Responses

5.1.4 Test 3

The simulation for Test 3 proved to be the best programmer-only simulation. While the peak acceleration is still lower than the experimental peak (87% of the true maximum value), it is relatively closer than the simulations at lower velocities. The duration is short as with the previous tests but also relatively better. Thus, the excellent representation seen in the resulting shock response spectrum is not surprising. The simulated progression of loading displayed in Figure 5.12 shows the initial contact between programmer and specimen, full compression of the programmer, and rebound of the specimen.

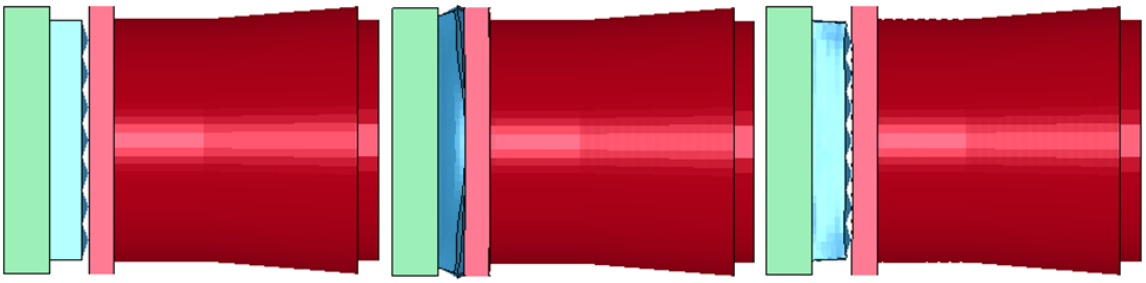

Figure 5.12: Test 3 - Simulated Progression of Loading

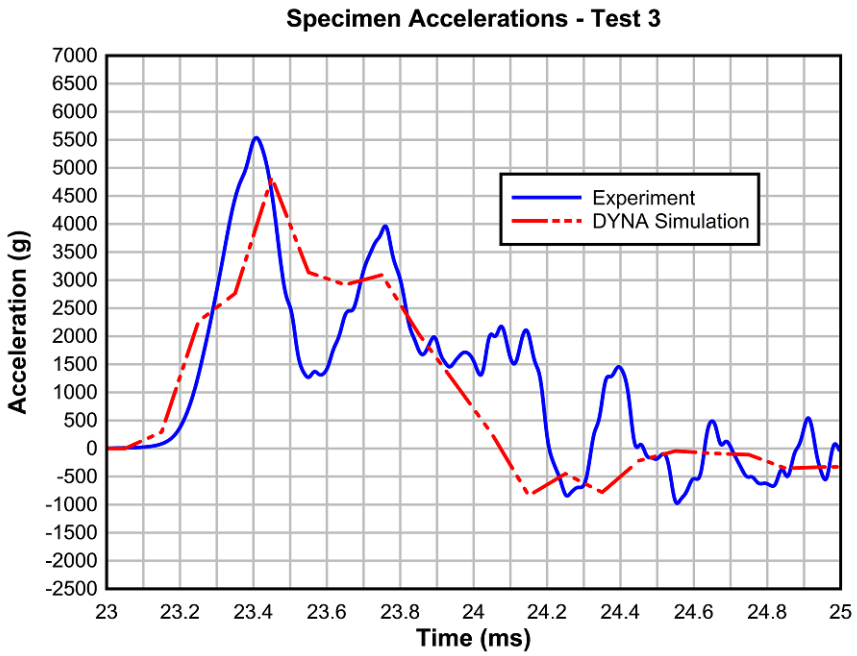

Figure 5.13: Test 3 - Comparison of Experimental and Simulation Results

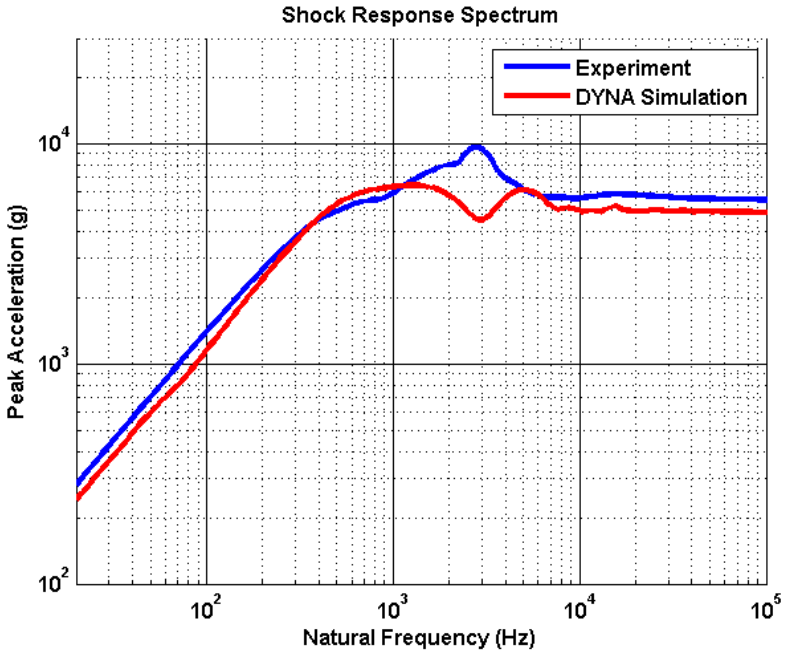

Figure 5.14: Test 3 - Comparison of Experimental and Simulation Shock Responses

5.2 Leather

5.2.1 Material Models

The simulations for Tests 9 and 10 included an aluminum mass, programmer, leather, and the test article. Five different material models were required to characterize the parts. The aluminum mass, programmer, and test article properties are explained in the Tests 1-3 material models section. The mesh used for the leather is shown in Figure 5.15.

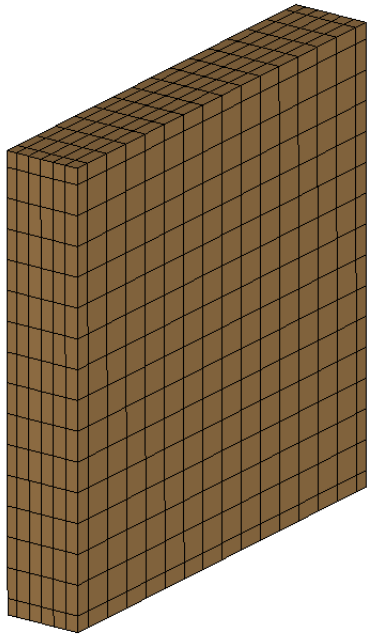

Figure 5.15: Leather Mesh

Because the characteristics of the specific leather being used for the experiments was unknown, a static force-displacement test was used to determine the mechanical properties of the material. A stack of 12x12x1/8 in leather sections was placed into the UCSD SATEC test machine (see Figure 5.17), and the depth of the stack was measured at eight different locations around the perimeter to determine an average initial thickness for strain calculations. The leather was loaded at a rate of 1 kip/sec to a maximum load of 300 kips (stress of 2,083 psi). Once the peak load was reached, the test machined paused for 3 seconds before unloading. Using the

acquired force-displacement data, the stress-strain curve shown in Figure 5.16 was produced. Because the material showed very little lateral expansion during the test, the engineering stress was calculated and assumed to be equal to the true stress. The progression of loading is shown in Figure 5.17.

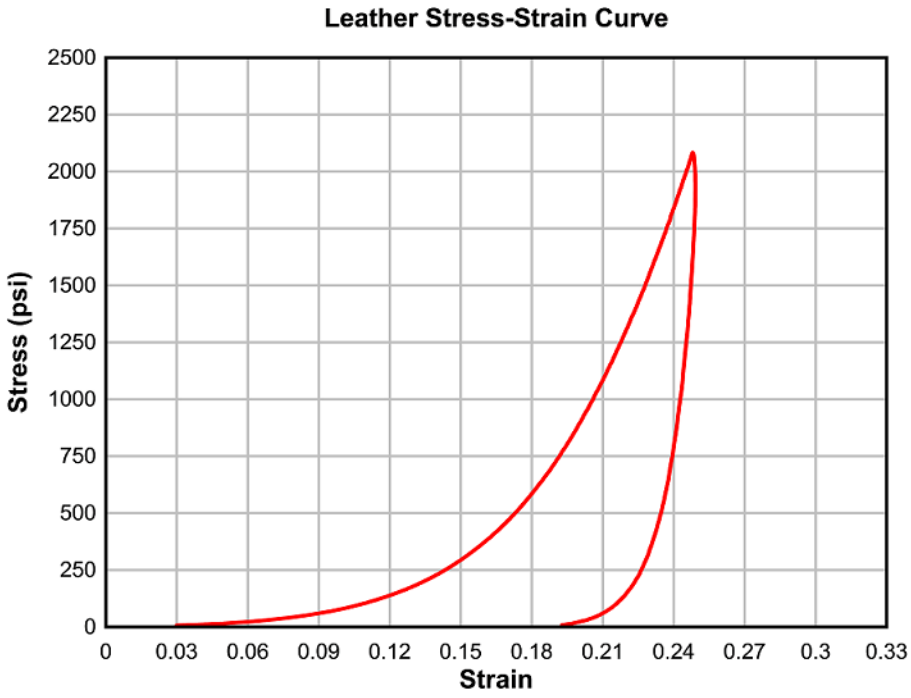

Figure 5.16: Leather Stress-strain Curve Acquired from Static Testing

The leather was modeled using *MAT_LOW_DENSITY _FOAM, which allows the user to input a stress-strain loading curve to characterize the response of the material model. In order to account for the significant difference in strain rates between the static testing ($\approx$.001 s^{-1}) and blast simulator testing ($\approx$100 s^{-1}), the stress values in the loading portion of curve seen in Figure 5.16 were doubled to better account for the rate effects of the material. As seen in [16], the adjustment of strengthening the material in the model to this degree is reasonable for leather-like materials. Figure 5.18 shows the modified input curve for the leather material model. In addition to the stress-strain curve, the model also calls for hysteretic unloading (HU), viscous damping (DAMP), and energy dissipation (SHAPE) factors to further modify the response curve. These values were iteratively adjusted to account for the

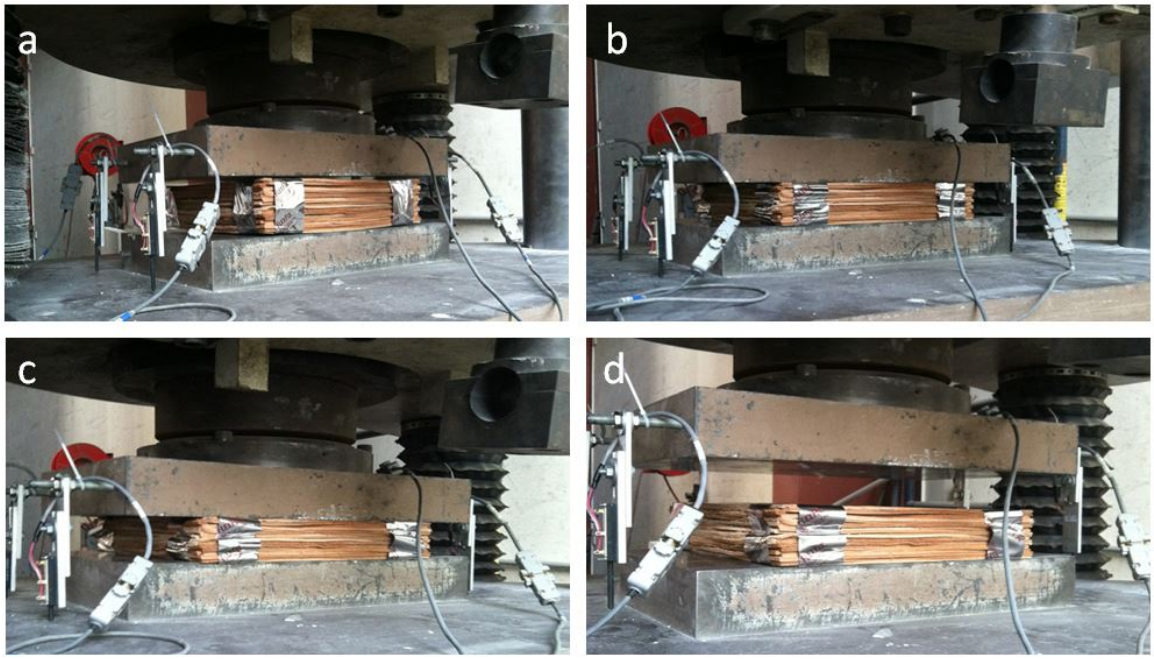

Figure 5.17: Static Testing of Leather

unloading response.

The interaction between the programmer, leather, and specimen was modeled using *CONTACT_SURFACE_TO_SURFACE to prevent the materials from penetrating one another during impact.

A comparison between the experimental impacting mass and model for Test 9 is shown in Figure 5.19. The model for Test 10 is identical with the exception of the leather thickness in the loading direction being doubled.

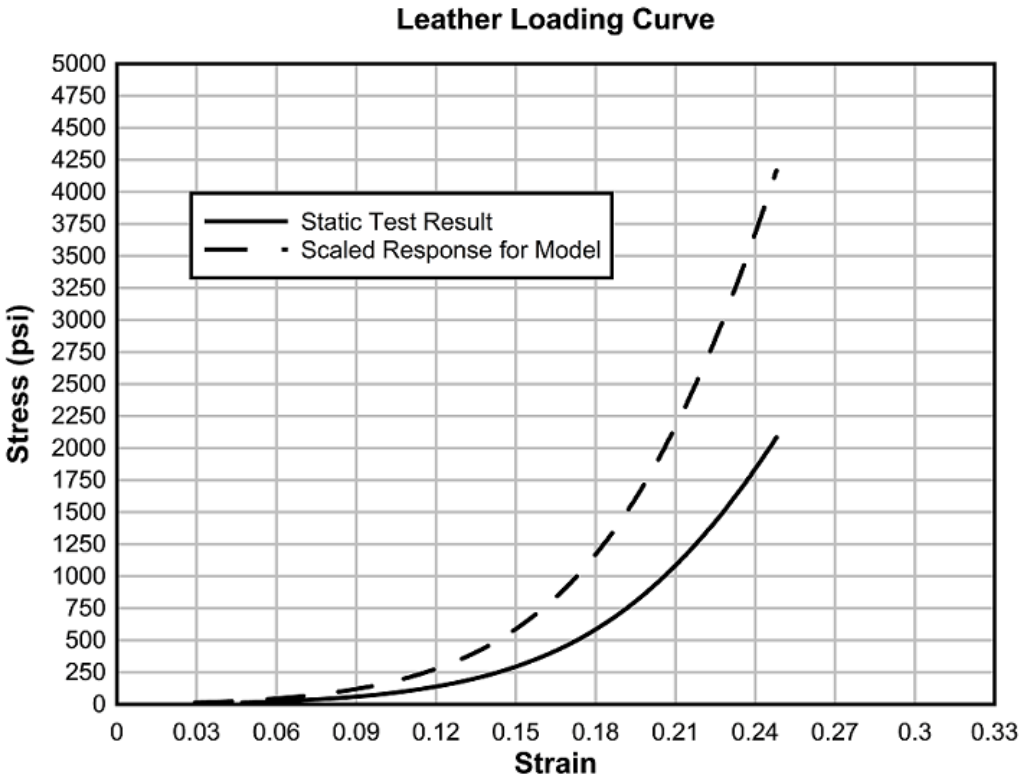

Figure 5.18: Scaling of Stress-strain Curve to Account for Rate Effects in Material Response

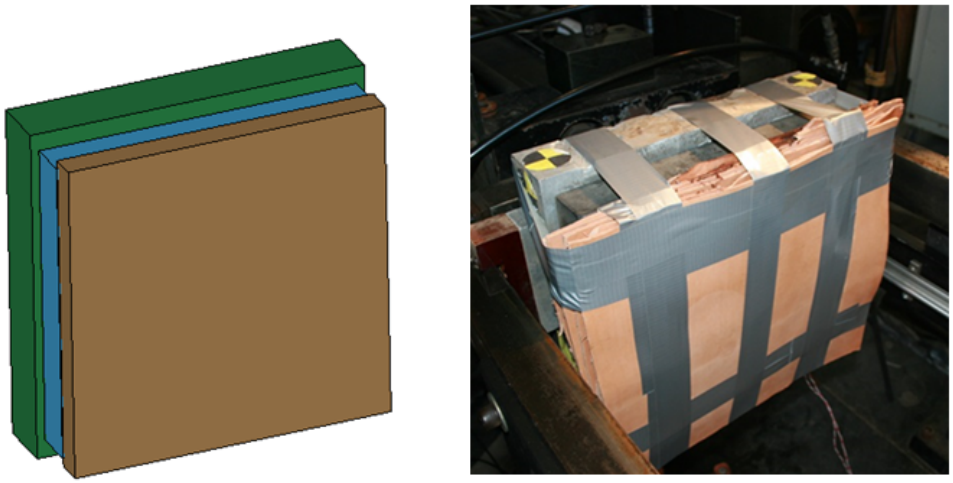

Figure 5.19: Comparison of Numerical and Experimental Impacting Mass Configurations

5.2.2 Test 9

The simulated progression of loading displayed in Figure 5.20 shows the initial contact between the leather and specimen, full compression of the programmer and leather, and rebound of the specimen. As in the experimental test, the leather stack flies away from the impacting mass (following the specimen) after impact.

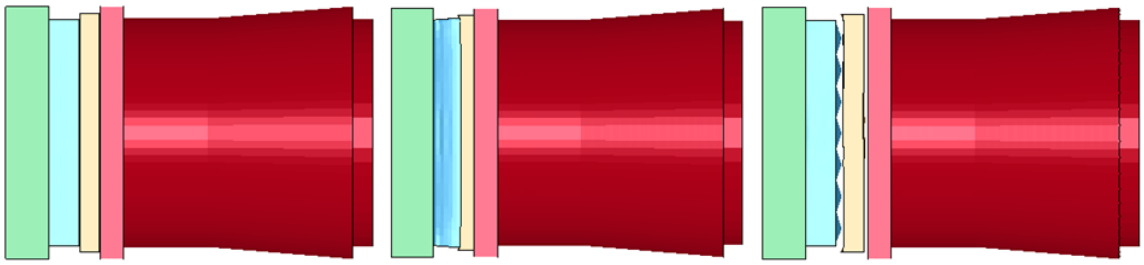

Figure 5.20: Test 9 - Simulated Progression of Loading

Both the pulse duration and peak acceleration values obtained in the experimental test are simulated well by the model as seen in Figure 5.21. The maximum acceleration is only 5% higher than the experimental value, and the duration is only slightly shorter as seen at the right end of the pulse. Because of these results, it should be expected that the experimental and numerical shock response spectrums match very well in the high-frequency range and show the numerical response being slightly lower in the low-frequency range. Figure 5.22 shows that these expectations are accurate.

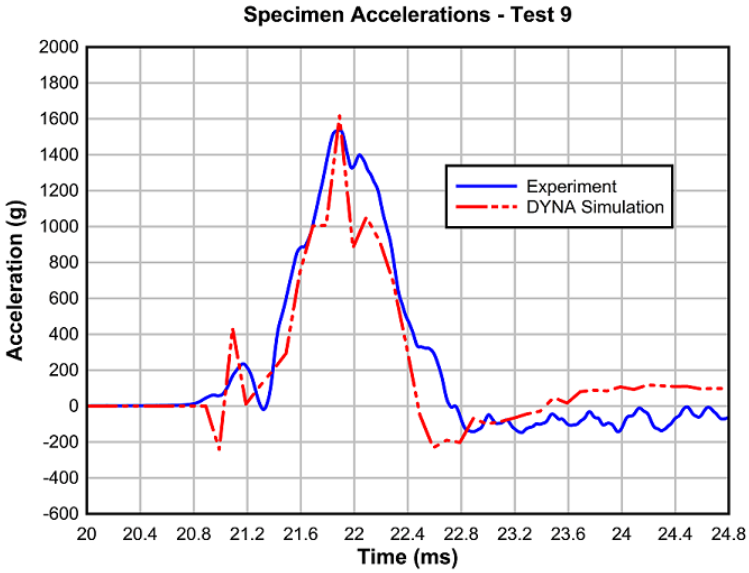

Figure 5.21: Test 9 - Comparison of Experimental and Simulation Results

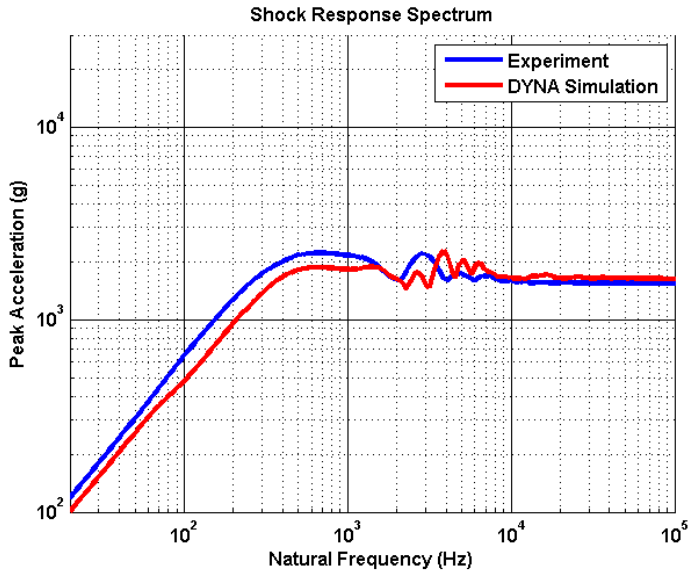

Figure 5.22: Test 9 - Comparison of Experimental and Simulation Shock Responses

5.2.3 Test 10

The progression of loading displayed in Figure 5.23 shows the initial contact between the leather and specimen, full compression of the programmer and leather, and rebound of the specimen. As in the experimental test, the leather stack flies away from the impacting mass (following the specimen) after impact.

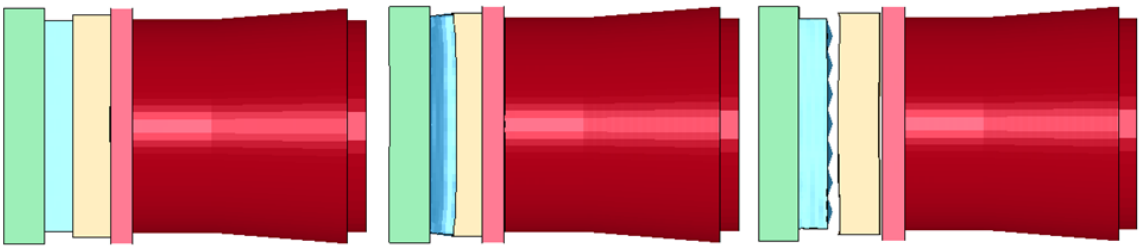

Figure 5.23: Test 10 - Simulated Progression of Loading

The model for Test 10 provided an excellent simulation for the experimental test as seen in Figure 5.24. Both the peak acceleration and pulse duration values match the experimental results nearly perfectly. In addition, the model was able to capture the initial smaller peak which occurs before the main pulse. The excellent representation by the DYNA simulation in the shock response spectrum comparison plot (Figure 5.25) in both the low-frequency and high-frequency regions is expected.

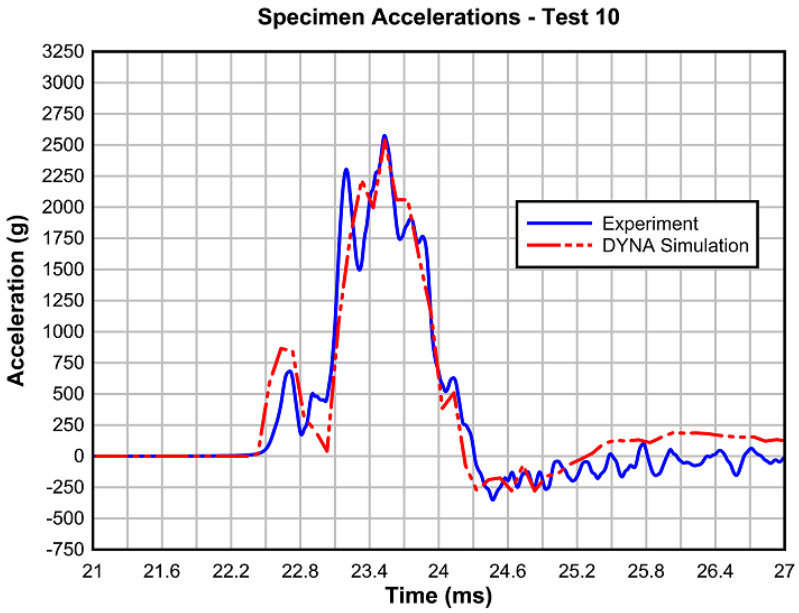

Figure 5.24: Test 10 - Comparison of Experimental and Simulation Results

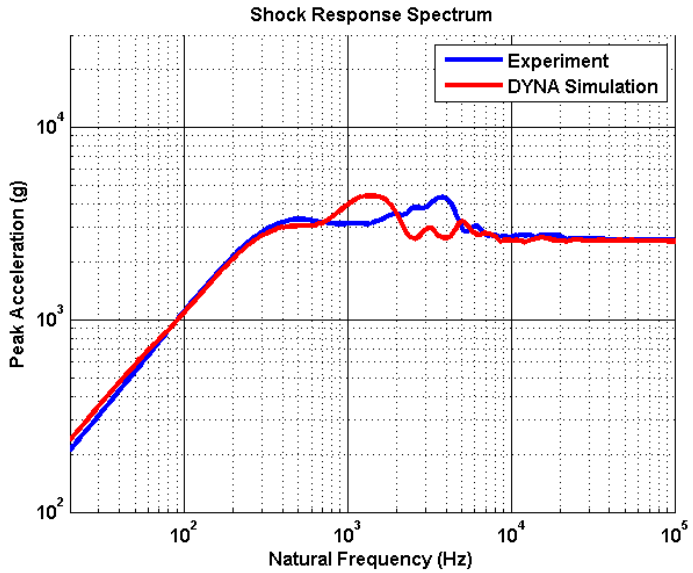

Figure 5.25: Test 10 - Comparison of Experimental and Simulation Shock Responses

5.3 Confined Sand

5.3.1 Material Models

The simulations for Tests 16 and 17 included an aluminum mass, programmer, sand, steel confining box, and the test article. Five different material models and six different parts were required to characterize the components. The aluminum mass, programmer, and test article properties are explained in the programmer material models section.

The confining box was modeled using *MAT_PLASTIC_KINEMATIC and typical steel properties explained in the material models section for Tests 1-3. Because the rapid lateral expansion of the sand often induced significant bending in the perimeter plates of the box, rate effects were included. The model allows the option of using a Cowper Symonds strain rate model which automatically scales the yield stress in proportion to the following factor:

$$1 + \left(\frac{\dot{\epsilon}}{C}\right)^{1/p} \tag{5.1}$$

where $\dot{\epsilon}$ is the strain rate and C and p are user-defined parameters which relate to the material sensitivity to strain rate. Alves [3] provides a range of appropriate values for these parameters for mild steel. The model uses $C = 550s^{-1}$ and $p = 3.4$.

To properly reproduce the geometry of the experimental confining box, outer dimensions of 19x19x7.5 in and inner dimensions of 18x18x6.5 in were specified for the model. As in the experiments, the aluminum plate extended 1 in into the box.

The layer of soft foam which held the sand in place in the confining box was modeled using *MAT_BLATZ-KO_FOAM, which simply allows the user to define a density and shear modulus for the material. The density was set to .01 lbs/in^3, and the shear modulus was set to 20,000 psi. Because modeling instabilities were encountered when using a small shear modulus, the value was artificially increased to this unrealistically large value in order to avoid these problems. In comparison to the other components, the foam has minimal effect on the transfer of load from the mass to the specimen and, thus, the adjustment is not critical. The mesh for the steel confining box and foam perimeter is shown in Figure 5.26.

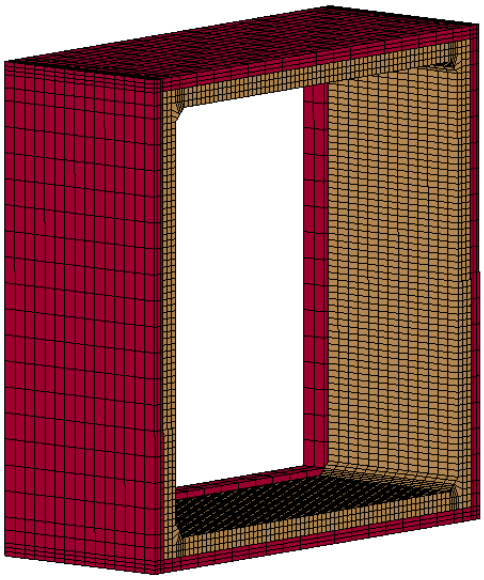

Figure 5.26: Confining Box and Foam Perimeter Mesh

The sand was modeled using *MAT_SOIL_AND_FOAM, which uses the deviatoric perfectly plastic yield function:

$$\phi = J_2 - \left[a_0 + a_1 p + a_2 p^2\right] \tag{5.2}$$

where $J_2 = \frac{1}{2}\sigma_{ij}\sigma_{ij}$ is the second invariant, p is the pressure, and a_0, a_1, a_2 are coefficients determined by the user. A study on impact testing of confined sand was conducted by NASA [5] and produced input material property values for the same LS-DYNA material model. Because the Blast Simulator testing included confinement of the sand, these values were determined to be good starting points for characterizing the material for the Test 16 and 17 simulations. After further analysis was conducted, the values shown in Table 5.1 proved to be the most effective for modeling the sand used in the Blast Simulator tests. The yield surface coefficients correspond to the a_0, a_1, and a_2 coefficients in the yield function.

Because the impact face of the sand in the experimental layout was not perfectly flat with respect to the specimen impact plate, the model includes a curved surface for characterizing the impact side of the sand mass. The mesh used for the sand in Tests 16 and 17 is shown in Figure 5.27.

Table 5.1: Sand Material Model Properties

Material Property	Value
Density	.063 lbs/in^3
Bulk Unloading Modulus	7,500 psi
Shear Modulus	375 psi
Yield Surface Coefficient (a_0)	0 (psi)^2
Yield Surface Coefficient (a_1)	0 (psi)
Yield Surface Coefficient (a_2)	0.6

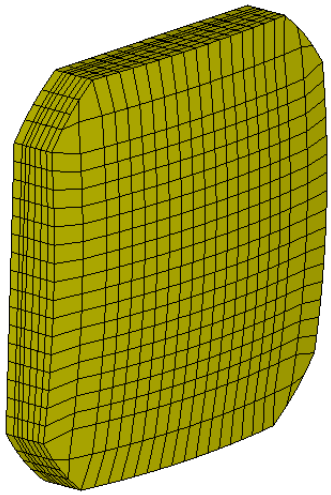

Figure 5.27: Sand Mesh

The sand model elements experienced significant deformation after the completion of loading and became unstable. To eliminate the unrealistic stretching of the elements as the sand was released from the confining box (following the specimen), *MAT_ADD_EROSION was used to delete the elements at a particular maximum principal strain level. Because these high strains were not encountered for nearly all elements until after loading was completed, this approach had very minimal effect on the acceleration-time history response of the specimen model.

The confining box was fixed to the aluminum using *CONTACT_ AUTOMATIC_SURFACE_TO_SURFACE_TIEBREAK, and the interaction between the sand and the programmer, aluminum, and confining box was modeled using *CONTACT _SINGLE_SURFACE, which is useful for materials undergoing large deformations be-

cause it prevents penetration of both surfaces of other parts and other surfaces of the same part. Because of the unpredictable nature of the sand model as it expanded within the confining box, the single surface option proved to be the most effective option for keeping the sand within the rest of the assembly.

A comparison between the experimental impacting mass and numerical model is shown in Figure 5.28. Because only the impact velocity varied between Test 16 and 17, this geometry was used for both simulations. Figure 5.29 provides a wire view of the assembly displaying the stacking of the programmer and sand.

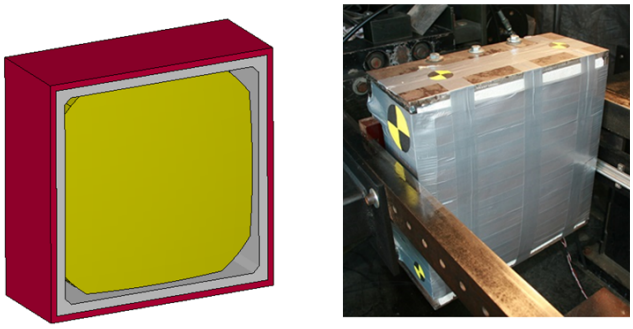

Figure 5.28: Comparison of Numerical and Experimental Impacting Mass Assemblies

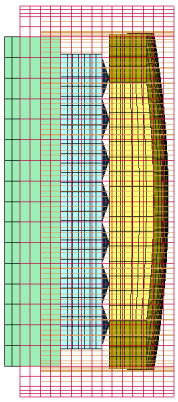

Figure 5.29: Impacting Mass with Wire View of Confining Box

5.3.2 Test 16

The simulated progression of loading displayed in Figure 5.30 shows the initial contact between the sand and specimen, full compression of sand within the confining box, and rebound of the sand and specimen. A transparent view is prescribed to the confining box and foam perimeter in order to show the response of the sand. It is important to note the gap between the perimeter edges of the programmer (blue) and confining box. The expanding sand seen in the second and third frames is filling in this air void rather than penetrating into the programmer material.

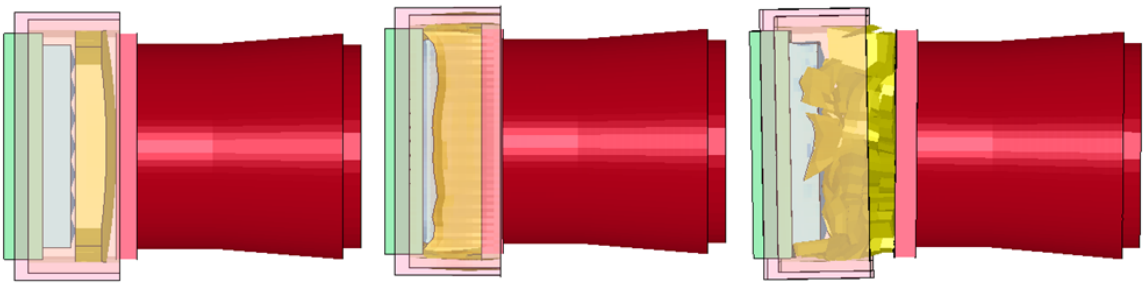

Figure 5.30: Test 16 - Simulated Progression of Loading

As seen in Figure 5.31, the simulation for Test 16 captured the shape of the experimental acceleration-time history very well in the first half of the signal. After representing the pulse well up to the peak acceleration, the model shows lower acceleration values in the second half of the pulse than those obtained by the experimental data acquisition. Also, it shows a longer duration by almost 1 ms. Despite these differences, it is reasonable to expect that the shock response spectrums may still correspond reasonably well for two reasons. First, the area under the numerical acceleration curve approximately matches that of the experimental curve due to the combination of the low values within the experimental pulse range and high values beyond the end of the experimental pulse. Second, the peak response is matched very well, which will cause the responses in the high-frequency range to be very similar. Figure 5.32 shows the shock response spectrum results.

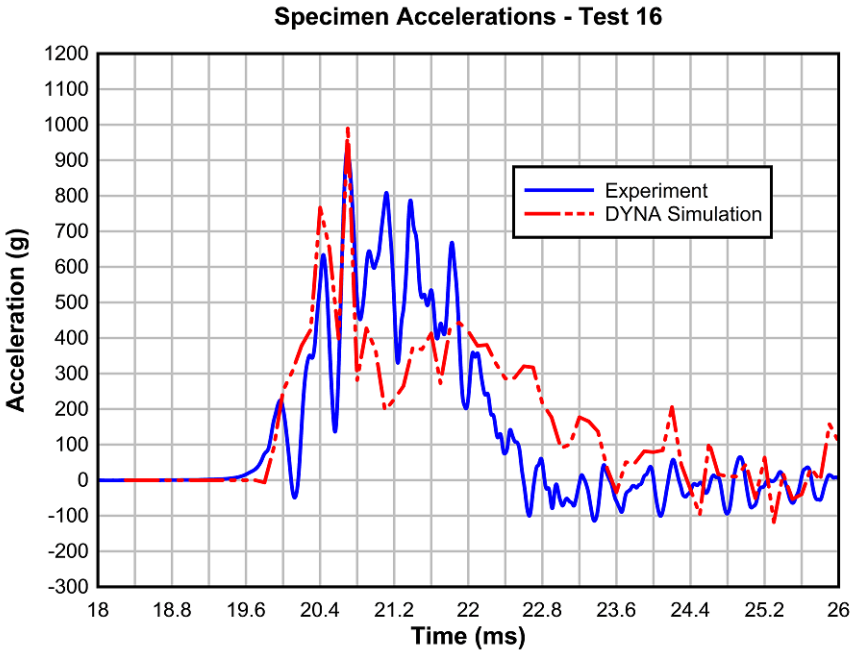

Figure 5.31: Test 16 - Comparison of Experimental and Simulation Results

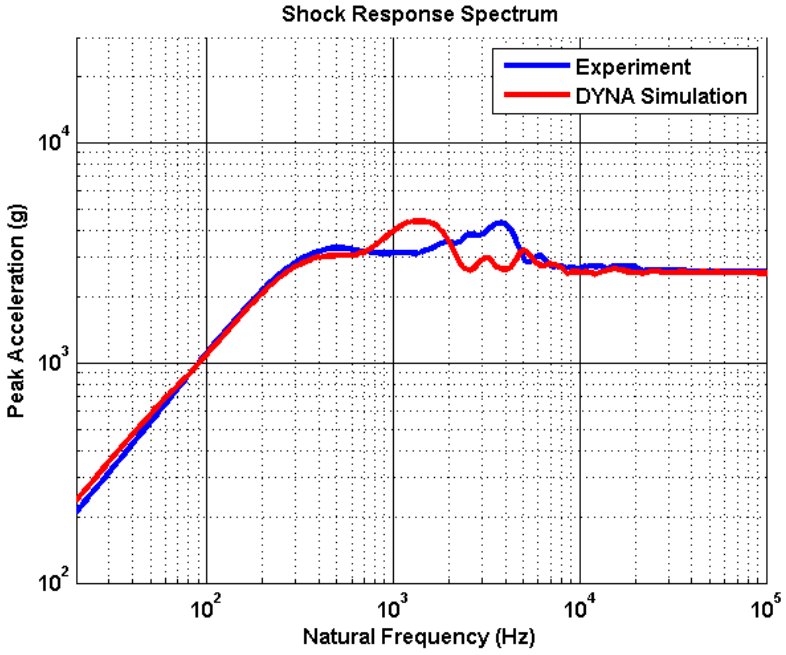

Figure 5.32: Test 16 - Comparison of Experimental and Simulation Shock Responses

5.3.3 Test 17

The simulated progression of loading displayed in Figure 5.33 shows the initial contact between the sand and specimen, full compression of sand within the confining box, and rebound of the sand and specimen. While deformation of the confining box perimeter plates was observed during the experimental series, the bending seen in the second frame of the simulation progression is larger than that observed during the test. The confining box model could be improved by tuning the strain rate parameters in the material model to better limit these deformations.

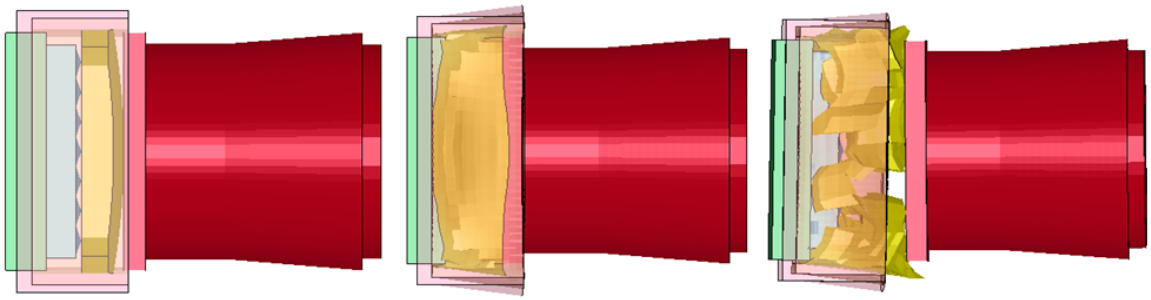

Figure 5.33: Test 17 - Simulated Progression of Loading

The simulation for Test 17 produced an acceleration-time history response which matches the experimental results very well as displayed in Figure 5.34. The peak acceleration is slightly low (93% of the true peak), but the duration and trend of the curve is represented well across the entirety of the signal. Based on these observations, it would be expected that the shock response spectrum would show approximately matching curves in the low-frequency region but slightly lower values for the numerical study in the high-frequency region. These expectations are shown to be true in the response spectrum displayed in Figure 5.35.

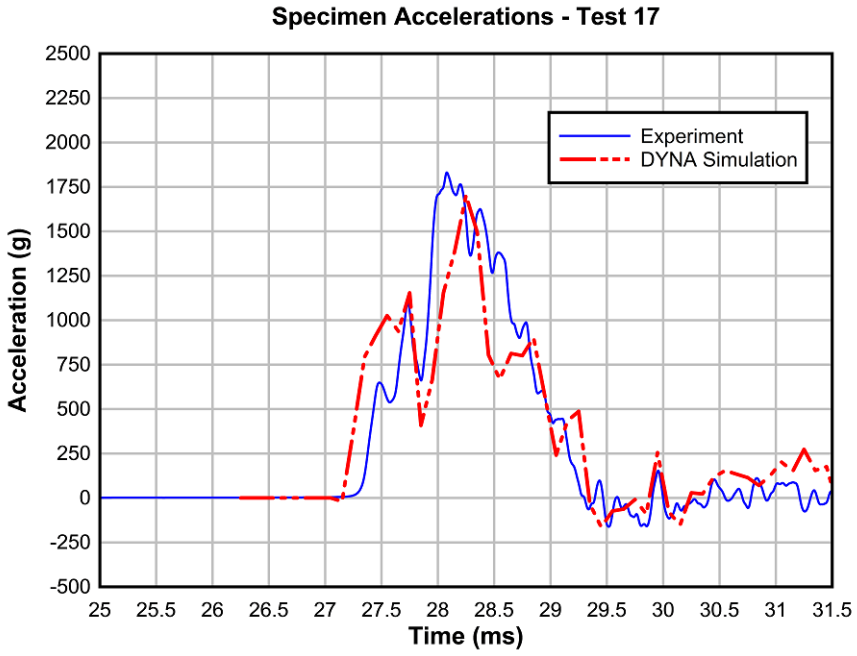

Figure 5.34: Test 17 - Comparison of Experimental and Simulation Results

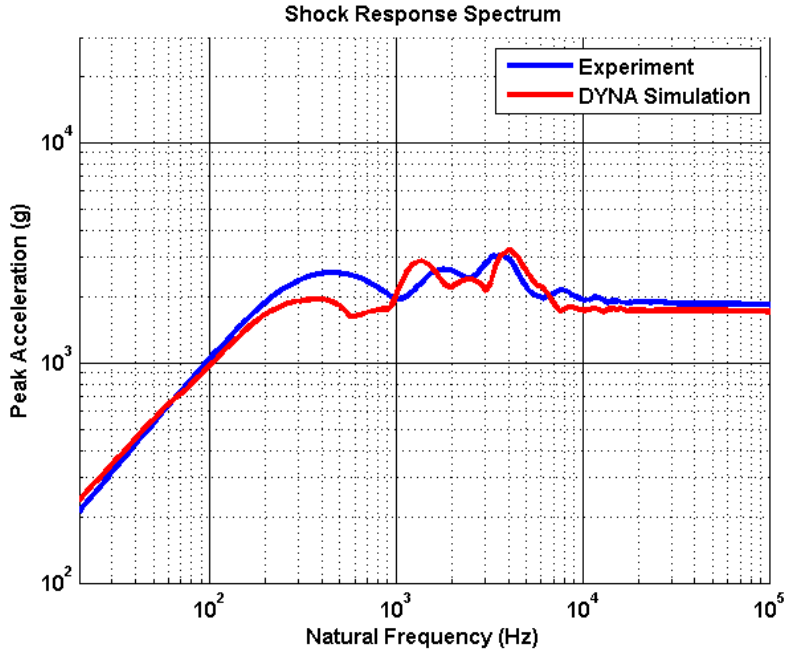

Figure 5.35: Test 17 - Comparison of Experimental and Simulation Shock Responses

5.4 Confined Sand and Leather

The most impressive shocks in the experimental series were produced using a combination of sand and layered leather. Thus, producing a reliable model which represented the loading patterns produced by this configuration was important. Upon successful calibration of the leather and sand models individually, the materials were combined to produce an assembly which simulated the impacting mass used in Test 18, which was conducted with a target impact velocity of 40 m/s in the experimental series. Because the weight of sand in the test was equal to 60 lbs rather than 40 lbs as in Test 16 and 17 and the leather was stretched over the sand with an arched layout, the geometry of the DYNA models had to be adjusted. Figure 5.36 shows the mesh of the new sand and leather geometries, and Figure 5.37 shows a comparison of the experimental and numerical impacting mass assemblies.

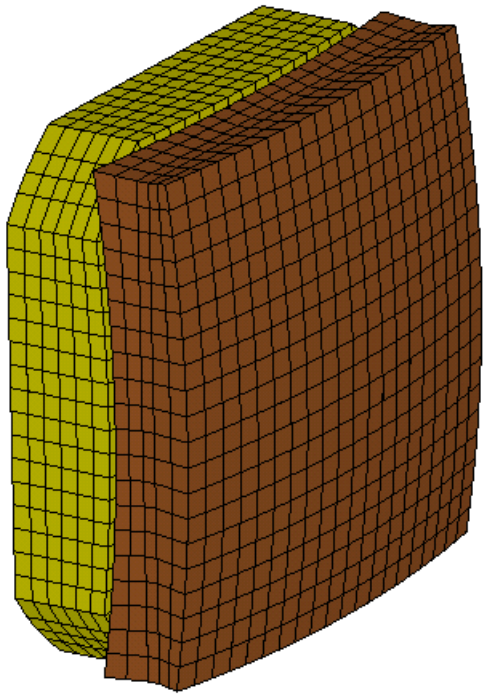

Figure 5.36: Mesh for Combined Sand and Leather

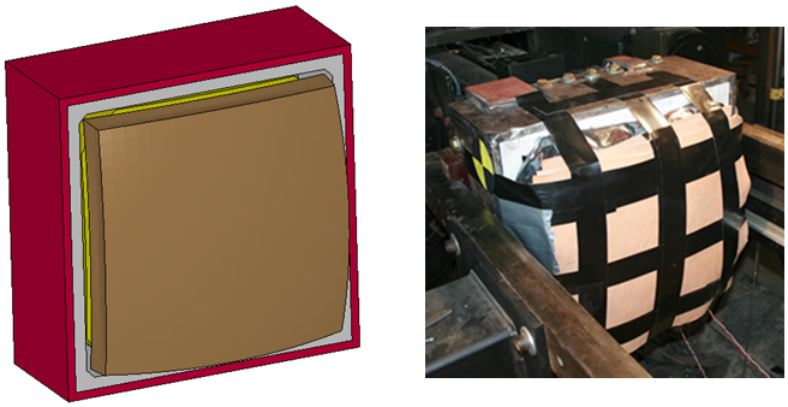

Figure 5.37: Comparison of Numerical and Experimental Impacting Mass Assemblies

5.4.1 Test 18

The simulated progression of loading displayed in Figure 5.38 shows the initial contact between the leather and specimen, full compression of the sand and leather within the confining box, and rebound of the sand, leather, and specimen. A transparent view is prescribed to the confining box and foam perimeter in order to show the response of the sand and leather.

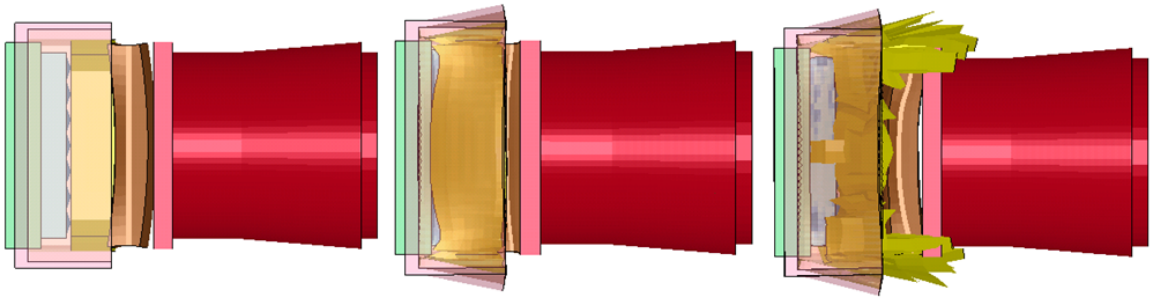

Figure 5.38: Test 18 - Simulated Progression of Loading

Considering the complexity of the loading arrangement and high energy levels present from the impact at approximately 40 m/s, the simulation for Test 18 produced an acceleration-time history response which matches the experimental results reasonably well (Figure 5.34). The peak acceleration is noticeably high (15% higher

than the true peak), but the trend of the curve is represented well, particularly in the first half of the pulse. The duration seen in the simulation corresponds well to the experimental value, but the area under each of the curves is different due to the sharp drops seen in the model response. Because of these oscillations in the response, the outcome of the shock response spectrum is somewhat unpredictable. While it is obvious that the model will produce larger values in the high-frequency region than the experimental results, it is difficult to say where the values in the low-frequency region will fall. The shock response comparison between the numerical and experimental results is shown in Figure 5.35.

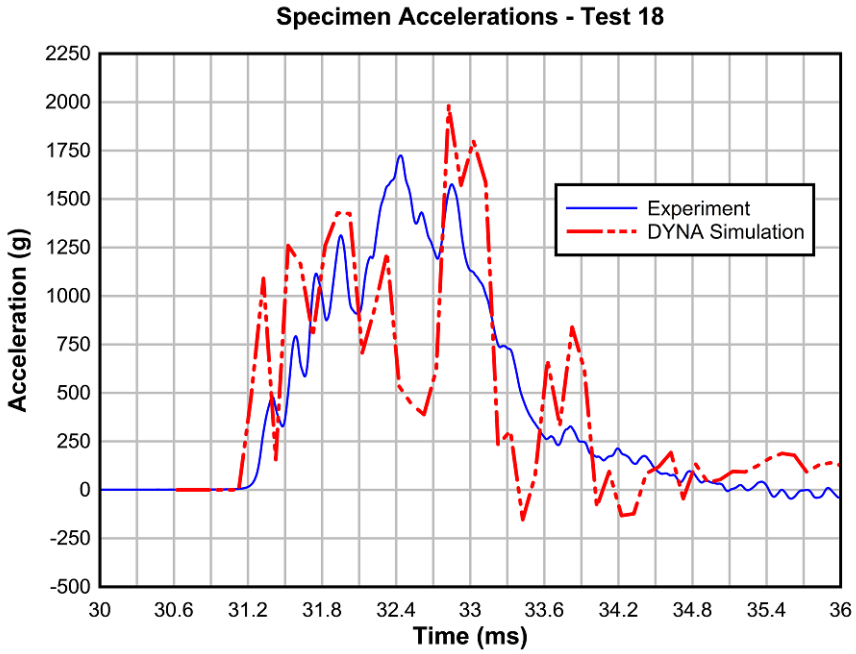

Figure 5.39: Test 18 - Comparison of Experimental and Simulation Results

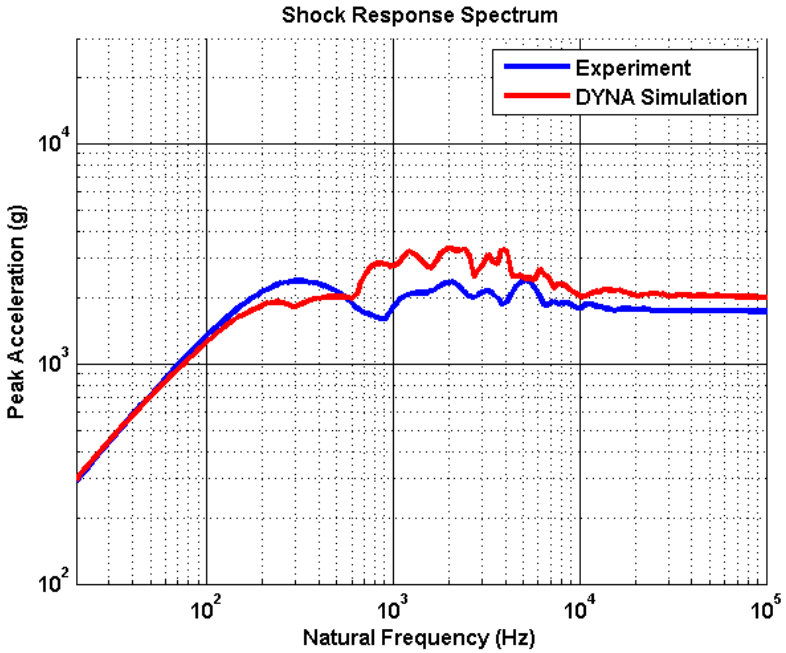

Figure 5.40: Test 18 - Comparison of Experimental and Simulation Shock Responses

5.5 Predictive Models

The set of calibrated models provided in the previous sections can be used to extrapolate to other loading arrangements for the purpose of predicting the expected specimen responses in corresponding experimental tests. The following three simulations with programmer, sand, and a combination of leather and sand show the acceleration-time history results which should be anticipated (after filtering) from tests conducted with an impact velocity of 25 m/s. In addition to the specimen acceleration response, a shock response spectrum is provided for each model. Because no tests were actually run at 25 m/s, these simulations provide valuable insight into the usefulness of running tests for these impactor configurations at this impact velocity. If a specific shock response objective was provided for the steel specimen as discussed at the end of Chapter 4, the models would show with a reasonably high level of accuracy whether or not such an objective would be met with the arrangement. Should the simulations show that the specified impactor arrangements and target velocity were not acceptable for producing the desired specimen response, the models could be adjusted until this goal was met. Consequently, less experimental test iterations, time, and money would be required to characterize the specified shock environment.

5.5.1 Programmer with Impact Velocity of 25 m/s

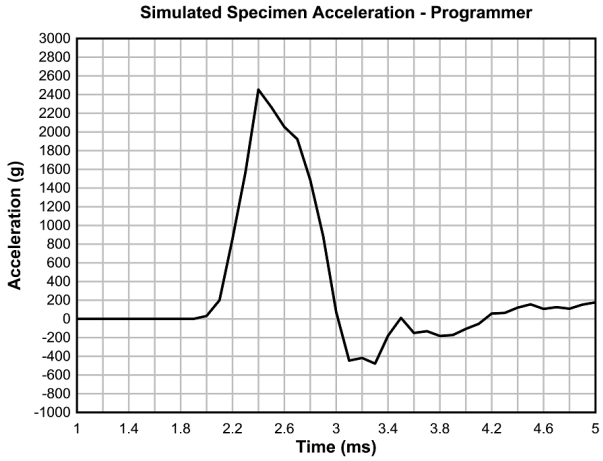

Figure 5.41: Simulation Result for Programmer Impact at 25 m/s

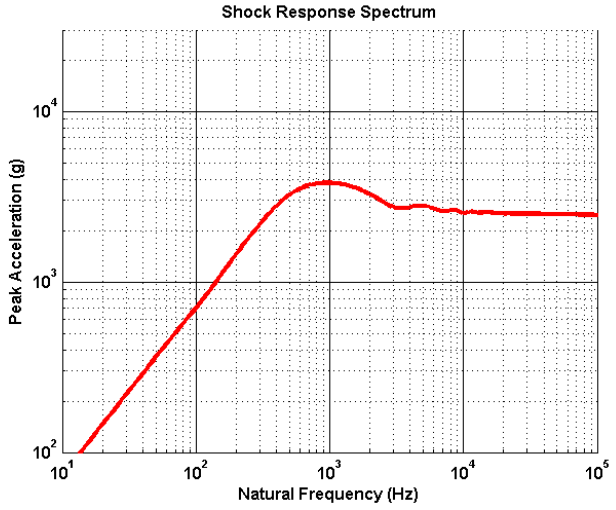

Figure 5.42: Simulated Shock Response for Programmer Impact at 25 m/s

5.5.2 Sand with Impact Velocity of 25 m/s

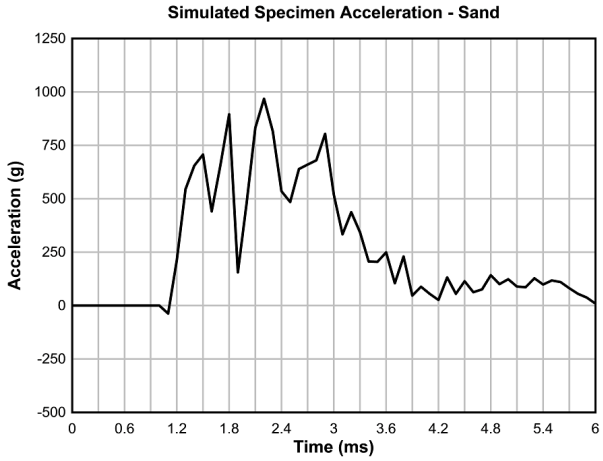

Figure 5.43: Simulation Result for Sand Impact at 25 m/s

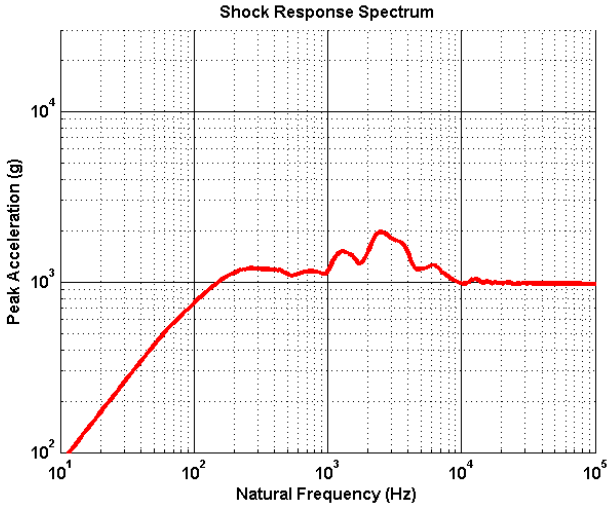

Figure 5.44: Simulated Shock Response for Sand Impact at 25 m/s

5.5.3 Combination of Sand and Leather with Impact Velocity of 25 m/s

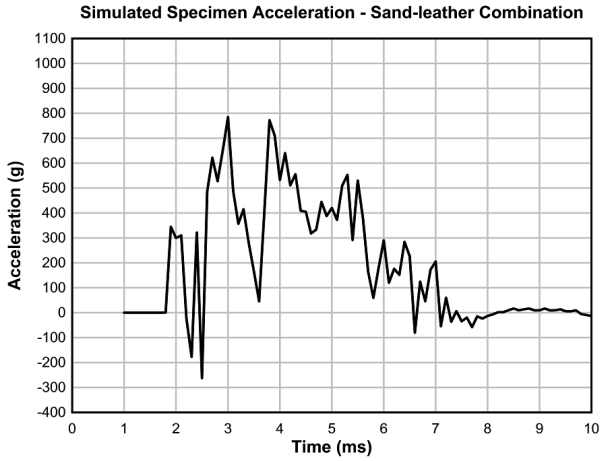

Figure 5.45: Simulated Result for Sand-Leather Impact at 25 m/s

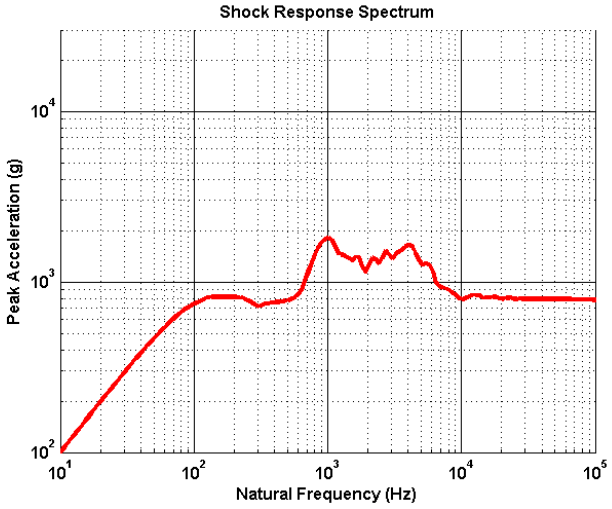

Figure 5.46: Simulated Shock Response for Sand-Leather Impact at 25 m/s

Chapter 6

Conclusions

6.1 Summary

This thesis provided an examination of the response of a steel cylinder to shock loading. Using various loading techniques with the UCSD Blast Simulator, a wide range of shock loads was produced. The shock response spectrum was used to analyze the results and make comparisons between data sets of different experimental arrangements. Numerical models were developed and calibrated for the purpose of predicting the ability of the Simulator to produce shock loads which were not seen in experimental testing.

Chapter 2 presented information on the fundamentals of shock loading and application to specific structures and testing techniques. The effectiveness of the shock response spectrum for both analysis and design of structural and mechanical components was described, as well as the underlying theory upon which the method operates. The chapter provided insight into the usefulness of the acceleration-time history and shock response data plots which are seen in Chapters 4 and 5.

Chapter 3 provided information on the UCSD Blast Simulator and its function of inducing both blast-like loads and mechanical shock loads. Operational components of the simulator and previous test series which showed the use of device for various types of test arrangements was also discussed. The explanations were valuable for showing the ability of the Blast Simulator to produce the types of loading which would be seen in Chapter 4 for the experimental series.

Chapter 4 presented a full description and analysis of the experimental test series. The test and data acquisition setup was briefly described to provide insight into the approach for loading the test article. Loading configurations for programmer, foam, leather, sand, and a combination of sand and leather at various impact velocities were discussed. Acceleration-time histories and corresponding shock response spectrums were provided to show the effectiveness of each approach as a shock-loading technique. Comparisons were made between the methods in order to display the varying types of shocks which were produced by the Blast Generators. The results showed that the Blast Simulator is capable of producing a wide range of shocks with varying characteristics in the high-frequency and low-frequency ranges of the shock response spectrum by adjusting the impactor material and impact velocity.

Chapter 5 presented the numerical simulations of eight different tests from the experimental series. Tests at three different impact velocities for programmer, two different velocities for leather and sand individually, and one impact velocity for the leather-sand combination were modeled in order to provide a thorough characterization of the experimental testing. The calibrated models were used to extrapolate to loading arrangements which were not used in the experiments and show the usefulness of the simulations for prediction of various shock loads.

6.2 Recommendations for Future Work

The research presented in this thesis can be supplemented by further work in several areas. Improvements and additions can be made in the areas of shock analysis, experimental techniques, and numerical methods for the simulation of shock loading.

Analysis of the shock response spectrum provided in this thesis focused specifically on the low-frequency and high-frequency response trends. However, the response is quite complex and is often characterized by spikes in the mid-frequency or high-frequency regions. The understanding of these deviations from the basic trends requires a more thorough investigation of the development of the underlying functions which form a shock response from an acceleration-time history. Research which includes a characterization of the jumps and spikes seen in shock response spectrums is recommended.

The experimental testing of foam and a double programmer configuration produced a significant amount of high-frequency noise in the specimen response to the extent that shock responses could not be reliably calculated. Because this noise was not observed in other test sets, determining the source of this problem is difficult. Further study of the specimen, accelerometer mounting, and interaction between these types of loading arrangements and the specimen plate should be conducted in order to determine a cause for the problems seen in the data.

While numerical models always have room for improvement, two specific needs are worthy of noting. First, the foam perimeter model for the confining box should be improved to include a lower shear modulus value while still remaining stable throughout the loading of the specimen model. Because the material model being used was very simple, considering more complex models would be a good starting point for improving this foam. Second, the perimeter plates for the confining box experienced excessive bending which was clearly beyond that which was seen in the experiments. A material model which better handles strain rate effects in the elastic response of the steel should be considered.

Appendix A

Additional Test Images

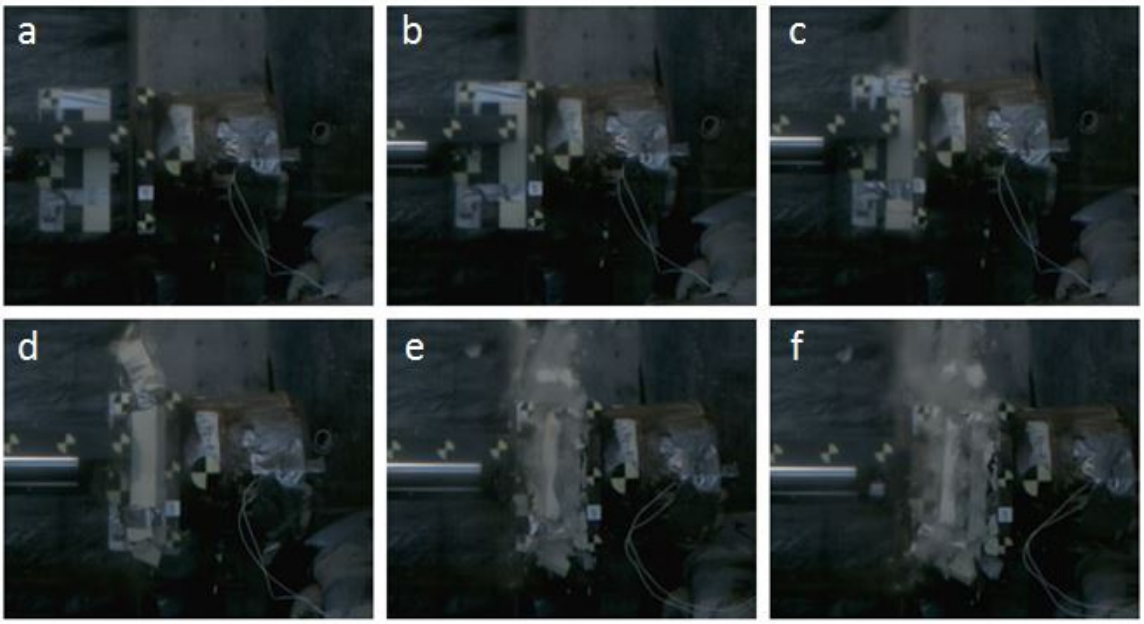

Figure A.1: Test 5 - Progression of Shock Loading

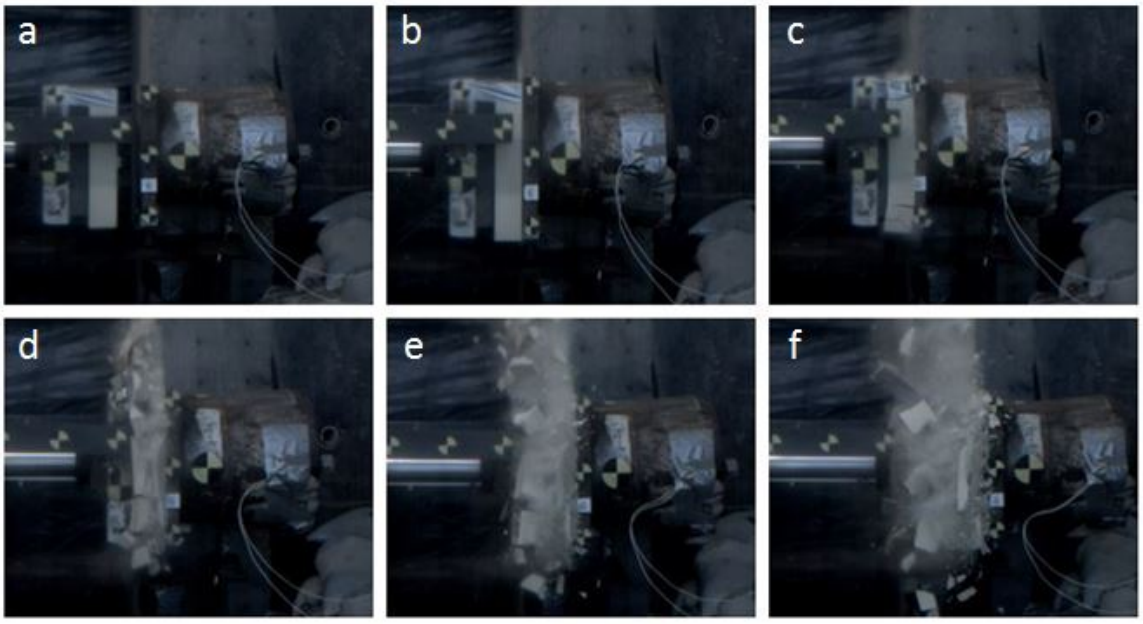

Figure A.2: Test 6 - Progression of Shock Loading

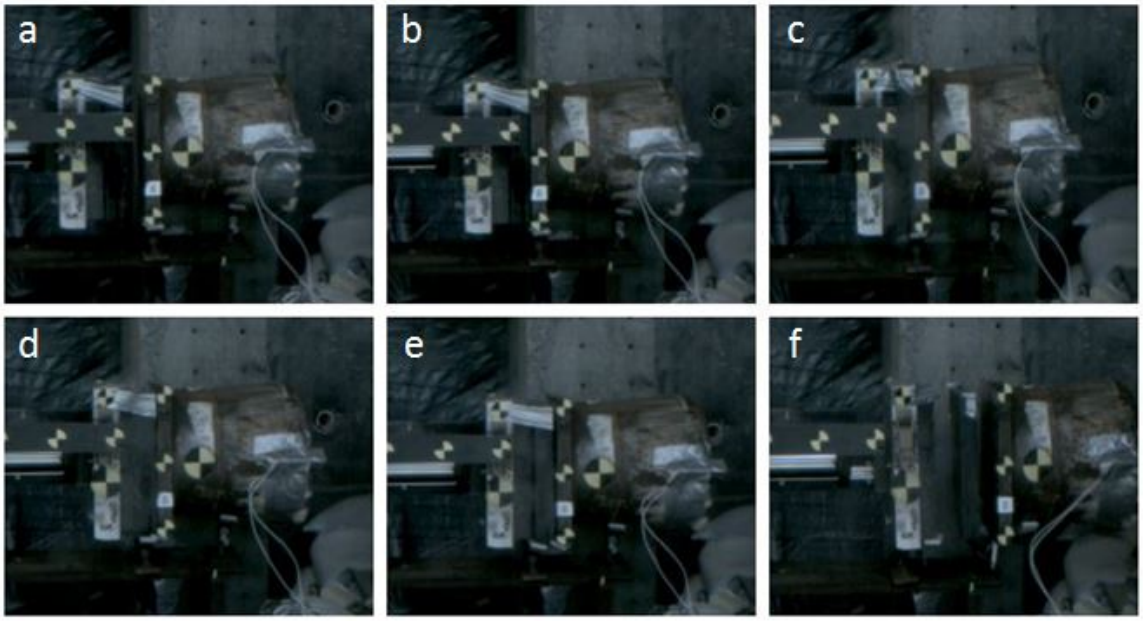

Figure A.3: Test 8 - Progression of Shock Loading

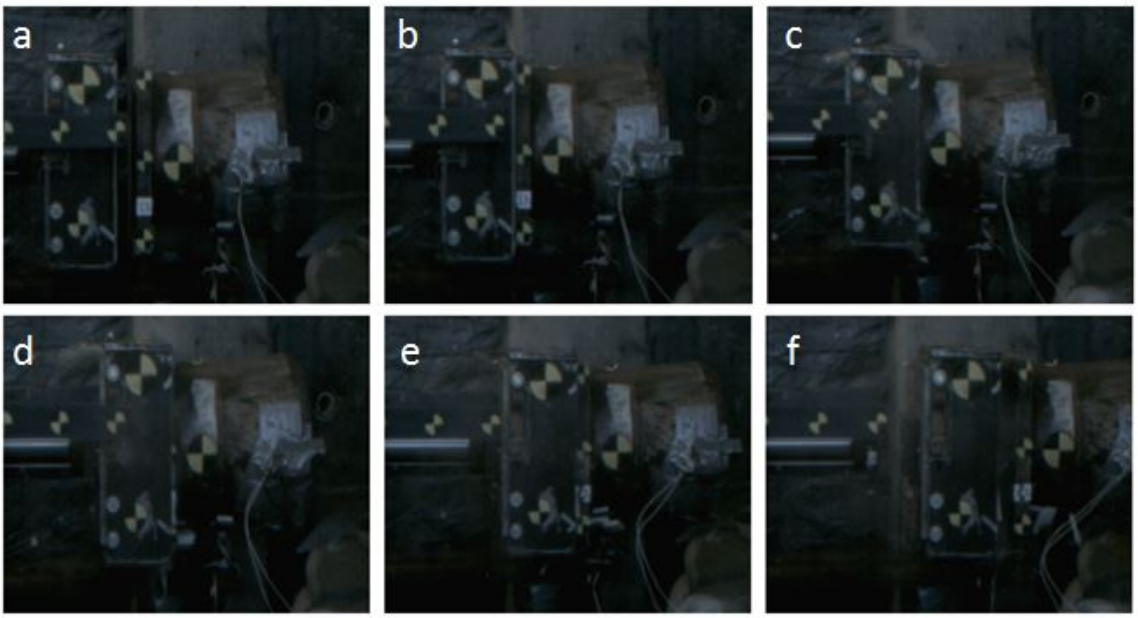

Figure A.4: Test 13 - Progression of Shock Loading

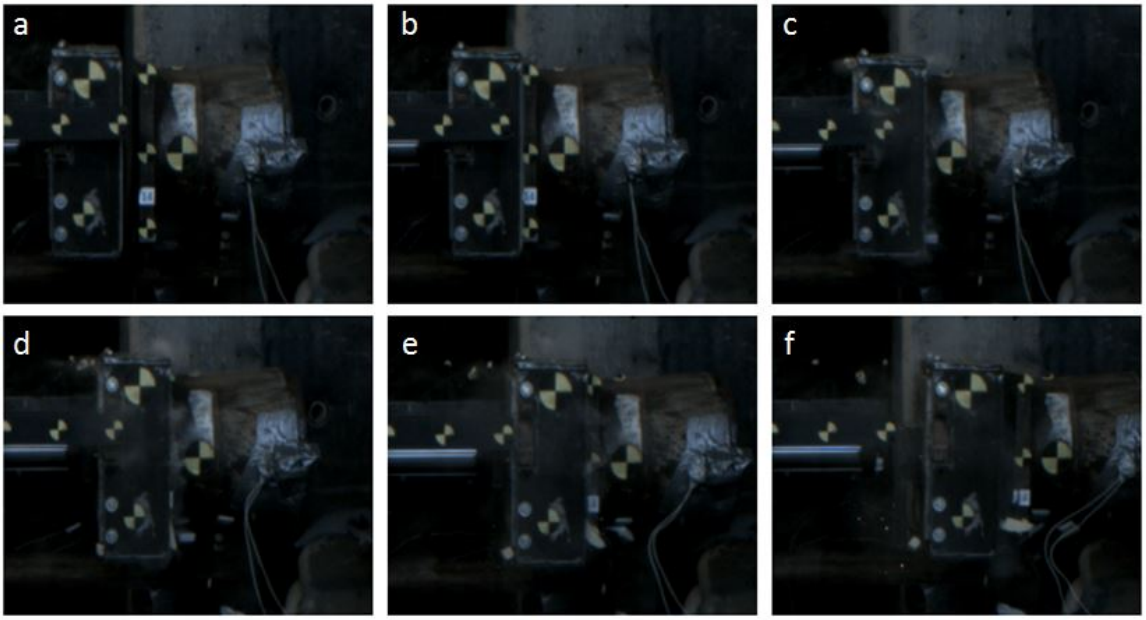

Figure A.5: Test 14 - Progression of Shock Loading

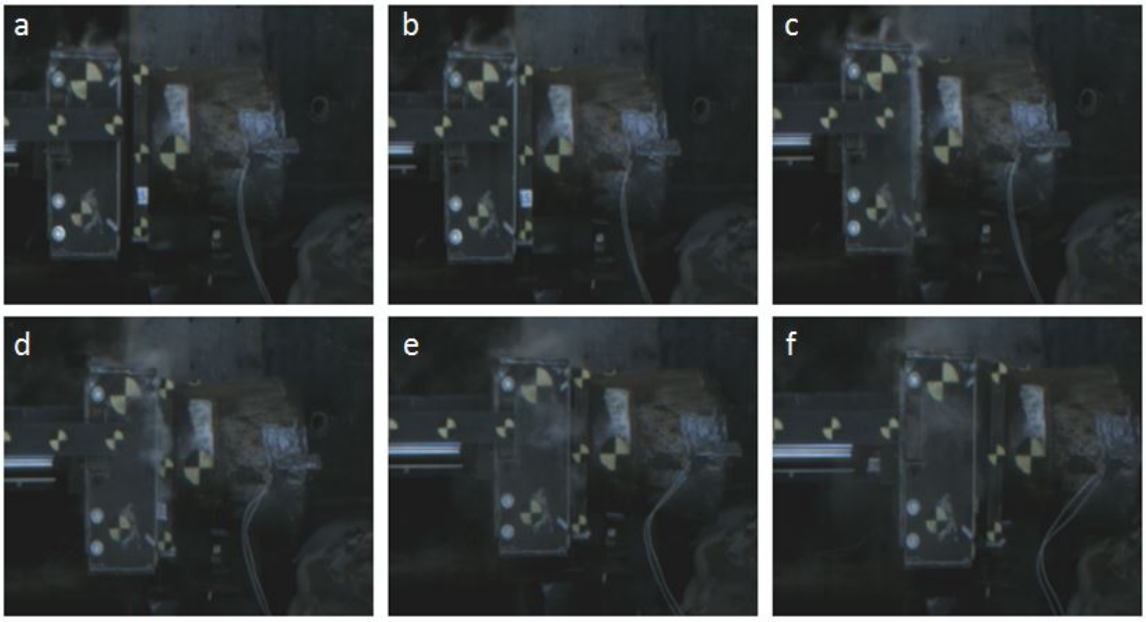

Figure A.6: Test 15 - Progression of Shock Loading

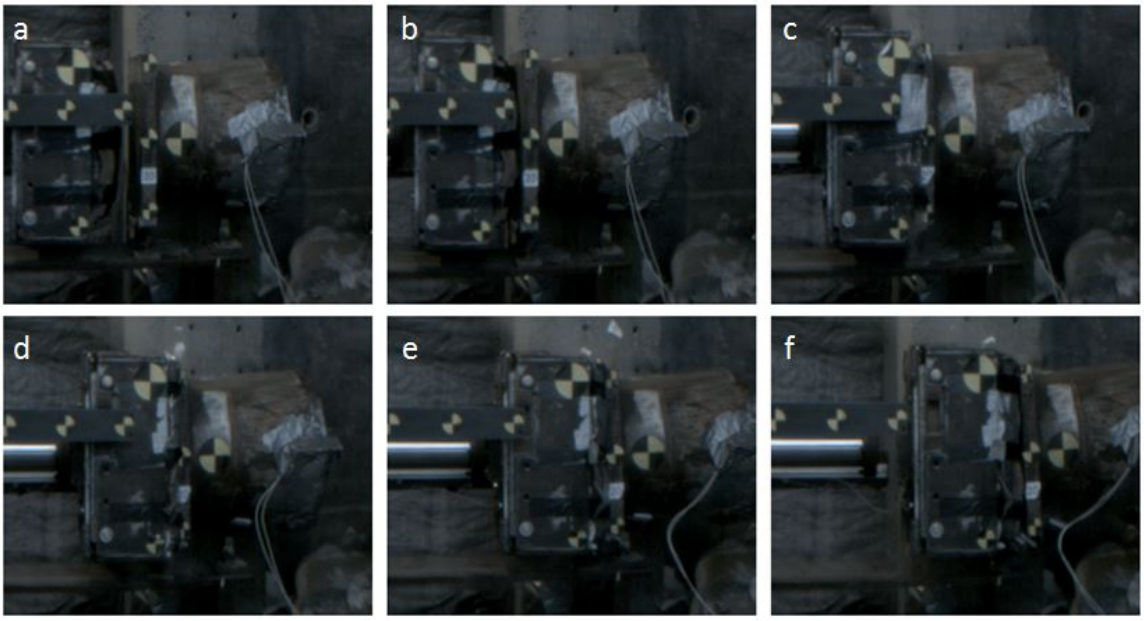

Figure A.7: Test 20 - Progression of Shock Loading

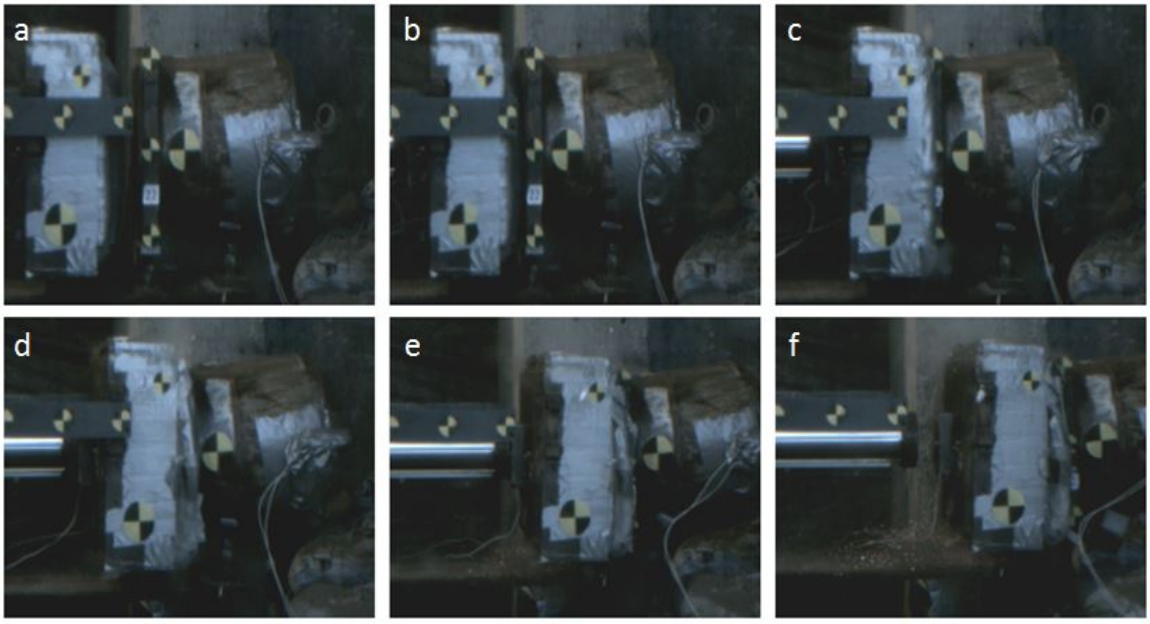

Figure A.8: Test 22 - Progression of Shock Loading

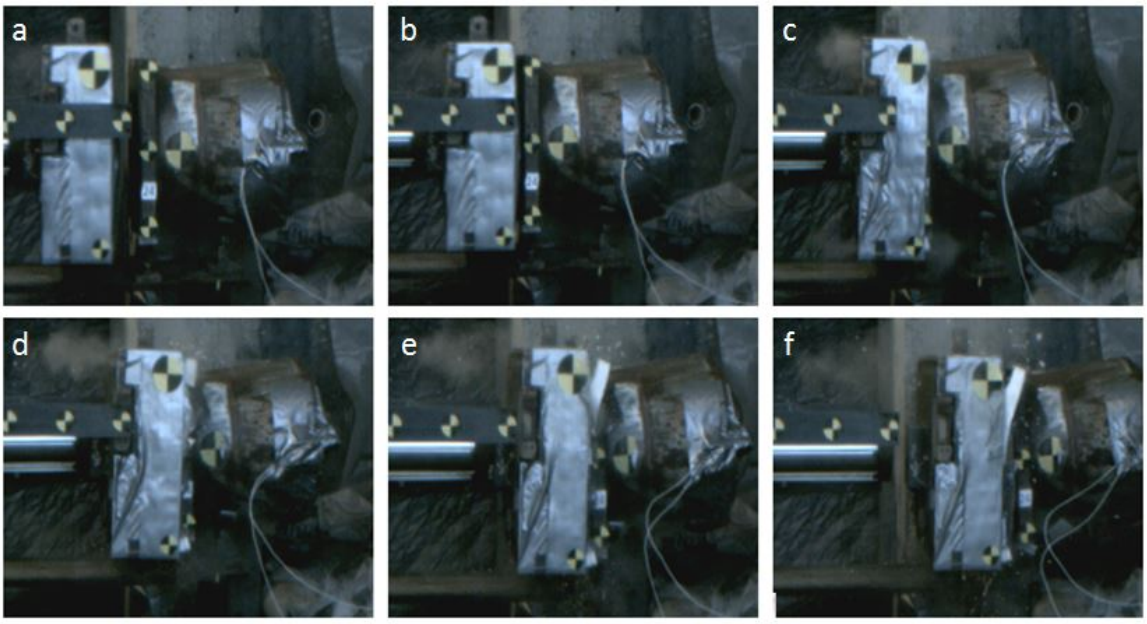

Figure A.9: Test 24 - Progression of Shock Loading

Appendix B

Additional Data

B.1 Impacting Mass and Specimen Velocities for Additional Tests

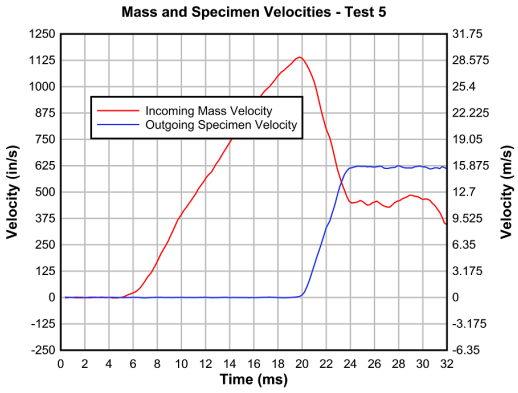

Figure B.1: Test 5 - Foam

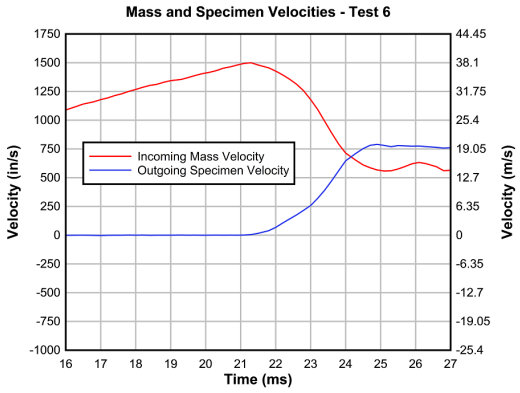

Figure B.2: Test 6 - Foam

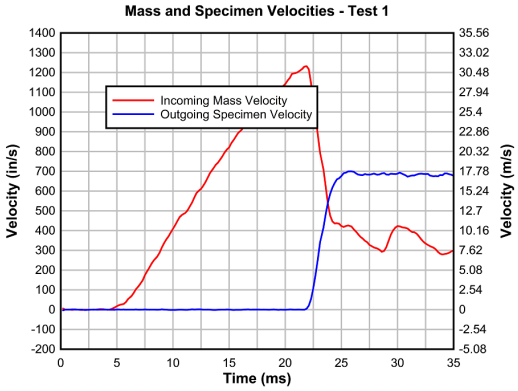

Figure B.3: Test 8 - Double Programmer

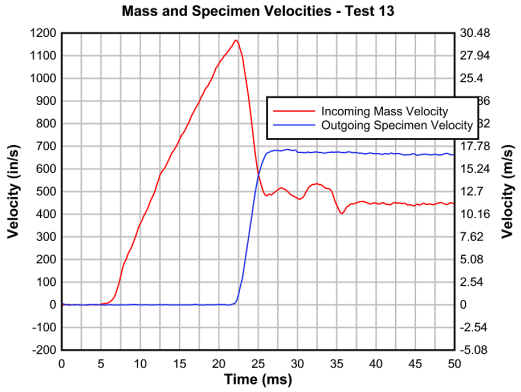

Figure B.4: Test 13 - Confined Foam

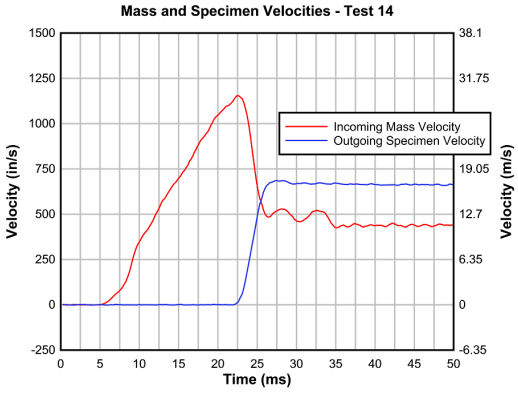

Figure B.5: Test 14 - Confined Foam

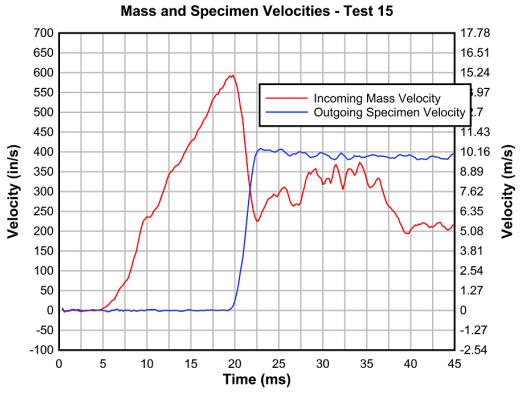

Figure B.6: Test 15 - Confined Foam

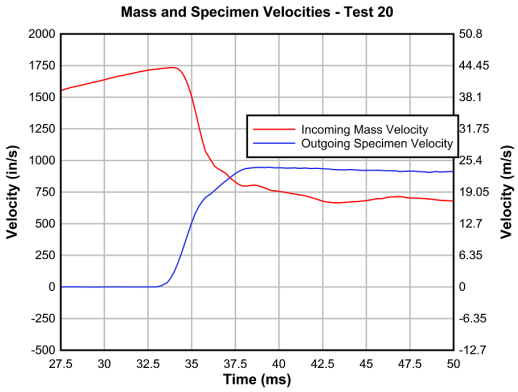

Figure B.7: Test 20 - Sand and Leather

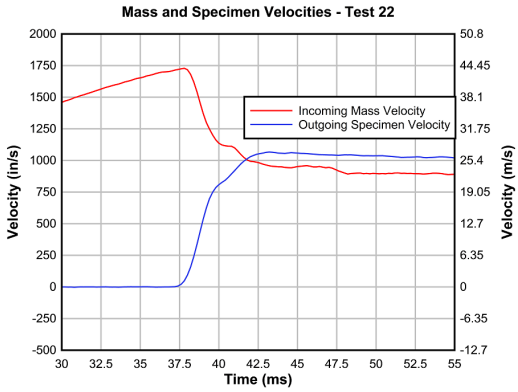

Figure B.8: Test 22 - Sand and Leather

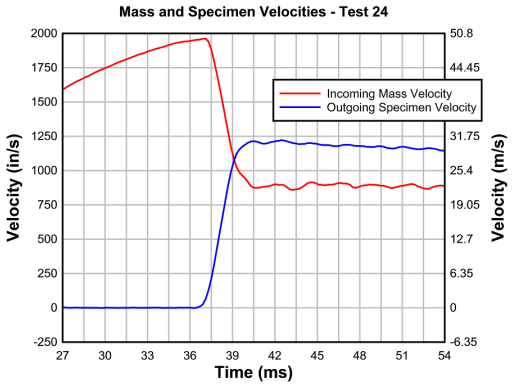

Figure B.9: Test 24 - Sand and Leather

B.2 Specimen Accelerations for Additional Tests

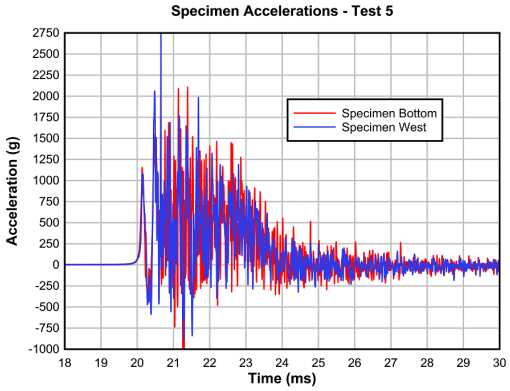

Figure B.10: Test 5 - Foam

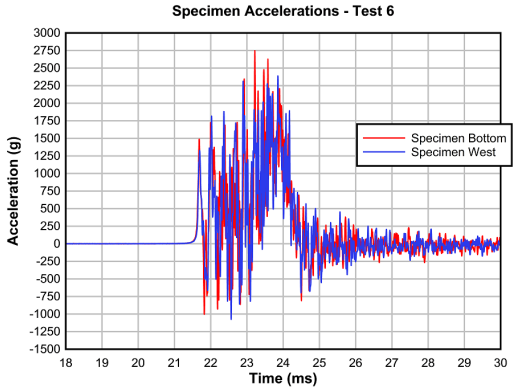

Figure B.11: Test 6 - Foam

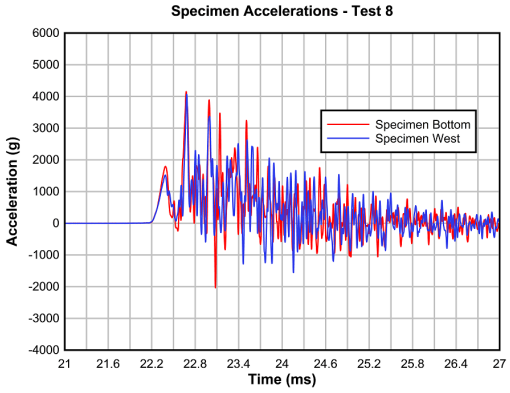

Figure B.12: Test 8 - Double Programmer

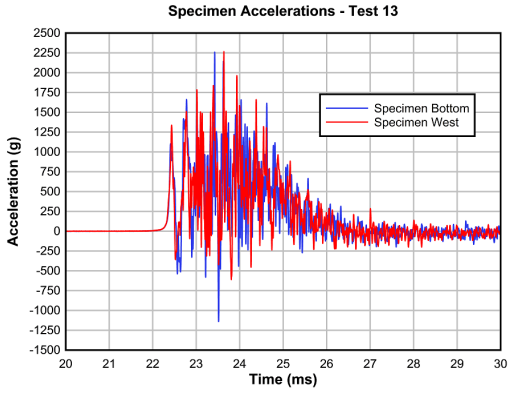

Figure B.13: Test 13 - Confined Foam

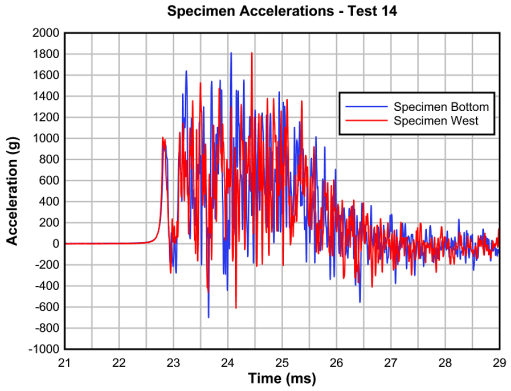

Figure B.14: Test 14 - Confined Foam

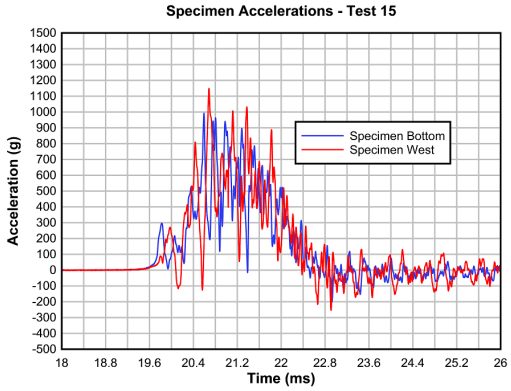

Figure B.15: Test 15 - Confined Foam

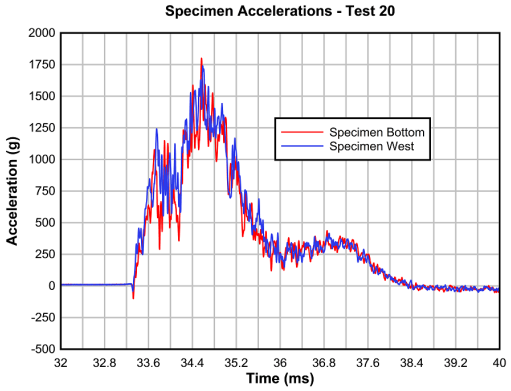

Figure B.16: Test 20 - Sand and Leather

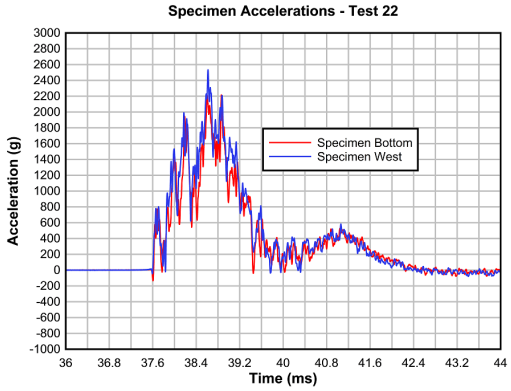

Figure B.17: Test 22 - Sand and Leather

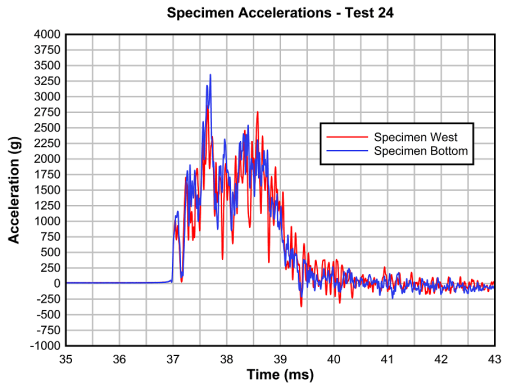

Figure B.18: Test 24 - Sand and Leather

B.3 Shock Response Spectrums for Additional Tests

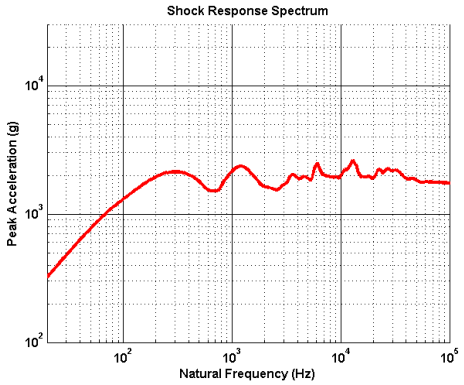

Figure B.19: Test 20 - Sand and Leather

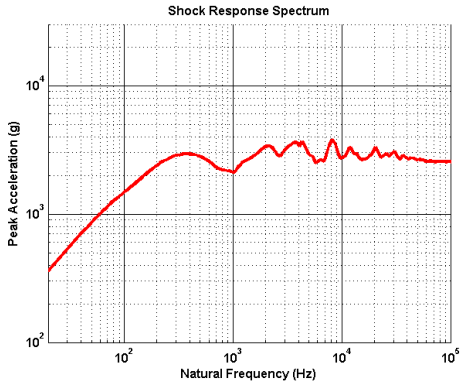

Figure B.20: Test 22 - Sand and Leather

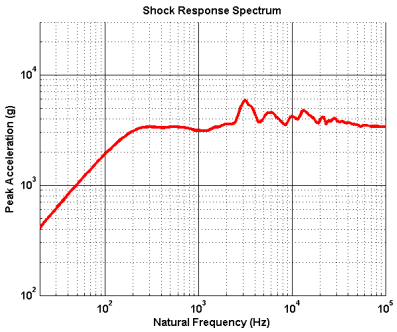

Figure B.21: Test 24 - Sand and Leather

Bibliography

[1] Test Operations Procedure (TOP): 5-2-521 Pyrotechnic Shock Test Procedures. Technical Report TOP 5-2-521, US Army Developmental Test Command, Aberdeen Proving Ground, MD, November 2007.

[2] J. Edward Alexander. The Shock Response Spectrum - A Primer. In *Proceedings of the IMAC-XXVII*, February 2009.

[3] Marcilio Alves. On the Prediction of the Dynamic Flow Stress. *Structural Engineering and Mechanics*, pages 3–4, 2005.

[4] Livermore Software Technology Corporation. *LS-DYNA Keyword User's Manual (2007)*. Livermore, CA, 971 edition.

[5] Edwin L. Fasanella, Karen E. Jackson, and Sotiris Kellas. Soft Soil Impact Testing and Simulation of Aerospace Structures. Technical report, NASA Langley Research Center, Hampton, VA.

[6] Aaron Freidenberg, C.W. Lee, Bradley Durant, Vitali Nesterenko, Lauren Stewart, and Gilbert Hegemier. Characterization of the Blast Simlator Elastomer Material Using a Pseudo-Elastic Rubber Model. *International Journal of Impact Engineering*, 2013.

[7] H. George Hammon. Properties of Three Adiprene Adhesives. Technical Report UCRL-52044, Lawrence Livermore Laboratory, Springfield, VA, April 1976.

[8] Cyril M. Harris and Allan G. Piersol. *Harris' Shock and Vibration Handbook - Chapter 26*. McGraw-Hill, New York, NY, 5 edition, 2002.

[9] George R. Henderson and Allan G. Piersol. Evaluating Vibration Environments Using the Shock Response Spectrum. *Sound and Vibration*, 37(4):18–20, 2003.

[10] Harry Himelblau, Allan G. Piersol, James H. Wise, and Max R. Grundvig. IES Recommended Practice 012.1: Handbook for Dynamic Data Acquisition and Analysis. Technical Report IES-RP-DTE012.1, Institute of Environmental Sciences, Mount Prospect, IL, 1995.

[11] Tom Irvine. An Introduction to the Shock Response Spectrum. Technical Report Revision S, Vibrationdata, July 2012.

[12] Christian Lalanne. *Mechanical Shock*. Wiley, Hoboken, NJ, 2 edition, 2009.

[13] S. N. Luo, B.J. Jensen, D.E. Hooks, K. Fezzaa, K. J. Ramos, and J. D. Yeager. Gas Gun Shock Experiments with Single-pulse X-ray Phase Contrast Imaging and Diffraction at the Advanced Photon Source. *Review of Scientific Instruments*, 83(073903):1–10, 2012.

[14] Michael G. Oesterle. *Blast simulator wall tests: experimental methods and mitigation strategies for reinforced concrete and concrete masonry*. PhD thesis, University of California, San Diego, 2009.

[15] Allan G. Piersol. Pyroshock data acquisition and analysis for u/rgm-109d payload cover ejection tests. *Engineering Department - Naval Weapons Center*, 1988.

[16] Oliver A. Shergold, Norman A. Fleck, and Darren Radford. The uniaxial stress versus strain response of pig skin and silicone rubber at low and high strain rates. *International Journal of Impact Engineering*, pages 1384–1432, 2006.

[17] David Smallwood. An Improved Recursive Formula for Calculating Shock Response Spectra. In *51st Shock and Vibration Symposium*, October 1980.

[18] Lauren K. Stewart. Experimental and Computational Methods for Steel Columns Subjected to Blast Loads. *WIT Transactions on The Built Environment*, 126, 2006.

[19] Jacob Job Wijker. *Spacecraft Structures*. Springer, Netherlands, 2008.